Gypsum Scale Formation on a Heated Copper Plate under Natural Convection Conditions and Produced Water Remediation Technologies Review

by

Mohamad H. Mirhi

BE in Mechanical Engineering, American University of Beirut (2011)

Submitted to the Department of Mechanical Engineering
in partial fulfillment of the requirements for the degree of

Master of Science in Mechanical Engineering

at the

MASSACHUSETTS INSTITUTE OF TECHNOLOGY

June 2013

ARCHIVES
MASSACHUSETTS INSTITUTE OF TECHNOLOGY
JUN 25 2013
LIBRARIES

©2013 Massachusetts Institute of Technology. All rights reserved

Author . . . . . .
Department of Mechanical Engineering
May 20, 2013

Certified by . . . . . .
John H. Lienhard V
Collins Professor of Mechanical Engineering
Thesis Supervisor

Accepted by . . . . . .
David E. Hardt
Chairman, Committee on Graduate Students

Gypsum Scale Formation on a Heated Copper Plate under Natural Convection Conditions

by

Mohamad H Mirhi

Submitted to the Department of Mechanical Engineering
on May 24, 2013, in partial fulfillment of the
requirements for the degree of
Master of Science in Mechanical Engineering

Abstract

Scaling or crystallization fouling of unwanted salts is one of the most challenging and expensive problems encountered in different applications such as heat exchangers and thermal water treatment technologies. Formation of dihydrated calcium sulfate scale, also known as gypsum, on a heated copper plate is studied in lab. The copper plate, held at a given temperature, is immersed in a supersaturated solution of calcium sulfate prepared at a given concentration. The flow conditions are governed by natural convection. A parametric study, in which surface temperature and the degree of supersaturation are varied, is set up and a scale inception time curve is plotted. No scale is observed at a supersaturation index smaller or equal to 1.4. Both higher temperatures and higher concentrations result in faster scale induction; however, the effect of temperature is more significant at lower degrees of supersaturation. SEM images of scale samples show needle-like crystals, the thinnest of which formed at a supersaturation index of 2.0. The classical nucleation theory of Mullin provides an excellent fit for the results. Interfacial energies calculated out of this model are in the reported ranges.

Thesis Supervisor: John H. Lienhard V
Title: Collins Professor of Mechanical Engineering

Acknowledgements

It is my absolute joy to look over the journey and remember all the people who have helped and supported me along the road. I would like to express my heartfelt gratitude to the inspirational Professor John Lienhard who patiently provided invaluable advice. I would also like to express my great appreciation for the support provided by the Center for Clean Water and Clean Energy at MIT and KFUPM, and my Rohsenow Kendall labmates who have spared no effort to help my research grow (Leo, Ronan, Greg, Ed, Karan, Prakash, Kishor, Jai, David, Emily, Anand, Steven, Max, and Fahad) . I would like to extend my special thanks to Trevor and Jeff for their contribution to the work.

This thesis would not be possible without the love and support of mama Salwa and baba Hussein who instilled within me a love of life and kept me in their prayers all the time. I also wish to express my sincere thanks to my sister Sahoura, my brother Abo Samra and his fiancee Miriam, my brother Assoumeh and his wife Rana, and the proud-of-her-uncle queen, Reine.

Moreover, I could not have survived the road without the love of an awesome group of friends who knew enough not to stray too far when I needed some time alone. I thank Ahmad T, Khalid, Baassiri, Abed, Obaidah, Tawfiq, Bardan, Fadel, Ragheb, Karim, Nabil, Dahlia, Hiba, Deeni, Lana, Afrah, Farah, Tania, Noor, Dima, Hana, Zeina, Shadab, Surekha and Rayan K.

يا نفس مرساك قريب!
أتدرين الفتى الذي خبأ مسودات أحلامه تحت الوسادة ما عاد متفرجاً من على رصيف الحياة، ها هو قد راح بذكرياته إلى قلب الحياة موقظاً كل حلم قديم.
إلى كلام الله، إلى أناقة الكلام،
إلى عائلتي التي صورت لي حكايا من العشق.
إلى اصدقائي الذين أشركوني الرقص على دربي، صديقاتي اللواتي علمنني كيف اصنع اللون وكيف أراه. إلى روحٍ تسكن الموسيقى منذ ألف سنة، إلى قهوة الصباح والمساء. إلى مدينةٍ منسوجة بذكاءٍ من ذكاء، إلى نبض وطنٍ يسكنني بجرحه.
إلى كل من زود موقدي بالحطب، إلى كل من أثرى تجربتي حتى أبصر هذا العمل النور.
أنا منكم فلكم حبي!
ويا نفس أنت اليوم من اشكر
تحملت عبء الإنتقاء وعبء الوقت عبء البداية وعبء الطريق
ولم تنوئي يوماً بحمل ذاك الفتى! يا نفس لا تخافي الحلم
يا نفس مرساك قريب!

Contents

List of Figures

List of Tables

Chapter 1

Introduction

1.1 Fouling Definition

Fouling is defined as the accumulation of unwanted extraneous materials on surfaces [1]. The surfaces could refer to any processing equipment in which some type of heat transfer is involved. Fouling is known to occur on solid-fluid surfaces. Examples include heat exchangers, boilers, cooling systems, membrane technologies (RO, FO) and a group of water remediation thermal systems. Fouling is one of the most serious challenges faced by the operators of this processing equipment. It has recently gained a lot of attention because a pressing need to outsmart the problem is steadily emphasized. Fouling is a challenge in terms of heat transfer as well as economics and environmental acceptability.

The problem with fouling lies with deteriorating the heat transfer capacity of the surfaces on which the unwanted materials accumulate [2] . The overall thermal resistance of a system increases and the surfaces fail to transfer heat under the temperature gradient for which they were designed [3]. For example, in heat exchangers fouling - due to low thermal conductivity of deposits-fouling introduces additional resistance to heat transfer, reducing their

operational capacity [4]. Also, in many cases the deposits are large and heavy enough to reduce the cross sectional area and interfere with fluid flow and boost the required pressure drop to maintain the flow rate across the exchanger.

A number of complex interactions are involved in fouling which makes it an extremely intricate phenomenon. Most scientists label it as a heat transfer problem, and it has been often described as the major unresolved problem in heat transfer. Fundamentally, fouling may be characterized as a combined, unsteady state, momentum, mass and heat transfer problem with chemical, solubility, corrosion and biological processes taking place [5].

Fouling of heat exchangers costs the U.S. industries hundreds of millions of dollars every year in increased equipment costs, maintenance costs, energy losses and losses in production [6]. Whatever the cause or nature of the deposits is, the problem of fouling has grown as a recognized, yet poorly understood phenomenon for a wide range of industries. Examples of industries include, but not limited to, chemical and process industries, oil refineries, paper manufacturing, polymer and fiber production, desalination, oil and gas separation, food processing, power generation, and energy recovery. It is obvious that these industries possess different types of streams that in turn have different operating conditions. Thus, formalizing a general analysis of fouling might be quite complicated of a task.

1.2 Foulants

Foulants are unwanted extraneous materials that form on a surface. Because fouling is a problem in a wide-ranging spectrum of industries and because foulant deposition is a function of different operating conditions, any solid or semi-solid depositing on a surface in the system is considered a foulant. However, some materials are commonly encountered in industrial operations. Examples include: [5]

1. Organic Materials

   (a) Biological Substances

      i. Bacteria: Bacterial fouling can take place under either aerobic or anaerobic conditions [7]. The layer formed is typically a complex structured biofilm known as slime.

      ii. Fungi: Fungi can actively grow in several systems in which they can cause dense degradation of pipelines [8]. Thriving of fungi can be attributed to special behavior like hydrophilicity or acidophilicity.

      iii. Algae: Algae, which are highly versatile and adaptive organisms, are a common active agent of biofouling. The adversity with algae is associated with the fact that they can grow on any surface in a moist atmosphere.

   (b) Oils: Oil fouling is one of the very complex problems faced in applications like oil preheat exchangers and refrigeration systems in which oil buildup causes substantial reduction in heat transfer.

   (c) Waxes and Greases: Wax fouling is very common in oil mixtures. An example is paraffin film fouling on cold surfaces [9].

   (d) Heavy Organic Deposits

   (e) Polymers: Polymer fouling is often deemed impossible to remove. While organic polymers are usually used as flocculants, they are potential membrane foulants. The problem lies with the fact that these heavy compounds are very commonly used in pretreatment technologies; hence, it is necessary to deal with them before they are carried over to the filtration membranes.

   (f) Tars: These heavy compounds often accumulate on distillation trays and packings especially in quenching systems where they condense out as gas temperatures drop.

   (g) Carbon: Carbon fouling is most commonly encountered in spark plugs.

2. Inorganic Materials

   (a) Airborne Dusts and Grit

   (b) Waterborne Mud

   (c) Silts: Silt fouling poses high-risk challenges like high pressure differentials and high turbidity in water systems. It is one form of colloidal fouling.

   (d) Calcium Salts: The most common calcium foulants are

      i. Calcium Carbonate (Calcite, Aragonite, Vaterite): a mineral scale that is a very common in membrane technologies. Calcium carbonate crystals deposit on the active layers of membranes hindering their performance. Scale formation might be caused by failure of antiscaling of the feedwater or in acid injection.

      ii. Calcium Sulfate (Gypsum, Plaster of Paris, Anhydrite): a scale that much harder than calcium carbonate and is much harder to remove as well. They are caused by incompatibility of streams containing compunds that tend to react or excess of sulfuric acid injection.

   (e) Magnesium Salts like Magnesium Hydroxide which deposits on membranes operating at high recovery at high pH

   (f) Barium Salts: Salts like Barium Sulfate are very hard to remove because they are insoluble in almost all cleaning solvents.

   (g) Strontium Salts like Strontium Sulfate

   (h) Iron Oxides: These scales could result from corrosion products in pipes or oxidation of solube iron with air.

1.3 Types of Fouling

There are several types of fouling, categorized according to the origin of the precursors of fouling or, in other words, the underlying chemical, physical, or biological processes. Although one cannot speak of fouling as a single commodity in real applications because different types coexist, researchers have grouped them into six types: [10]

- Particulate Fouling

  Particulate fouling is the accumulation of suspended particles on heat transfer surfaces [11]. Settling of particles in process streams could be driven by gravity force, case in which it is called sedimentation. Fine particles that are not settled by gravity settle instead on heat transfer surfaces at different inclinations, typically driven by suction or other mechanisms. This type of fouling is encountered in deposition of corrosion products in working fluids, ash deposition on boiler tubes, soot suspensions of incomplete combustion, magnetic particles in economizers, and mineral particles in river water [12]. Like many other types of fouling, particulate fouling is highly affected by concentration, flow conditions, temperature and heat flux at surfaces.

- Precipitation or Crystallization Fouling

  Crystallization fouling, also known as scaling is crystallization of dissolved salts from saturated or supersaturated solutions onto heat transfer surfaces. Generally, this type of fouling is caused by solubility variations with temperature [12]. A number of salts precipitate at higher temperatures, exhibiting what is called inverse solubility behavior. Precipitation fouling is common when aqueous solutions of untreated water undergo some kind of cooling or heating. Scaling is visible in applications where process streams that are mixed contain chemicals that reach with each other to form solid precipitates. For example, in underground oil and gas extraction, sulfates from seawater injected for enhanced recovery might readily interact with calcium from the mineral formation layers to cause a hard scale of calcium sulfate. Normally, crystallization is triggered at

especially active sites known as nucleation sites. These sites might occur at scratches, pits, or rough surfaces and they accelerate the rate of fouling until the scale forms a full layer on the surface. This kind of fouling is very difficult to remove and requires vigorous chemical and mechanical treatment [13]. Fig 1.1 shows scale buildup in a water distribution plant [14].

Figure 1.1: Fouling Curves

- Chemical Reaction Fouling

  When accumulation of unwanted material is a result of a chemical reaction, it is called chemical reaction fouling. In this type of fouling, one or more reactions taking place between substances in the flowing fluid cause deposition of a solid layer in the vicinity or on the surface. The surface material is not usually one of the reactants but could behave as a catalyst sometimes as in the cases of cracking, coking, or polymerization [12] [5]. Chemical reaction fouling is common in applications such as petrochemical industries, oil refining, gas cooling and vapor-phase pyrolysis. It is often extremely tenacious and requires very special treatment measures [13].

- Corrosion Fouling

  Typically, corrosion is a product of a chemical or an electrochemical reaction; however, in this case the heat transfer surface is one of the reactants [2]. So, it is a case where

one of the reactants is consumed. If the produced corrosion product is not dissolved in the aqueous solution, it changes the thermal characteristics of the surface and deposits on it. In other cases, the corrosion products are transported through the solution to another site in the system where deposition is more favorable. Examples include corrosion caused in oil fired boilers due to the presence of sulfur in the used fuel [15]. It is important to mention that this type of fouling is very sensitive to the pH of the working fluid.

- Biofouling

  Biofouling is the attachment and growth of microorganisms or macroorganisms on heat transfer surfaces. When the products of algae, molds, fungi or bacteria grow on a surface, they bring about serious microbial fouling. The slime layer formed is usually uneven and may be a trigger for further corrosion fouling. Biofouling is one of the challenging problems faced by food processing industries and power plants in which seawater is used.

- Freezing Fouling

  Freezing fouling involves solidification of pure liquids onto subcooled surfaces. Examples include formation of ice during chilled water production and formation of waxes as paraffin during their cooling. The rate of fouling is very sensitive to surface temperature and shear stress [16].

1.4 Fouling Stages

In order to reduce the complexity of the mechanism behind fouling processes, fouling was divided into five stages, each of which is influenced by other intricate phenomena. These stages can be grouped into two groups: transport of molecules from bulk to liquid-crystal interface and the integration of molecules at the heat transfer surface into crystal lattices.

The different steps are discussed below: [17]

1. Initiation

   Initiation is the formation of foulant materials in the bulk of the fluids. A seed for crystallization must exist in order to initiate nucleation. The time of induction of the first nucleus might be in the order of seconds, minutes, hours, days or even several weeks. The main driving factor is the increase in the degree of supersaturation with respect to the heat transfer surface temperature. The time it takes nuclei to crystallize, also known as the delay period, decreased with increasing temperature. With the increase in surface roughness, the delay period tends to decrease [7].

2. Transport

   In this stage, foulant material is transported to the fluid-deposit interface across the boundary layer [18]. Transport is carried on by a number of phenomena including: [19]

   (a) Diffusion which is mass transfer of the scaling products from the flowing fluid with higher concentration to the heat transfer surface down the concentration gradient.

   (b) Thermophoresis whereby a thermal force moves fine particles from a hot to a cooler region. In the case of deposition on the surface, an absolute value of the temperature gradient at the wall induces attachment.

   (c) Electrophoresis due to electric forces. Fouling particles will carry a charge toward or away from the surface based on the polarity of each side. Electric forces are usually brought about by surface phenomena like London-van der Waals interaction forces.

   (d) Inertial Impaction during which large particles have an inertia that is high enough to prevent them from following a streamline; hence they deposit on a surface.

   (e) Sedimentation which is deposition of particles under the action of gravitational interaction. It is usually observed in cooling tower waters.

(f) Turbulent Downsweeps thought of as suction regions distributed across the surface. The flux during transport is evaluated as the product of the concentration difference and the transfer coefficient that is a function of Sherwood number.

3. Attachment

In this stage, adherence of deposits to the surface takes place [12]. This process is influenced by different factors including:

(a) Particle Size and Density which affect both sticking and reentrainment probabilities.

(b) Surface Conditions like wettability, interfacial tension and heat of immersion. Surface roughness also increases the area of contact and hence induces nucleation [20], substantially reducing the time of induction of fouling.

4. Removal

Surface shear forces that are guided by velocity gradients at the surface and properties like roughness is the main driving force behind removal of deposits [21]. The general effect of these forces is not yet completely understood. New molecules form only after the deposit bond resistance is larger than the shear forces at the interface. Other mechanisms causing removal are randomly distributed turbulent bursts, erosion and re-solution [5].

5. Aging

Aging starts as soon as deposition takes place. The properties are function of the mechanical properties of the deposits.

A schematic diagram reproduced from the work of Awad et al. [5] shows the deposition and removal mechanisms.

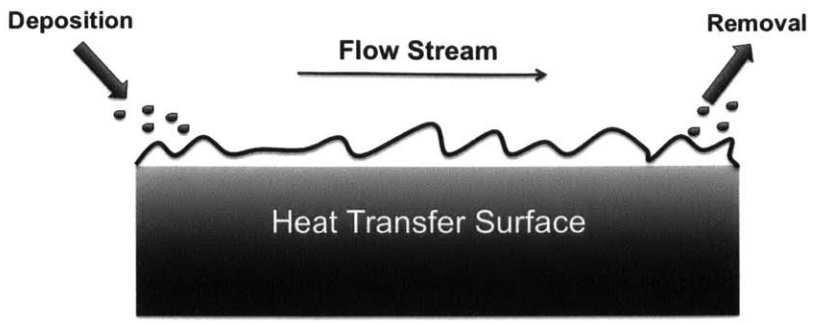

Figure 1.2: Fouling Process

1.5 Fouling Curve

The process of fouling is usually represented by a fouling resistance R_f that reflects the decreased heat transfer capacity of heat exchangers. By convention, a fouling curve is a plot of the fouling resistance versus time. Typical fouling curves are shown Fig 1.3 [12]. The

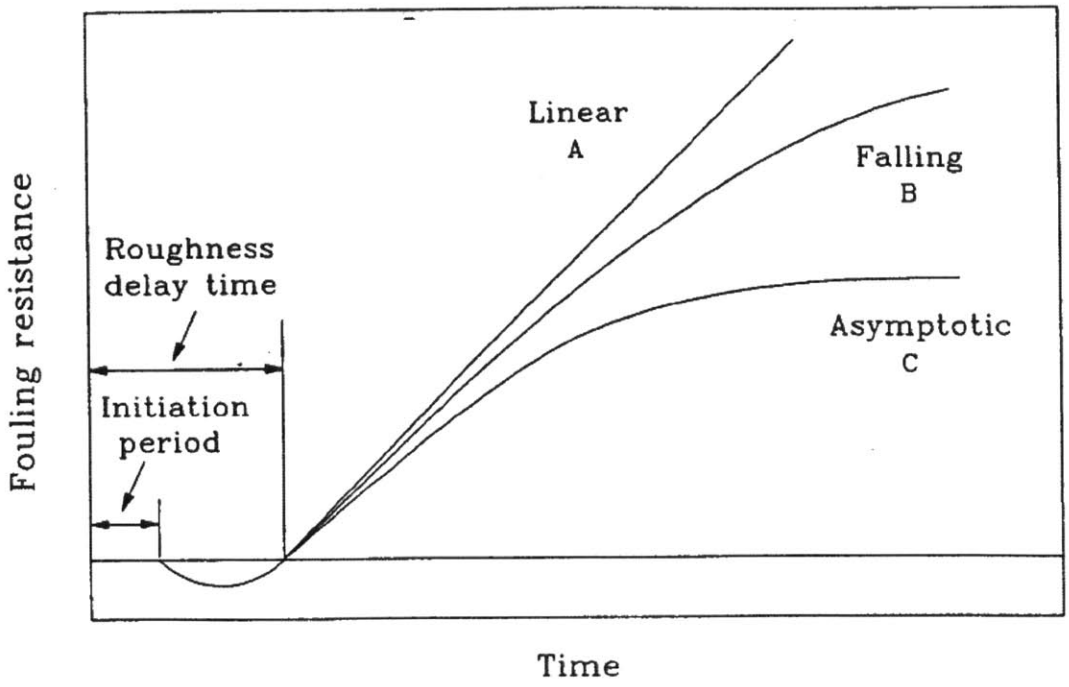

Figure 1.3: Fouling Curves

initiation period is the time during which no scale is formed anywhere in the system after it starts its operation. Right at the end of this period, the initial growth of deposits causes

the heat transfer coefficient in the system to increase as the deposits penetrate the viscous sublayer. Therefore, the flow characteristics at the heat transfer surface change and the increase in the heat transfer coefficient overcomes the thermal resistance associated with the deposits, thereby increasing the effective coefficient. Some authors have as a result reported negative fouling resistances [22] [23].

The process goes on until the increased heat transfer coefficient due to increased turbulence lags behind the thermal resistance. The time period from the beginning of the fouling process until the fouling resistance again becomes zero is called roughness delay time [24]. The initiation period and the roughness delay time for particulate fouling are very small [25] in comparison to the fairly long delay time for crystallization fouling [26]. The fouling curve starts its monotonic increase crossing the zero level at the end of the roughness delay time, taking one of three routes:

- Linear

  Curve A represents the linear case which is common in cases when the deposits are strong enough for removal to be negligible relative to deposition. Also, when the removal rate is constant the fouling curve is linear. A linear fouling curve was reported by Reitzer et al. and in this case, the deposits exhibit powerful mechanical strength [27].

- Falling

  The fouling curve is falling (curve B) when the deposition rate drops down as deposits have low mechanical strength.

- Asymptotic

  Asymptotic curves like curve C are the most reported as the fouling resistance increases for some time after which it takes a steady value when the removal rate becomes equal to the deposition rate. A closer representation of asymptotic fouling practical curve might be as shown in Fig. 1.4 [12].

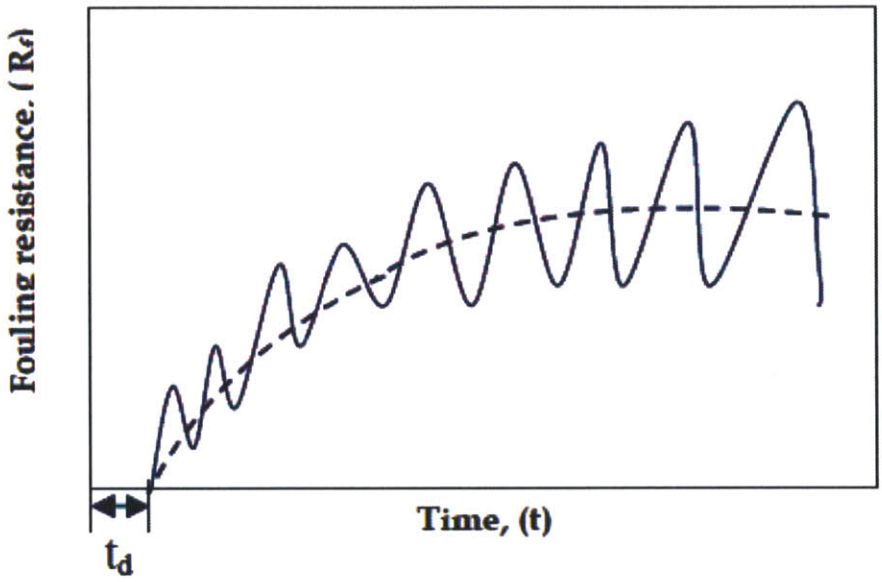

Figure 1.4: Practical Fouling Curve

1.6 Crystallization Fouling

This thesis deals with one specific type of fouling that is crystallization fouling or scaling. Since dihydrated calcium sulfate or gypsum is one of the most common crystallizing salts spanning different applications and industries, the kinetics of gypsum crystallization are studied.

1.6.1 Governing Parameters

The kinetics of scale formation are influenced by a number of operating conditions and design parameters. These parameters include:

- Surface Temperature

  The temperature of the heat transfer surface has a major influence on fouling size and fouling rate. For salts that have an inverse solubility behavior, higher temperatures

is equivalent to lower solubility; hence, more fouling is expected. For salts whose solubility increases with temperature, cooling results in more fouling. Literature has also reported cases where temperature had no effect on fouling [19]. The real effect cannot be studied independently of other parameters particularly the supersaturation degree.

- Bulk Temperature

  The temperature of the pool of the working fluid has its own effect on fouling as well. Higher bulk temperatures are said to result in more fouling in the case of inverse crystallization because bulk precipitation is induced and deposition follows.

- Degree of Supersaturation

  Fouling and fouling rate increases with supersaturation. This is expected because the driving force for surface reactions increases when the concentration is higher. At the later stages of operation, the influence of concentration becomes less pronounced because of enhanced shear stresses and lower interfacial temperatures. Demopolous reported that supersaturation is the most important controlling factor of aqueous precipitation [28]. De Yoreo et al. report a trend of induction time versus supersaturation as shown in Fig. 1.4 [29]. Tlili et al. found that the concentration has a stronger effect than temperature in precipitation of calcium sulfate when using a gold layered nickel foil [30].

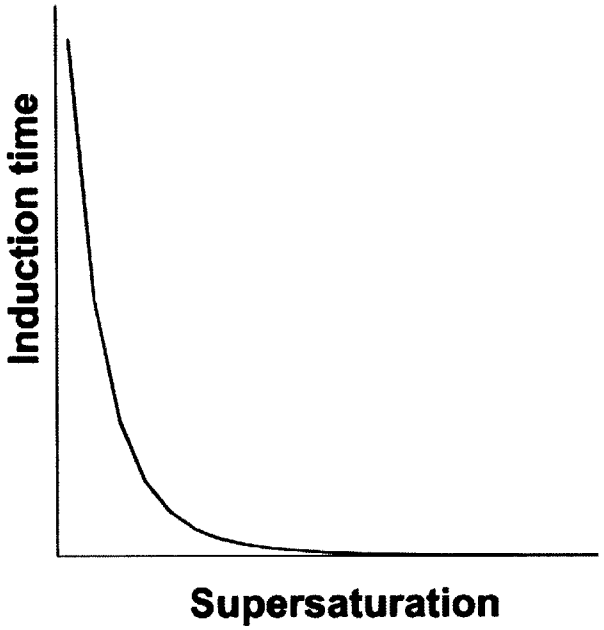

Figure 1.5: Change of Induction Time with Supersaturation

- Velocity

  Although in most applications less fouling is expected at higher velocities, there are some reported cases of diffusion-controlled processes during which more fouling occurred at higher velocities [31]. Moreover, increasing the velocity enhances shear forces, which causes higher removal effects. The effect of velocity variation is tightly linked to the size and mechanical strength of the deposits. When the deposits are so fine, increasing the velocity might even eliminate fouling. However, when they are strong, the positive effect of increasing velocity decreases after some point.

- Surface Material

  Different materials have different catalyzing action; hence, there are ones that induce fouling more than others. Kazi et al. reported that surfaces with higher thermal conductivities promote more fouling and they ranked different metal surfaces in decreasing extent of fouling as follows: copper, aluminum, brass, stainless steel [20].

- Surface Structure (Roughness)

The initial rate of nucleation is highly dependent on surface structure because sites like pits and scratches serve as seeds for crystallization as they significantly reduce flow velocities. Rankin et al. reported that surface roughness leads to a much larger effective contact area than the projected surface area and hence deposit adhesion is stronger [32]. Hence, a rough surface induces deposition at a rate that is faster than what takes place in the case of a smooth surface. Junghahn et al. developed a theoretical explanation of the fact that the free energy needed for nucleus crystallization is much less with rough surfaces [33]. On the other hand, rough surfaces cause more turbulence in the flow, which enhances shear effects and removal. In heat exchanger applications, mirror finished surfaces are usually used to reduce fouling [34].

Other conditions affecting fouling initiation, transport and attachment are heat exchanger types [35], impurities in solution, fluid properties like viscosity and density and design considerations. It was also found that the rate of scale formation is a function of the area and the metallurgy of the heat exchanger [36].

1.6.2 Time of Induction

The time that elapses between the onset of supersaturation and the formation of critical nuclei or embryos-clusters of loosely aggregated molecules that have the same probability to grow as crystals or redissolve into solution- is an important parameter when it comes to the study of the kinetics of nucleation [37]. This time is called the time of induction. Sohnel and Mullin suggested that this time is impossible to experimentally measure; hence, it is necessary to let crystals grow to reach a detectable size [38]. It has been shown that $CaSO_4$ nucleation on the heat transfer surface of a non-boiling flow exchanger is a transient nucleation phenomenon [?]. Branch et al. correlated the reciprocal of the delay time as if it were independent of solute concentration. An Arrhenius dependence on wall temperature

was suggested instead [39]. Najibi et al. showed that the degree of supersaturation is one of the most governing parameters affecting the delay time and a zero-order model is definitely a wrong representation [40].

1.6.3 Calcium Sulfate Crystallization

The formation of crystalline calcium sulfate on heat transfer surfaces is one of the most challenging problems in heat exchanger applications as well as thermal desalination systems. Calcium sulfate is the most common naturally occurring sulfate. It is frequently encountered in geology, medicine, art, industry and chemistry. Gypsum ($CaSO_4 \cdot 2\,H_2O$) is the most common sulfate scale in oil and gas industries, followed by anhydrite calcium sulfate ($CaSO_4$) and barium sulfate. The third form of calcium sulfate is the hemihydrate or what is commercially referred to as the Plaster of Paris ($CaSO_4 \cdot \frac{1}{2}\,H_2O$). The most thermodynamically stable form of calcium sulfate at a given temperature is decided based on the solubility equilibrium curve in Fig 1.6 published by Rausoor et al. [41].

According to Amjad et al. gypsum is the most commonly encountered calcium sulfate in cooling water and reverse osmosis based systems [42]. Hemihydrate and anhydride forms are the most frequently formed salts in high temperature processes such as boilers and multi-stage distillation [43].

1.6.4 Gypsum

1.6.4.1 Morphology and Crystal Structure [44]

Built in 3000 BC, the pyramid of Cheops in El-Giza, Egypt is the first verification of the use of gypsum in construction [44]. Gypsum occurs in nature as sedimentary rocks and as a scale. Someone who works in an oilfield would describe it as a hard, dirty-brown deposit

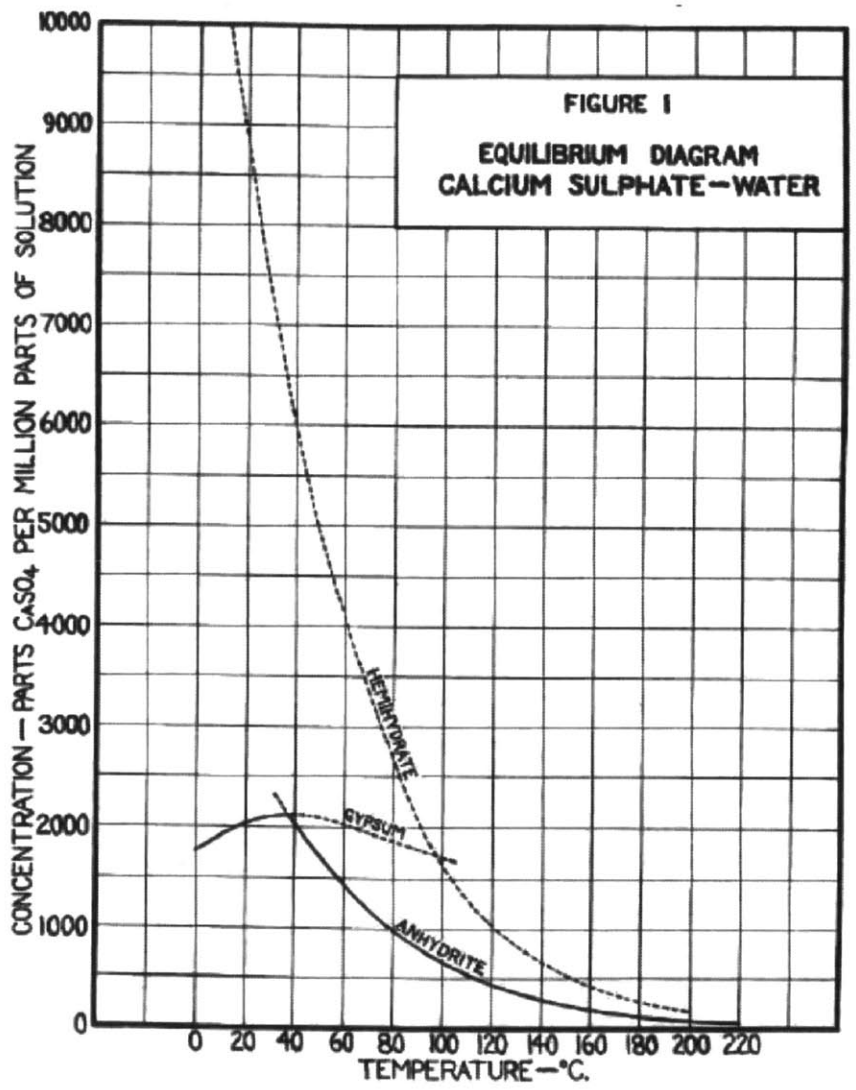

Figure 1.6: Solubility Equilibrium Diagram of Calcium Sulfate in Water

coating the inside of tubes. The crystal structure of gypsum is described as monoclinic prismatic. Pure gypsum is snow-white as shown and commonly exists with layers of anhydride calcium sulfate.

At temperatures higher than 38-40°C, calcium sulfate solubility starts decreasing with temperature as shown in Fig. 1.4 [41]. In that range, gypsum is the most thermodynamically stable form of calcium sulfate and is expected to be the primary foulant in thermal desalination systems where calcium and sulfate exist in streams.

Selenite gypsum mineral is shown in Fig. 1.7 [45].

Figure 1.7: Gypsum Mineral

Chapter 2

Experimental Setup: Description and Methodology

This chapter discusses the details of the experiment done in lab. The experimental setup, materials used, building procedure, instrumentation, operation steps, measurement methods, cleaning measures, and precautions are thoroughly described. The theory underlying a number of the taken steps is also depicted throughout.

2.1 Experimental Setup Description

Because the kinetics of scale formation are dependent on a complex system of parameters, studying the phenomenon experimentally becomes cumbersome. Investigating how the time of scale induction varies cannot be achieved without being able to control a number of the influencing parameters. The experimental method followed here is intended to draw out a parametric study, which outlines the variation of scale formation time versus salt concentration and surface temperature. In order to obtain a comprehensive data matrix, all other parameters that affect the kinetics or thermodynamics of scale formation need be fixed.

Therefore, the experimental setup had to be formulated in the light of the need for a system that facilitates access to parameter control. In particular, the system to be built had to offer the ability to fix surface roughness, fluid flow conditions, solution purity level, fluid properties and pH. In fact, a number of possible setups were excluded for the fact that fixing some parameters was not possible. For example, studying the kinetics of sulfate scale formation on a plate placed horizontally under a stirrer was not the best candidate. This is because flow conditions for such a system are not well studied and minimal information about the fluid flow velocity could be obtained.

In the light of this constraint along with space requirements, the devised setup consists of three simple component systems that allow, to a large degree of control, the measurement of the time of scale inception on a heated copper plate in a supersaturated solution of dihydrated calcium sulfate. A schematic diagram of the apparatus is shown.

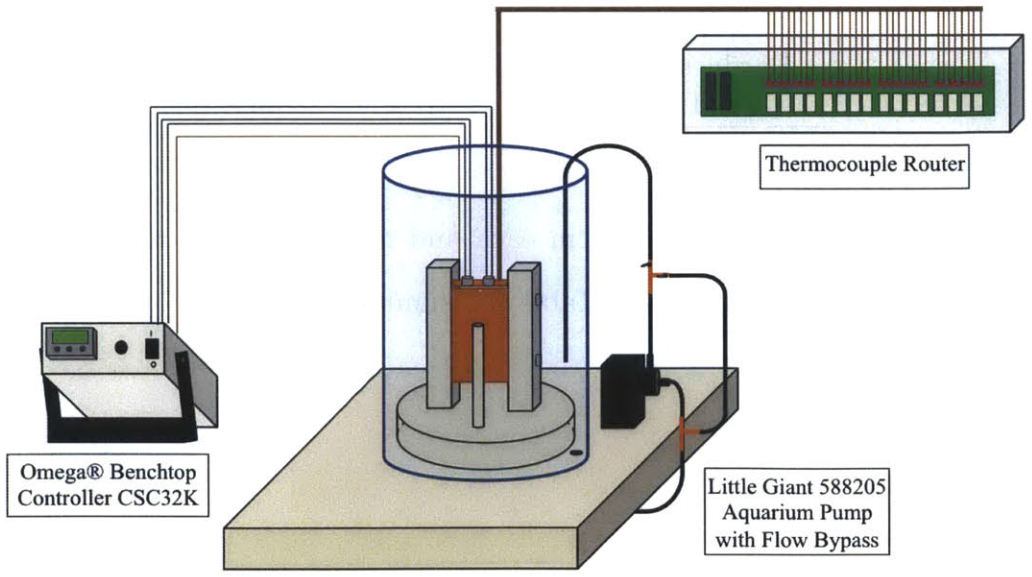

Figure 2.1: Schematic Diagram of the Experimental Apparatus

2.1.1 First Component System

The first component system is the fouling surface or the heat transfer plate. In this system, a solid machined $15 \times 8 \times 2.5\ cm^3$ copper block is vertically mounted to two vertical Delrin® Acetal resin rails that are in turn mounted normal to a circular Delrin® base.

The copper block is a multipurpose alloy (110) that is 99.9% copper with some traces of lead. Copper is selected mainly because it has a high thermal conductivity value that would speed up heat transfer to the entire block leading to a thermally uniform surface. More information about the physical and chemical properties of the copper block is given in Table 2.1

Table 2.1: Copper Plate Properties

Property	**Unit**	**Value**
Nominal Density	kg/m^3	8912.9
Modulus of Elasticity	GPa	117
Thermal Conductivity	W/m.K	392
Electrical Resistivity	Ω	10.6
Temper	-	Hard (H04)
Hardness Rockwell	-	F65-F80
Yield Strength	MPa	303

The Delrin® square poles are 25 cm each and they are bolted to a circular piece of Delrin® that is 20 cm in diameter. Table 2.2 summarizes some of the properties of the Delrin® support system.

Table 2.2: Delrin®Properties

Property	Unit	Value
Tensile Strength	MPa	69
Rockwell Hardness	-	M89-M94
Friction Coefficient	-	0.2
a Dielectric Strength	V/0.001"	435-500
Water Absorption	%	0.2-0.4%
Thermal Expansion	$1/°C$	$8.47 - 21.2 \times 10^{-5}$
Density	kg/m^3	1411

In addition to providing strength and support, the Delrin® system is employed to keep the copper block in a vertical position in the solution so that the flow conditions can be modeled using the integral method for natural convection against a vertical plate in water. Delrin® Acetal resin is selected for its good tensile strength, machinability and convenient thermal properties that would conserve the heat in the attached copper block within a desired range.

The front surface of the copper block is brushed smooth so that no rough pits can serve as nucleation sites that induce gypsum crystallization.

The back surface of the block has nine holes drilled symmetrically about the principal axes, which contain the ends of nine temperature sensors held in place by epoxy. The holes are drilled through the back surface deep enough to reach 6.4 mm depth below the front surface. The purpose of these points is to accurately monitor surface temperature and ensure that the copper block remains thermally uniform throughout the testing procedure.

The temperature sensors embedded in the back surface are ready-made Omega insulated K-type thermocouples supplied with a subminiature connector and a spool cap. The thermocouple wire is 0.25 mm in diameter and the insulation is made of Kapton®. The ends of the wires are glued in the drilled holes that are blocked to prevent interaction with

the aqueous solution. In order to fix the thermocouples, Loctite® epoxy adhesive is used. The epoxy provides ultra-fast hardening and resists high temperatures. It is of clear color and reaches maximum hardness within 1 hour.

The top surface of the copper block has two large bores, which house two Joule-heater cores. The 1.27 cm diameter, 11.4 cm long, 200 W cylindrical cartridge heaters transfer heat through metal surfaces. They are insulated with magnesium oxide and encased in a Type 304 stainless steel sheath. They operate on 120 V AC, are single phase, have leads for hardwiring, and designed to be used with a temperature controller. Cartridges withstand a maximum temperature of 1000°F, which is far beyond the desired operation range. The heating elements are tightly wound and compressed to ensure high resistance to impact and vibration.

The cores are embedded with OMEGATHERM® thermally conductive silicone paste to improve heat transfer to the copper block. The paste is thermally conductive 'heat sink' silicone grease. It has a very high thermal conductivity coupled with high insulation resistance and high dielectric strength. It is rated for continuous use between 40°C and 200°C. This white thick smooth paste provides an excellent route of heat conduction increasing the heat-path area from the cartridge heaters to the copper block body.

The two cartridge heaters and the thermocouple embedded in the center of the block are connected to an OMEGA® CSC32K mini benchtop controller that regulates the temperature of the copper block during operation. This temperature controller is a 4-digit display, 0.1°C resolution heater. Pre-wired input and output receptacles on the rear panel enable quick and easy connections to main ac power, signal input, control output and two-way digital communications. The leads of the two cartridge heaters are connected to the back of the controller. The feedback temperature sensor is the thermocouple connected to the center of

the block, which proved to be uniformly isothermal. The controller was programmed to a PID Autotune Control mode. The desired temperature was set on the front panel and the controller maintained it constant throughout operation. The machining orthogonal views of the copper block are shown in Fig 2.2.

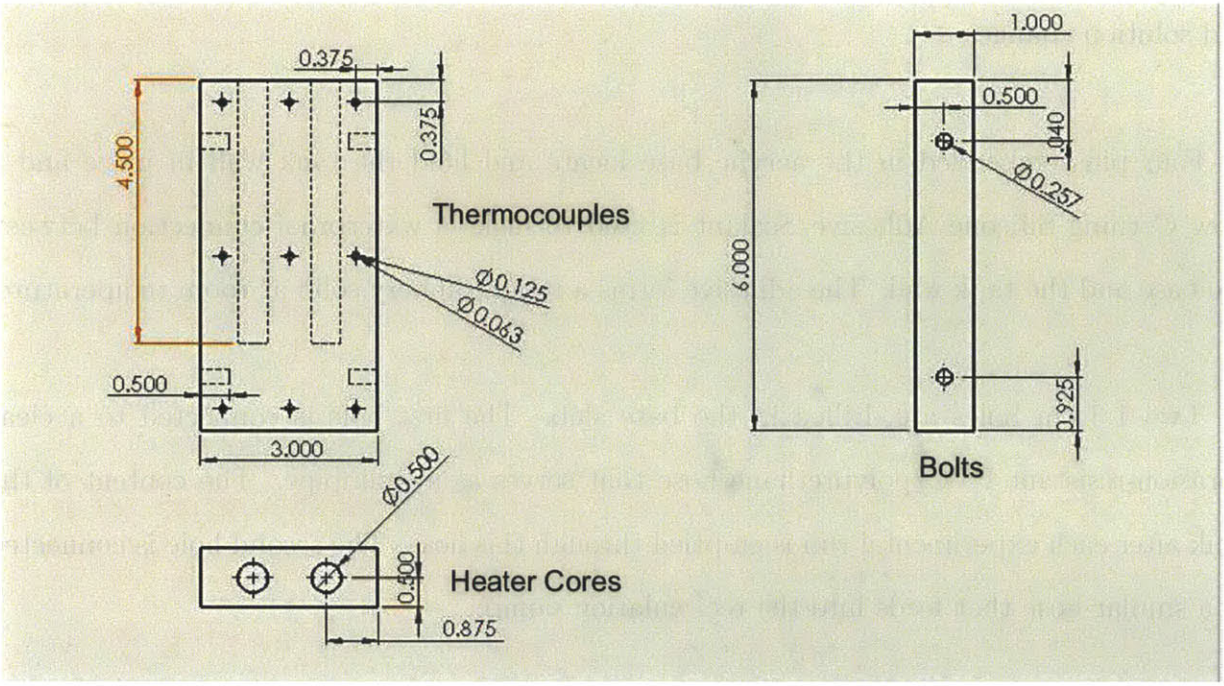

Figure 2.2: Orthographic Views of the Plate

2.1.2 Second Component System

The second component system is the test tank. The base of the tank is made from a square slab of optically clear MIL-Spec Cast Acrylic 0.64 cm thick, 30.5 cm ×61 cm in cross section. The base has excellent tensile strength, convenient thermal operation range and it is easily machineable, as a number of holes have to be drilled through.

Four threaded rods, used for support, are located at the corners of the base, one of which holds the circulation pump and another the wye valve in the recirculation system,

explained later.

The tank's cylindrical tube is made from Scratch-Resistant Clear Cast Acrylic that has an outer diameter of 30.5 cm and an inner diameter of 29 cm. The tank material has an excellent tensile strength, and its transparency allows for accurate visualization of surface and solution changes.

Four pins embedded in the acrylic base locate and hold the tank wall in place and a Dow Corning Silicone Adhesive/Sealant is used to make a waterproof connection between the base and the tank wall. The adhesive forms a tough rubbery solid at room temperature.

Two 1.3 cm holes are drilled in the base slab. The first hole is connected to a clear abrasion-resistant PVC/polyurethane hose that serves as a drainpipe. The content of the tank after each experimental run is emptied through this hose. The second hole is connected to a similar hose that feeds into the recirculation pump.

2.1.3 Third Component System

The third component system is the recirculation pump network. The purpose of installing this pump is to ensure that the solution is not thermally stratified and that enough mixing of the solution is taking place. The unmixed stagnant solution could cause layers of water at different temperatures to form; hence, a pump is necessary. However, because the flow conditions are modeled as natural convection, the flow rate of the circulated water is low enough not to disrupt the free convection behavior. In fact, the flow rate of the pump is roughly calculated to be less than 10% of the flow rate at the top of the plate induced by convection effects.

Because the pump used operates at a flow rate that is relatively higher than the desired one, a bypass system is installed. A wye valve is installed to pass the desired amount of water back to the tank. The pump sucks the water from the top.

The pump is made from plastic, because the apparatus has to have no corrosion potential. A stainless steel pump that was first used caused iron corrosion in the solution especially that deionized water in which the solution is prepared is very aggressive and leaches out impurities easily.

The valve is a wye-shaped three-port chrome-plated brass ball valve, and the bypass network is made up of PVC/polyurethane hoses, durable nylon multi-barbed tube fitting adapters, thick-wall dark gray PVC threaded pipe fittings, durable nylon multi-barbed tube fitting tees, worm-drive hose clamps with zinc plated steel screws and standard-wall white PVC pipe fitting sockets. All parts exhibit high resistance to impact, abrasion, and corrosion. Also, multi-barbed components provide extra gripping power because of enhanced contact.

In addition to these three component systems, a video camera is used to monitor the changes taking place at the level of the plate. The clear acrylic tank allows for good-quality imaging of crystal nucleation and growth on the surface. Also, a chemical dosing window is made in the wall of the tank to facilitate adding chemicals to the solution to maintain a constant initial concentration.

These three component systems make up an apparatus in which a smooth copper plate is heated to a desired temperature, a calcium sulfate solution is prepared to a desired concentration, and a recirculation pump mixes the solution at a desired flow rate.

2.2 Methodology

A systematic procedure is used throughout the experiment to achieve the desired objective, which is a parametric study that outlines the variation of surface scale induction time as a function of surface temperature and solution salt concentration. The procedure can be divided into four main steps.

2.2.1 Copper Plate Heating

The copper plate's smooth surface serves as a heat transfer medium that attracts retrograde solubility salts leading to their crystallization on surface. In order for dihydrated calcium sulfate to nucleate on the plate, the plate has to be heated enough to exceed the saturation temperature at the prepared concentration. Heating of the plate is achieved using the benchtop temperature controller.

In order to complete the plate heating step, two possible routes are evaluated. One is to heat the plate while it is already immersed in solution. Another is to heat the plate separately to be slowly immersed in solution when the needed temperature is attained.

Several points are taken into consideration while selecting the better route. These points are summarized below:

- The aim of the experiment is to achieve surface crystallization of dihydrated calcium sulfate. Hence, it is vitally important to make sure that bulk precipitation does not take place before particles nucleate on surface. While several authors have experimentally showed that the salt particles migrate to the hottest surface in the system, it is important to keep the surface temperature higher than the pool temperature. This is mathematically explained using the Kern and Seaton approach [46] that models surface

fouling as

$$\frac{dm}{dt} = \dot{m}_d - \dot{m}_r \tag{2.1}$$

where the rate of deposition for diffusion controlled scaling is

$$\dot{m}_d = \beta(c_b - c_w*) \tag{2.2}$$

and for reaction controlled scaling is

$$\dot{m}_d = k_r(c_b - c_w*)^n \tag{2.3}$$

For $CaSO_4$ crystallization, n was found to be 2. The rate of reaction follows an Arrhenius term in temperature dependence

$$k_r = C \exp(-\frac{E}{RT}) \tag{2.4}$$

Symbols	Variable Name	Units
$\dot{m}_d$	rate of deposition	kg/m^{2}sec
$\dot{m}_r$	rate of removal	kg/m^{2}sec
β	mass transfer coefficient	m/sec
c_b	bulk concentration	ppm
c_w*	concentration at surface	ppm
n	order of reaction	
C	Arrhenius constant	m^4/kg sec
E	activation energy	J/mol
R	ideal gas constant	J/mol.K
T	solution temperature	K

The removal rate depends on deposit strength and fluid shear forces. The rate of deposition serves as a driving force; hence, in case the driving force is positive, the wall temperature has to be higher than the bulk temperature and gypsum would crystallize on the heat transfer surface.

- It is advisable to keep a relatively constant temperature difference between the plate and the pool. Several experimental runs showed that with the absence of any cooling system, the thermal difference was maintained by virtue of the properties of solution as well as the heating provided through the cartridge heaters by the temperature controller.

- A supersaturated solution has to be prepared in a way that the salt is perfectly mixed in the beginning because any particle within the system can serve as a seed for crystallization, which would give an inaccurate depiction of the times of induction.

Keeping these points in mind, heating the plate and preparing the solution separately is selected as a better option for completing this step. Heating the plate while it is in solution creates an obstacle against the perfect mixing of the solution due to space restrictions. Also, several runs showed instances of bulk precipitation because the solution is being heated by convection from the copper surface at the same time the plate is being heated by the heating elements. In these cases, the solution attained a temperature higher than the saturation temperature corresponding to the prepared concentration at equilibrium conditions.

Dihydrated calcium sulfate, or gypsum, starts to exhibit an inverse solubility behavior at a temperature of 38°C after which its solubility decreases with increasing temperature [41]. Hence, the solution is separately prepared at room temperature. This is particularly important in cases of testing at a surface temperature that is around 38°C.

2.2.2 Solution Preparation

Calcium sulfate is used as a hardness salt because it exhibits an inverse solubility behavior in water. It crystallizes from an aqueous solution in three forms: dihydrated or gypsum,

hemihydrate or plaster of Paris, and anhydrous. Gypsum crystallization is selected to test. Since calcium sulfate crystals do not easily dissolve in water, gypsum salt has to be prepared by the reaction of two separate solutions.

While there are several ways to prepare a dihydrated calcium sulfate $CaSO_4 \cdot 2\,H_2O$, it was shown that the simplest and fastest way is to mix a water soluble calcium compound and a water soluble sulfate compound together in the absence or in the essential absence of free water. At least one of the calcium and sulfate compounds is in the hydrated form.

Abiding by this recipe, the dihydrated calcium sulfate solution is prepared by mixing together stoichiometric proportions of tetrahydrate calcium nitrate and sodium sulfate. The solution is prepared in deionized water. This method is preferred to preparation from gypsum crystals because of the higher solubility of calcium nitrate and sodium sulfate in water. The products of the reaction are gypsum, sodium nitrate in the form of dissolved ions and water.

The reaction that takes place is:

$$Ca(NO_3)_2 \cdot 4\,H_2O + Na_2SO_4 \longrightarrow CaSO_4 \cdot 2\,H_2O + 2\,NaNO_3 + 2\,H_2O$$

The salts used in the reaction were purchased from Sigma Aldrich, and they have with the properties given in Tables 2.3 and 2.4.

Table 2.3: Tetrahydrated Calcium Nitrate

Other Names	Lime Nitrate or Nitrocalcite
Linear Formula	$Ca(NO_3)_2 \cdot 4\,H_2O$
Purity	$\geq 99.0\%$
Molecular Weight	M_1=236.15 g/mol
CAS Wumber	13477-34-3
Soluble in water	200 mg/mL
Yield	Clear Colorless Solution
Storage	Room Temperature

Table 2.4: Sodium Sulfate

Linear Formula	Na_2SO_4
Purity	$\geq 99.0\%$
orm	Anhydrous, Granular
Molecular Weight	M_2=142.00 g/mol
CAS Wumber	7757-82-6
Soluble in water	100 mg/mL
Yield	Clear Colorless Solution
Storage	Room Temperature

A supersaturation index SI is defined as

$$SI = \frac{C}{C_s} \tag{2.5}$$

$$SI \begin{cases} < 1 & \text{undersaturated} \\ = 1 & \text{saturated} \\ > 1 & \text{supersaturated} \end{cases}$$

C is concentration of the prepared solution and C_s is the concentration corresponding to the surface temperature at saturation conditions. If the solution is supersaturated, salt precipitation is expected to happen after a certain time determined by different influencing

operation and design parameters.

Hence, the variation in concentration is represented by a variation in the supersaturation index. Also, the amounts of the reacting salts needed are calculated based on the desired supersaturation index based on equimolar quantities. A sample case is presented.

Case when surface temperature T_s=80°C and supersaturation index SI=2.0

Values needed for the calculation are the molecular weights of each salt, calcium sulfate saturation curve values and the volume of solution to be prepared. Both reactants are mixed at room temperature. In this case, referring to the equilibrium curves of gypsum: C_s(T=80°C)=1800 parts $CaSO_4$ per million parts of solution. This corresponds to 1800 mg/L of solution.

$$C = C_s \times SI = 1800 \times 2 = 3600 \text{ g/L}$$

$$M_{CaSO_4}=136.14 \text{ g/mol}$$

Therefore, the molar concentration is

$$n_{CaSO_4} = \frac{C}{M_{CaSO_4}} = \frac{3600 \text{ mg/L}}{136.14 \text{ g/mol}} = 26.44 \text{ mmol/L}$$

By stoichiometry in the reaction

$$CaSO_4 \cdot 2H_2O \longrightarrow CaSO_4 + 2H_2O$$

$$n_{CaSO_4 \cdot 2H_2O} = n_{CaSO_4} = 26.44 \text{ mmol/L}$$

Equimolar quantities of the reacting salts are needed; hence

$$n_{Ca(NO_3)_2 \cdot 4H_2O} = n_{Na_2SO_4} = n_{CaSO_4 \cdot 2H_2O} = 26.44 \text{ mmol/L}$$

All the experiments are run with a solution volume V=10 L. Therefore, the amounts of salts needed are calculated as

$$m_{Ca(NO_3)_2 \cdot 4H_2O} = n \times M_1 \times V = \frac{26.44 \text{ mmol}}{\text{L}} \times \frac{236.15 \text{ g}}{\text{mol}} \times \frac{1 \text{ mol}}{1000 \text{ mmol}} \times 10 \text{ L}$$

$$m_{Ca(NO_3)_2 \cdot 4H_2O} = 64.22 \text{ g}$$

Also,

$$m_{Na_2SO_4} = n \times M_2 \times V = \frac{26.44 \text{ mmol}}{\text{L}} \times \frac{142.00 \text{ g}}{\text{mol}} \times \frac{1 \text{ mol}}{1000 \text{ mmol}} \times 10 \text{ L}$$

$$m_{Na_2SO_4} = 38.61 \text{ g}$$

After the required amounts of each of the salts are added to deionized water at room temperature, the solution has to be mixed well enough to ensure that no suspended particles exist. This is achieved with the help of an electric hand mixer. When this supersaturated aqueous solution is prepared, the plate that is separately heated to a desired temperature is slowly lowered into the tank.

Because of the temperature difference between the plate surface and the solution bulk, the plate temperature drops at the moment it is immersed in solution. However, the plate heaters are still kept connected to the temperature controller that will return the temperature back to the previously set value. At that moment, the recirculation pump starts its calm mixing function, time starts counting, and the video camera starts recording.

2.2.3 Instrumentation

In order to have a well-controlled system, several kinds of sensors are installed within the apparatus. A block diagram of the apparatus is shown here.

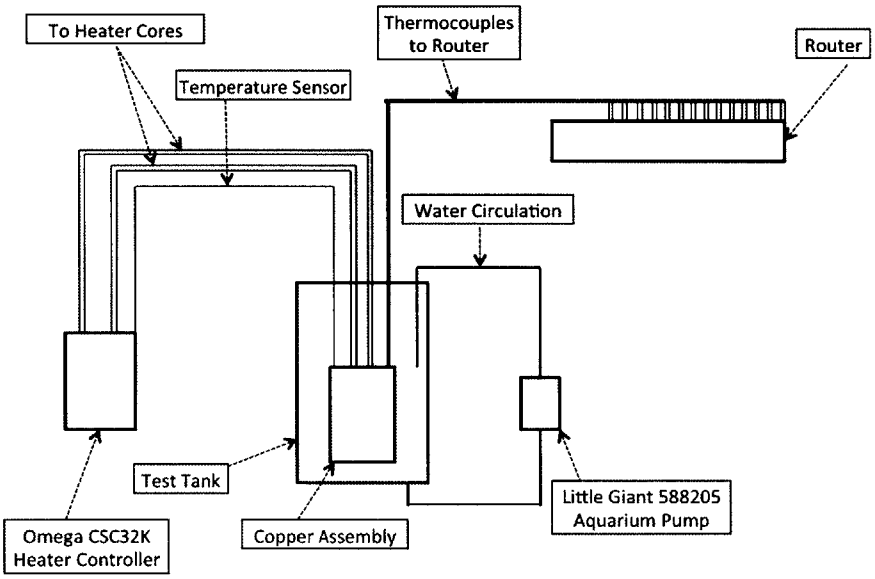

Figure 2.3: Block Diagram of the Experimental Apparatus

2.2.3.1 Temperature

One of the main concerns of the procedure is to maintain a spatially uniform, isothermal copper plate. And since heating to the desired temperature is achieved through a feedback thermocouple embedded in the center of the plate, it is necessary to make sure the temperature at the block center is a good indication of the entire plate. For that purpose, other eight K-type thermocouples are embedded in the plate with their ends attached to different depths on different axes. The exact locations are shown.

Figure 2.4: Locations of Monitoring Thermocouples

In addition, the temperature of the solution bulk is monitored through other K-type thermocouples planted at different locations to ensure that the recirculation of the aqueous solution is bringing about a thermally uniform medium with no stratified layers.

All the thermocouples are connected through a data acquisition system to an Agilent®34970A data logger which records values in real time. Measurements from all experiments revealed that both the copper plate and the solution are thermally uniform. Copper is highly conductive that the temperature at the block center is indicative of the entire plate.

2.2.3.2 Salinity/Conductivity

After gypsum salt crystallizes on the plate, calcium and sulfate ions are depleted from solution that the salinity and the electrical conductivity of solution decrease. One sample drop of the solution is extracted using a needle at different times to monitor the change in salinity of the solution. The salinity meter used is Atago ES-421 digital salt meter that measures the salt % in solution with automatic temperature compensation.

2.2.3.3 pH

Several authors reported a significant influence of the pH of solution on the kinetics and thermodynamics of crystallization. Although this influence is more pronounced with salts that interact with carbon dioxide like calcium carbonate (veterite, aragonite, calcite), a pH meter is used to monitor any change in solution acidity. The meter used is a McMaster-Carr®waterproof device that is equipped with an automatic temperature compensation system that adjusts readings to correct for any temperature variations.

2.2.3.4 Video

As mentioned before, a video camera is installed on record throughout the entire experimental procedure. It is focused on the smooth surface of the plate to monitor how the surface view changes. The experiment is kept running for some time (a couple hours) after the scale layer becomes visible on the plate. The video is used to detect the time at which salt molecules are first seen crystallizing. It is undoubtedly a difficult task to inspect the time the first molecule nucleated because the changes happen at a micro level. However, the video camera's resolution is high enough to visualize the first thin layer of salt that forms. Ideally, a critical particle radius should be used to decide what may be called a scale layer and what may not. However, since such sophisticated sizing technology was not available, scaling is decided upon based on a surface coverage basis. Videos showed that crystal growth happens after a uniform thin layer of salt first forms.

The camera used is Creative Live Connect HD 1080 Webcam which records videos at full HD 1080p resolution. The resolution rate is 1920×1080 pixels and the frame rate is up to 30 frames per second. Images at different stages and conditions of experimentation can be found in Appendix A.

2.2.3.5 Mass

Because scaling is more than a single phenomenon, crystal growth should be studied in addition to nucleation. One indicative of the kinetics of crystal growth is the rate at which the mass of the salts varies. Typically, a unit of grams per unit area per unit time is used to represent such a parameter. Hence, the salt collected on the surface is scraped off the plate a couple of hours after it forms. It is collected only after the layer dries off. A ScoutPro®digital scale is used to measure the mass of the collected sample that is saved in a Petri dish to be prepared for SEM imaging.

2.2.3.6 Imaging

Since crystallization fouling involves a number of complex phenomena, it is important to examine how the change in parameters like salt concentration and surface temperature impacts crystallographic orientation and structure. Therefore, the Scanning Electron Microscopy technology (SEM) is used as a tool to visualize the surface of the salt samples with various resolutions. The technology allows drawing out a number of observations.

2.2.4 Inter-experimental cleaning and preparation

Thorough cleaning of the system is significantly important because crystallization is largely induced by impurities, rough pits or other crystals. Hence, each and every component of the system has to be cleaned very carefully. The steps taken between two consecutive runs are summarized below:

1. Copper plate assembly is taken out of the solution and allowed to cool at room temperature.

2. A petri dish is weighed and a note of the weight is taken.

3. Using a clean Scoopula®lab scoop, the scale layer is scraped off the test surface.

4. The petri dish is set aside uncovered to allow collected sample to air dry. Once the collected sample has dried, it is weighed and the mass of the formed salt is calculated by subtracting the petri dish's mass noted in step 2 from the total mass.

5. The copper plate assembly is dismantled: the bottom bolts holding the vertical supports to the base along with the side bolts connecting the copper plate to the vertical supports are all unscrewed.

6. Using a wire brush, any scale that was formed on the bolts, vertical supports or circular base is removed. A pick is used to clear out the Phillips heads of the bolts.

7. The components are rinsed under deionized water and pat dried with clean paper towels.

8. The copper plate is patted dry and taken to a Scothbrite buffering wheel. The test surface sides, bottom and back are all buffed. The top surface of the plate is never submerged in the solution during the experimental procedure; hence, buffing is not necessary especially that the cartridge heater leads stick out the top surface. It is important to make sure all thermocouples are still anchored to the back surface via epoxy. This polishing step is important for two reasons. First. The plate's surfaces have to be smooth to eliminate the effect of surface roughness on seeding crystallization. Second, it would be easier to visualize a polished clean surface on the recorded videos to investigate the time of scale induction.

9. The copper plate system is reassembled. The vertical supports are attached to the plate from the sides and the base is in turn attached to the supports.

10. The copper plate assembly is plugged to the temperature benchtop controller that is turned on and the desired temperature is selected. During heating, it is important not to touch the plate to avoid burns. Wearing protective gloves is one precaution to take.

11. The aqueous solution bath is prepared to the desired supersaturation index using necessary amounts of the reacting salts.

12. Once the copper plate reaches the set temperature, the assembly us picked up (wearing thermally insulated gloves) and gently lowered to the solution pool.

Chapter 3

Heat Transfer Model of the System

In order to fully understand the kinetic behavior of gypsum salt crystallization on the heated copper plate, a heat transfer model of the system needs to be developed. Essentially, the kinetics of the crystallization fouling problem should never be isolated from the thermodynamics of the problem. In other words, the rate at which scale forms on a heat surface area is highly dependent on thermal variations and heat transfer parameters like heat transfer coefficients, the plate's thermal conductivity, the heat transfer rate within and out of the apparatus and the thermal profile of the flow in the vicinity of the plate as well as in the volume of the bulk.

Within the system's thermal network, there exist a number of heat transfers taking place. This chapter discusses the importance of each in order to better understand the conditions behind crystallization of gypsum.

3.1 Natural Convection on the Copper Surface

The main flow conditions are modeled as natural convection on an isothermal vertical wall. In natural or free convection, the aqueous solution's motion is not induced by an external source. It is rather caused by density differences or a density gradient within the flow fluid itself. Unlike analyses of forced convection, fluid properties in ntural convection are not constant. Moreover, another condition that is necessary for natural convection to occur is the presence of a body force that is proportional to the density. This body force along with the density gradient bring about a buoyancy force that is considered to be the main driving force of natural convection. The density gradient could be caused by a temperature or a concentration gradient. In this case, both fluid mechanics and heat transfer problems have to be simultaneously solved.

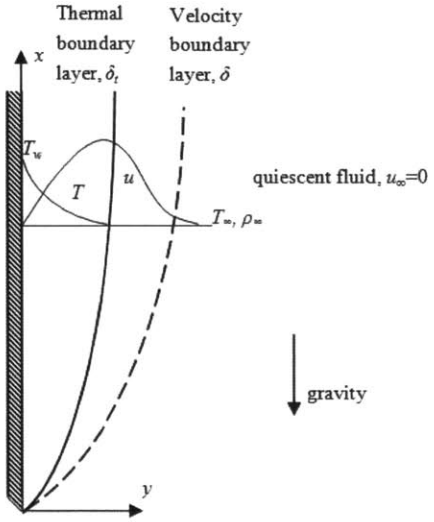

Figure 3.1: Laminar Natural Convection Velocity and Thermal Profiles

In the proximity of the heated copper surface, the surrounding fluid receives some of the heat, becomes less dense and rises. The cooler fluid then replaces it; however, it is then heated and becomes less dense. The process continues and a convection current forms. Overall, heat is transferred from the bottom of the cell to the top. Velocity, temperature and concentration

boundary layers are created. The thickness of the velocity layer is dependent on Prandtl number, and the thermal convection is predicted by Rayleigh number. Natural convection is the mode of heat transfer in various groups of applications especially in energy systems, electronics cooling, and materials processing. A schematic of the laminar natural convection boundary layer on a vertical wall showing expected velocity and temperature profiles is shown in Fig. 3.1 [47].

The equations governing velocity and temperature profiles can be solved using the integral method of analysis, which gives a particularly good approximation. The analysis is reported by Mills Heat Transfer book [48]

3.1.1 Momentum Conservation

The buoyancy force has to be considered in deriving the integral form of the momentum conservation equation. The Archimedes' expression of the buoyancy force per unit volume acting on an element of warmer fluid in the boundary layer is

$$f_b = g(\rho_e - \rho) \tag{3.1}$$

where g is the gravitational acceleration, ρ is the density of the fluid element that varies across the boundary layer, and ρ_e is the fluid density outside the boundary layer. ρ_e is spatially constant.The buoyancy force is a vertical upward force that is proportional to density change and opposes gravitational acceleration.

To derive the integral form of the momentum conservation equation, let's start with an elemental control volume shown in Fig. 3.2 reproduced from [48] The elemental control volume has a unit depth and it is extending to y=Y, where Y is greater than the boundary layer thickness. Applying Newton's second law of motion, the momentum outflow is equal

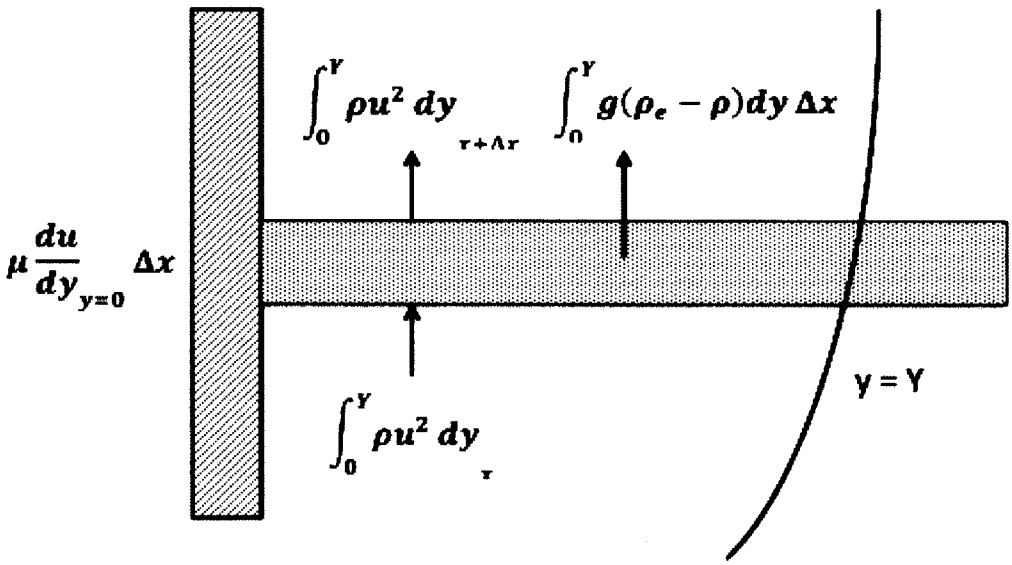

Figure 3.2: Elemental Control Volume

to the buoyancy force minus the viscous drag force exerted by the wall:

$$\int_0^Y \rho u^2 dy_{x+\Delta x} - \int_0^Y \rho u^2 dy_x = \int_0^Y g(\rho_e - \rho)dy\Delta x - \mu \frac{\partial y}{\partial x}_{y=0} \Delta x \tag{3.2}$$

Dividing by Δx and taking the limits at 0

$$\frac{d}{dx}\int_0^Y \rho u^2 dy = \int_0^Y g(\rho_e - \rho)dy - \mu \frac{\partial y}{\partial x}_{y=0} \tag{3.3}$$

Boussinesq Approximation can be used here. In essence, it states that the inertia difference is small; however the gravity forces are strong enough to make the specific weight appreciably different between the two fluids within and outside the boundary layer. Hence, density is constant except in the buoyancy term; dividing by ρ gives:

$$\frac{d}{dx}\int_0^Y u^2 dy = \int_0^Y g(\frac{\rho_e - \rho}{\rho})dy - \nu \frac{\partial y}{\partial x}_{y=0} \tag{3.4}$$

The variation in density within the system is a function of temperature and pressure; hence after expanding the term $\rho_e - \rho$ using **Taylor's** series expansion, considering that the pressure variation in our system is negligible, introducing β, the volumetric coefficient of thermal expansion, and letting Y tend to ∞, the integral form of the momentum equation becomes:

$$\frac{d}{dx}\int_0^\infty u^2 dy = \int_0^\infty g\beta(T - T_e)dy - \nu\frac{\partial y}{\partial x}_{y=0} \tag{3.5}$$

3.1.2 Energy Conservation

Similar to the case of forced convectional flow, natural convection has the following energy conservation equation

$$\frac{d}{dx}\int_0^\infty u(T - T_e)dy = -\alpha\frac{\partial T}{\partial y}_{y=0} \tag{3.6}$$

3.1.3 Boundary Conditions

Equations (5) and (6) are coupled; hence a simultaneous solution has to be worked through. The following boundary conditions apply

y	u	T
0	0	T_s
$\rightarrow \infty$	0	T_e

Table 3.1: Velocity and Thermal Boundary Conditions

3.1.4 Integral Method Solution

3.1.4.1 Integral Method Analysis

An integral solution involves assumption of the forms of solution for velocity and thermal profiles within the boundary layer. Solution forms suggested in **Mills** [48] are given using a scale velocity U that is a function of x under the assumption that the thicknesses of the

thermal and velocity boundary layers are identical and equal to δ

$$\frac{u}{U} = \frac{y}{\delta}(1 - \frac{y}{\delta})^2 \tag{3.7}$$

$$\frac{T - T_e}{T_s - T_e} = (1 - \frac{y}{\delta})^2 \tag{3.8}$$

Substituting equations (7) and(8) in equations (5) and (6), the equations to be solved are

$$\frac{d}{dx}(\frac{U^2\delta}{105}) = -\frac{\nu U}{\delta} + \frac{g\beta(T_s - T_e)\delta}{3} \tag{3.9}$$

$$\frac{d}{dx}(\frac{U\delta}{30}) = \frac{2\alpha}{\delta} \tag{3.10}$$

Variations of the boundary layer thickness δ and the scaling velocity U are given as per a power law assumption such that

$$\delta = Dx^m \tag{3.11}$$

$$U = Xx^n \tag{3.12}$$

Equation (9) reduces to

$$\frac{d}{dx}(\frac{X^2 D x^{2n+m}}{105}) = -\frac{\nu X x^{n-m}}{D} + \frac{g\beta(T_s - T_e)Dx^m}{3} \tag{3.13}$$

In order to cancel dependence on x, $2n + m - 1 = n - m = m$. Hence n=$\frac{1}{2}$. Therefore, the two conservation equations are

$$\frac{5}{4}\frac{X^2 D}{105} = -\frac{\nu X}{D} + \frac{g\beta(T_s - T_e)D}{3} \tag{3.14}$$

$$\frac{3}{4}\frac{XD}{30} = \frac{2\alpha}{D} \tag{3.15}$$

Hence

$$X = \frac{80\alpha}{D^2} \tag{3.16}$$

and

$$D = 3.94[\frac{(20/21)\alpha^2 + \nu\alpha}{g\beta(T_s - T_e)}]^{0.25} \tag{3.17}$$

The heat flux from the wall is given by

$$q_s = -k\frac{\partial T}{\partial y}_{y=0} = \frac{2k}{\delta}(T_s - T_e) \tag{3.18}$$

The ratio of convective to conductive heat transfer normal to the boundary is given by the following equation of the local **Nusselt** number

$$\mathrm{Nu_x} = \frac{\mathrm{h_{cx}x}}{\mathrm{k}} = \frac{2\mathrm{x}^{3/4}}{\mathrm{D}} = 0.508[\frac{\mathrm{Pr}}{0.952 + \mathrm{Pr}}]^{0.25}\mathrm{Ra_x}^{0.25} \tag{3.19}$$

where $Ra_x = \beta g(T_s - T_e)\frac{x^3}{\nu\alpha}$ is the **Rayleigh** number that defines the transition between a laminar and a turbulent flow regime.

3.1.4.2 Application on the $CaSO_4$ solution

Table 3.2 summarizes the variables used throughout the integral method solution derivation and the unit of each variable whose value will be used to model the heat transfer within the body of the aqueous solution of calcium sulfate prepared for the scaling test. In what follows, calcium sulfate solution is treated like a water solution. The reason lies in the fact that the concentration of the salt molecules during the experiments is low relative to the concentration of water molecules. Also, the change of the values of various properties with parameters like temperature and pressure can be ignored because the change is very small and would not affect the order of significance throughout the heat transfer model.

Symbol	Variable	Unit
ρ	Density	kg/m^3
c_p	Heat Capacity	J/kg.K
μ	Dynamic Viscosity	kg/m.sec
ν	Kinematic Viscosity	kg/m.sec
α	Thermal Diffusivity	m^2/sec
k	Thermal Conductivity	W/m.K
β	Thermal Expansion Coefficient	1/K
g	Gravitational Acceleration	m/sec^2
T_s	Plate Surface Temperature	K
T_e	Bulk Temperature	K
x	Surface Coordinate	m
y	Distance from Surface	m
u	Velocity	m/sec
Δ	Hydrodynamic BL Thickness	m
δ	Thermal BL Thickness	m
U	Scaling Velocity	m/sec
m	Constant	-
n	Constant	-
h	Heat Transfer Coefficient	$W/m^2.K$
q_s	Heat Flux	W/m^2

Table 3.2: Integral Solution Variables

The significance of the used dimensionless numbers is tabulated below.

Table 3.3: Dimensionless Parameters for Integral Solution

Symbol	Name	Significance	Formula
Pr	Prandtl	Viscous to Thermal Diffusion Rate	ν/α
Re	Reynolds	Inertial to Viscous Forces	uL/ν
Gr	Grashof	Buoyancy to Viscous Forces	$g\beta(T_s - T_e)L^3/\nu^2$
Ra	Rayleigh	Presence of Convection	$Pr \times Gr$
Nu	Nusselt	Convective to Conductive Heat Transfer	hL/k

Since the parameters required to evaluate the thermal and velocity profiles based on the integral solution for the problem of natural convection on an isothermal vertical wall, exhibit a very small change with temperature and pressure, a sample case with T_s=80°C and T_e = 70°C is analyzed here.

3.1.5 Integral solution for $T_s = 80°C$ and $T_e = 70°C$

Using MATLAB, different plots are generated to fully model the system.

First, copper plate dimensions (length, width, and thickness) are defined.

$$l = 6" = 0.1524 \text{ m}$$

$$w = 3" = 0.0762 \text{ m}$$

$$t = 1" = 0.0254 \text{ m}$$

Second, solution properties are evaluated at the film temperature T_f where

$$T_f = \frac{T_s+T_e}{2} = \frac{80+70}{2} = 75°C$$

At 75°C:

$$k = 0.669 \text{ W/m.K}$$

$$\rho = 973 \text{ kg/m}^3$$

$$c_p = 4196 \text{ J/kg.K}$$

$$\nu = 0.39 \times 10^{-6} \text{ m}^2/\text{sec}$$

$$\text{Pr}=2.4$$

$$\alpha = \frac{\nu}{Pr} = \frac{0.39\times10^{-6}}{2.4} = 0.1625 \times 10^{-6} \text{ m}^2/\text{sec}$$

$$\beta = 6.24 \times 10^{-4}$$

Third, other parameters are defined

$$g = 9.81 \text{ m/sec}^2$$

The flow regime is tested by the local Rayleigh number Ra_x where x is the coordinate along the 15.24 cm length of the plate

$$\text{Ra}_x = \frac{\beta(T_s-T_e)gx^3}{\nu\alpha} = \frac{(6.24\times10^{-4})(353.15-343.15)(9.81)}{(0.39\times10-6)(1.625\times10^{-7})}x^3 = 9.659 \times 10^{11}x^3$$

A Rayleigh number of 10^9 stands at the transition region between a laminar and a turbulent flow regime within the body of the fluid. This Ra value corresponds to an $x = 10.11$ cm. During the experimental runs, the plate is not entirely immersed in the solution to keep the leads of the cartridge heaters away from the aqueous solution and to keep the immersed

section within the laminar flow regime.

The boundary layer thickness is $\delta = Dx^{1/4}$ where D is given by

$$D = 3.94[\frac{(20/21)\alpha^2+\nu\alpha}{g\beta(T_s-T_e)}]^{0.25} = 0.0043 \text{ m}^{3/4}$$

Hence,

$$\delta = 4.3 \times 10^{-3}x^3$$

The scaling velocity is $U = Xx^{1/2}$ where X is given by

$$X = \frac{80\alpha}{D^2} = \frac{80\times1.625\times10^{-7}}{0.0043^2} = 0.6964 \text{ m}^{1/2}/\text{sec}$$

Hence,

$$U = 0.6964x^{1/2}$$

The local Nusselt number, local heat transfer coefficient, velocity profile and thermal profile are defined by

$$\text{Nu}_x = 0.508[\frac{\text{Pr}}{0.952+\text{Pr}}]^{0.25}\text{Ra}_x{}^{0.25} = 463.259x^{3/4}$$

$$h_{cx} = \frac{k\times\text{Nu}_x}{x} = 309.920x^{-1/4}$$

$$\frac{u}{U} = \frac{y}{\delta}(1-\frac{y}{\delta})^2$$

$$\frac{T-T_e}{T_s-T_e} = (1-\frac{y}{\delta})^2$$

where y is the vector of distance from the wall along the elemental control volume.

Plots of the (1) change in boundary layer thickness, (2) local Rayleigh number, (3) local Nusselt number, (4) local heat transfer coefficient, (5) velocity profile and (6) thermal profile within the boundary layer, are shown in the figures 3.3 to 3.8.

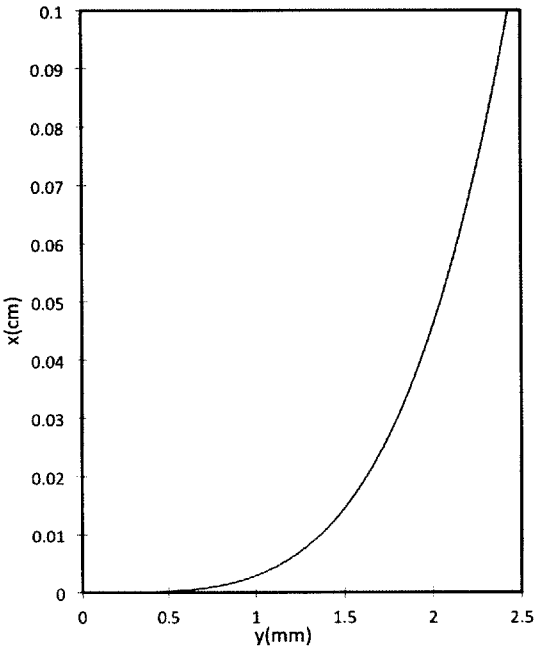

Figure 3.3: Boundary Layer Thickness

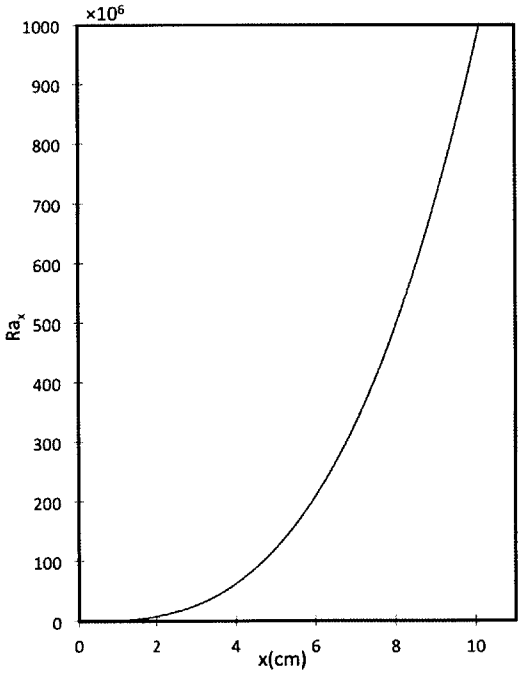

Figure 3.4: Local Rayleigh Number

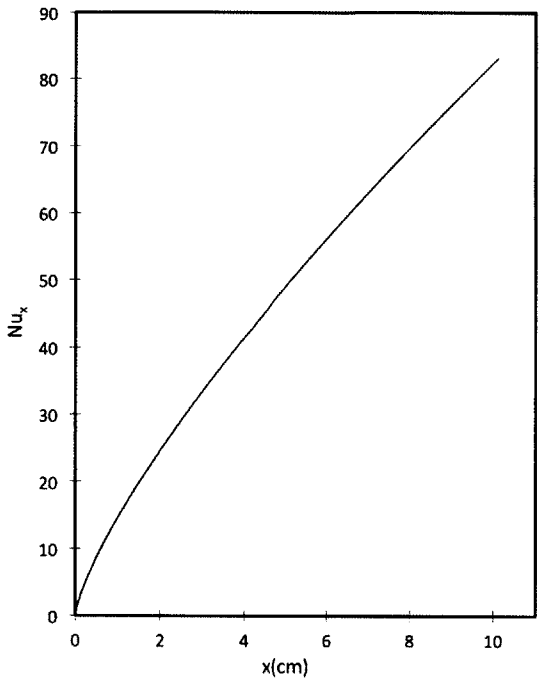

Figure 3.5: Local Nusselt Number

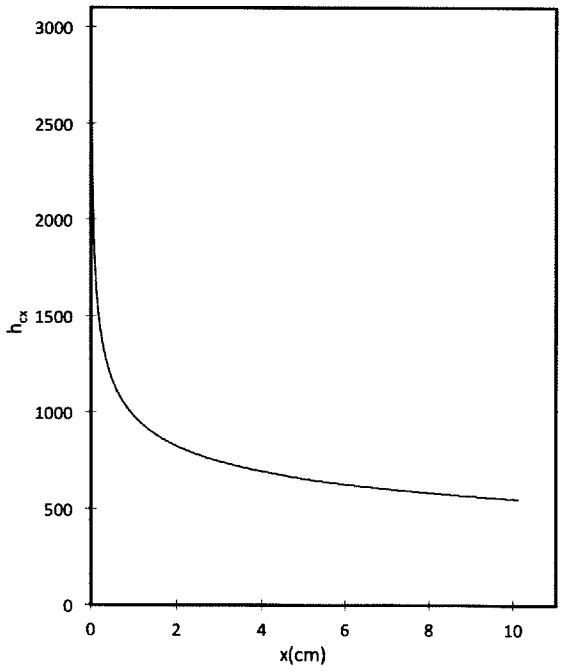

Figure 3.6: Local Heat Transfer Coefficient

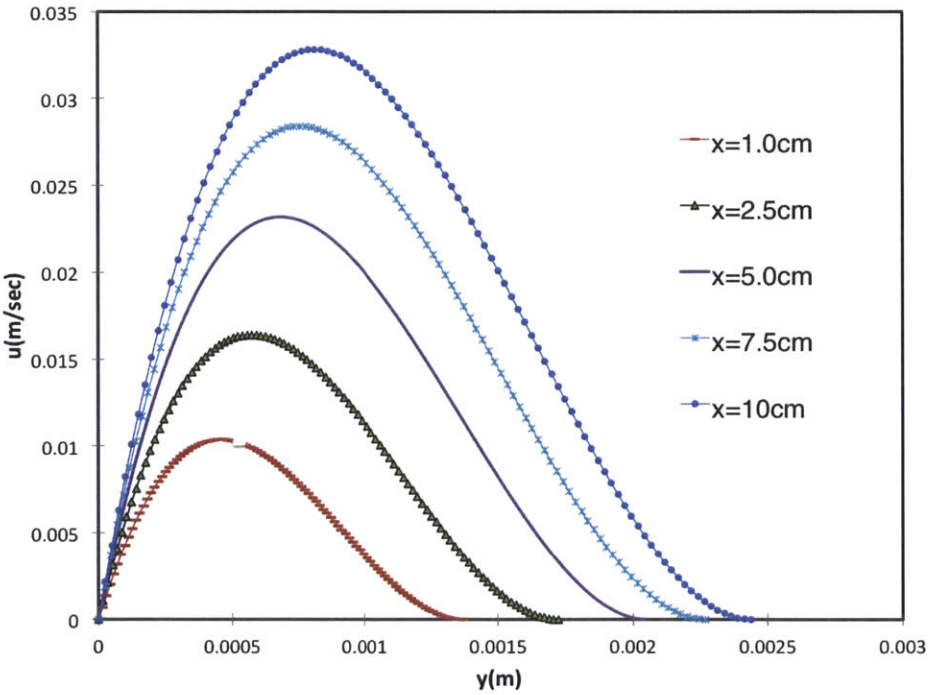

Figure 3.7: Velocity Profile within the Boundary Layer at Different Positions

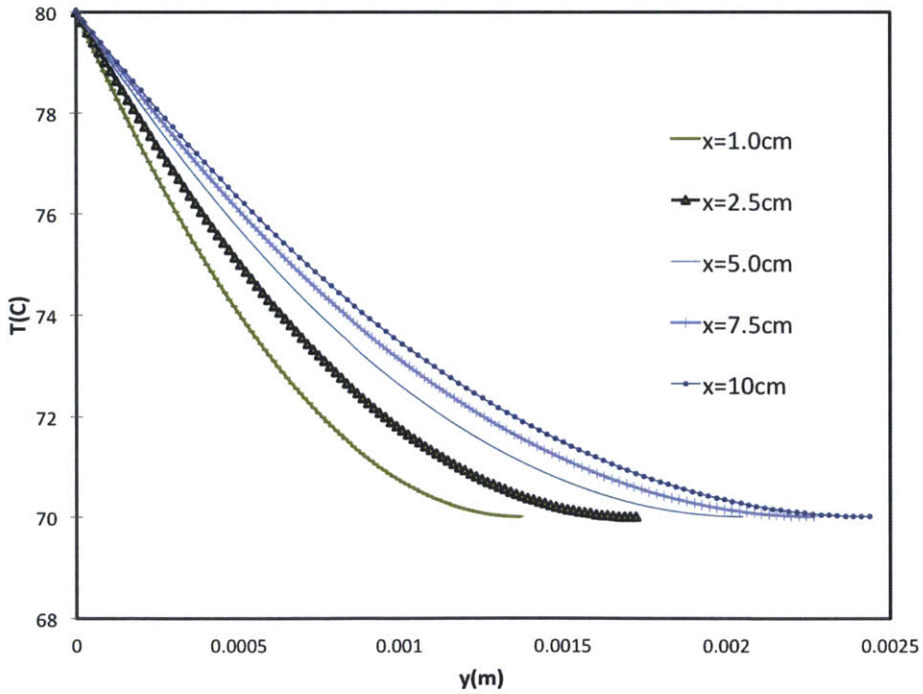

Figure 3.8: Temperature Profile within the Boundary Layer at Different Positions

3.2 Heat Transfer Average Resistance Comparison

3.2.1 Conduction within the Copper Block

The conduction resistance is

$$R_{cond} \times A_{cond} \approx l_c/k$$

where l_c is a characteristic length, A is the heat transfer area, and k is the thermal conductivity of copper. For an $l_c = t = 2.54$ cm where t is the plate thickness and $k = 392$ W/m.K,

$$R_{cond} \times A_{cond} \approx 6.5 \times 10^{-5} \text{ m}^2\text{K/W}$$

The heat transfer area is the area of the conduction wall. Hence,

$$A_{cond} = l \times w = 0.00774\text{m}^2$$

and

$$R_{cond} \approx 8.40 \times 10^{-3} \text{ K/W}$$

3.2.2 Natural Convection on the Isothermal Plate

The natural convection resistance can be represented by an average resistance midway along the plate at $x = 5$ cm calculated as

$$R_{ncplate} \times A_{ncplate} \approx 1/h_{avg} \approx l/k\text{Nu}_{\text{avg}}$$

where h_{avg} and Nu_{avg} are respectively the average heat transfer coefficients and average Nusselt number, and k is the thermal conductivity of the solution. Hence

$$R_{ncplate} \times A_{ncplate} \approx \frac{0.1}{0.669 \times 463.259 \times (0.05)^{3/4}} \approx 3.06 \times 10^{-3} \text{ m}^2\text{K/W}$$

The natural convection area is made up of the immersed surfaces areas of the block. The lateral faces have negligible significance. So the area is calculated as

$$A_{ncplate} = 2 \times l \times w = 0.0155 \text{ m}^2$$

and

$$R_{ncplate} \approx 0.395 \text{ K/W}$$

3.2.3 Natural Convection at the Tank Wall

At the tank wall, the existing modes of heat transfer are free convection with the aqueous solution at bulk temperature from inside, and free convection with air at room temperature from outside. Water is more thermally conductive than air. Hence, the resistance associated with tank to air convection is expected to be the limiting resistance. The tank wall can be modeled as an isothermal vertical plate with a characteristic length that is the height of the aqueous solution, i.e. 20 cm

3.2.3.1 Inside the Tank

$$\mathrm{Nu_x} = 0.508[\tfrac{\mathrm{Pr}}{0.952+\mathrm{Pr}}]^{0.25}\mathrm{Ra_x}^{0.25}$$

where Pr = 2.4 An average Nusselt number corresponding to an average Rayleigh number at $x = 10$ cm is calculated based on an assumed 10°C temperature difference between tank wall (60°C) and bulk(70°C) Hence

$$\mathrm{Ra_{10cm}} = 9.659 \times 10^{11}(0.1)^3 = 9.659 \times 10^8$$

$$\mathrm{Nu_{avg}} = 0.508[\tfrac{2.4}{0.952+2.4}]^{0.25}(9.659 \times 10^8)^{0.25} = 82.38$$

Therefore, the average natural convection resistance is

$$R_{inside} \times A_{wall} \approx \tfrac{0.2}{0.6\times 82.38} \approx 4.04 \times 10^{-3}\ \mathrm{m^2K/W}$$

The tank wall area is

$$A_{wall} = 2 \times \pi \times r \times h = 0.1596\ \mathrm{m^2}$$

Hence,

$$R_{inside} \approx 0.0253\ \mathrm{K/W}$$

3.2.3.2 Outside the Tank

The same analysis applies to the free convection from the tank to the air. However, the properties are evaluated for air at a temperature of 25°C and a film temperature of $\frac{25+60}{2} = 42.5$°C

$$Ra_{avg} = \frac{\beta(T_s - T_e)gx^3}{\nu\alpha} \approx \frac{(3.36\times10^{-3})(60-25)(9.81)(0.1)^3}{(1.568\times10^{-5})(1.9\times10^{-5})} = 3.872 \times 10^6$$

$$\mathrm{Pr} = \frac{\nu}{\alpha} = \frac{1.568\times10^{-5}}{1.9\times10^{-5}} = 0.825$$

$$\mathrm{Nu_{avg}} = 0.508[\frac{\mathrm{Pr}}{0.952+\mathrm{Pr}}]^{0.25}\mathrm{Ra_{avg}}^{0.25} \approx 0.508[\frac{0.825}{0.952+0.825}]^{0.25}(3.872 \times 10^6)^{0.25} = 18.602$$

Hence, the average natural convection resistance is

$$R_{outside} \times A_{wall} \approx \frac{0.2}{0.024\times18.602} \approx 0.448 \text{ m}^2\text{K/W}$$

and

$$R_{outside} \approx 2.807 \text{ K/W}$$

3.2.3.3 Scaling Analysis

At the tank wall, the resistance associated with natural convection with the air is at least 100 times the one associated with natural convection at the water side. Hence, it is safe to neglect the latter one. The conduction resistance is very small compared to any other resistance in the system. Therefore, the resistance network of the system is made up of two resistances in series. The thermal resistance circuit is shown in the Fig. 3.9 in which T_a is the outside room temperature, T_b is the bulk temperature of the aqueous solution, and T_s is the surface temperature of the copper block. A numerical analysis can be done to compute the bulk temperature using the fact that it is the same flux traversing the two resistors.

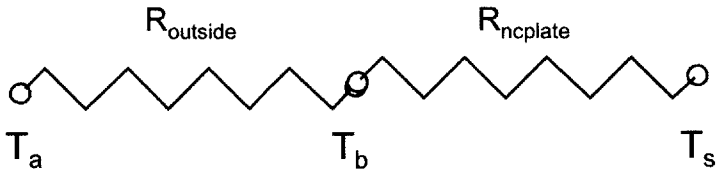

Figure 3.9: Thermal Resistance Circuit of the System

3.3 Thermal Time Constant

The thermal time constant is a feature of thermal systems under convective cooling of warming. It characterizes the response to a step input. Since the heat transfer is proportional to the temperature difference between the surface and the working fluid, the thermal time constant has been formulated as in the equation:

$$\tau = \frac{\rho c_p V}{h_{avg} A} \tag{3.20}$$

where ρV is the mass of the fluid being heated, c_p is its heat capacity, A is the heat transfer area, and h_{avg} is the area-averaged heat transfer coefficient due to convective warming. For a 10 L volume, the thermal time constant is:

$$\tau = \frac{973 \times 4196 \times 10 \times 10^{-3}}{730.5 \times 0.1524 \times 0.0762} = 80.2 \text{ min} \tag{3.21}$$

which means it takes 80 min to heat the solution to the steady state temperature.

Chapter 4

Results

This chapter summarizes the results of lab experimentation. Times of induction were recorded by the videos taken throughout operation. The effect of supersaturation index and temperature variations on the time it takes gypsum to form on a smooth copper plate under natural convection conditions is also discussed.

4.1 Lab Results

The matrix in Table 3.1 summarizes the results collected. An 'X' in the table denotes no significant formation of scale within the time of operation. Typically, for a supersaturation index as low as 1.4, 48 hours of operation is allowed. At the end of some runs, some crystals are visible on the copper surface; however, the amount is not significant enough to be considered a scale layer when it comes to surface coverage considerations.

Table 4.1: Times of Induction at Different Temperatures and Salt Concentrations

-	SI=2.4	SI=2.2	SI=2.0	SI=1.8	SI=1.6	SI=1.4
$T = 80°C$	1hr 23min	1hr 42min	2hr 30min	3hr 10min	6hr 01min	X
$T = 70°C$	1hr 26min	1hr 50min	2hr 45min	3hr 22min	14hr 16min	X
$T = 60°C$	1hr 27min	1hr 39min	3hr 05min	3hr 33min	21hr 04min	X
$T = 50°C$	1hr 26min	1hr 32min	3hr 15min	5hr 20min	23hr 13min	X
$T = 40°C$	1hr 57min	1hr 59min	4hr 00min	6hr 05min	25hr 15min	X

Since no scaling is formed at a supersaturation index of 1.4 for different test temperatures, a **Scale Inception Curve** can be defined above of which scaling forms. Typically, one expects gypsum to precipitate at any concentration above the solubility curve if the waiting time is long enough. However, this precipitation does not necessarily bring about a scale layer of interest. Also, the waiting times, as shown by a mathematical model later, can be on the order of tens of days. Figure 4.1 shows the scale inception curve relative to the published equilibrium curve of calcium sulfate solubility reproduced from the findings of [41].

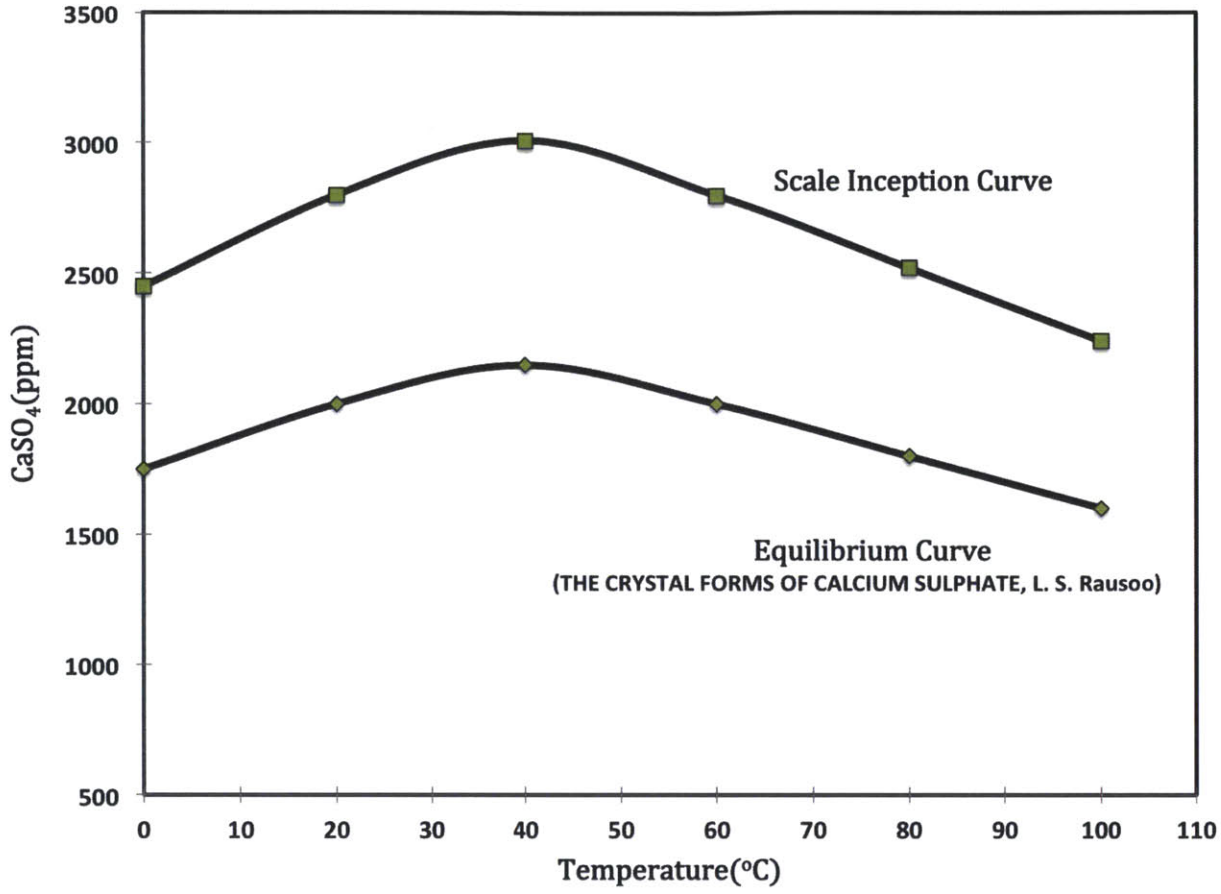

Figure 4.1: Scale Inception Curve

For more instructive visualization of the results, the variation of the gypsum scale induction time is shown as a function of temperature at different supersaturation degrees, and as a function of supersaturation at different temperatures.

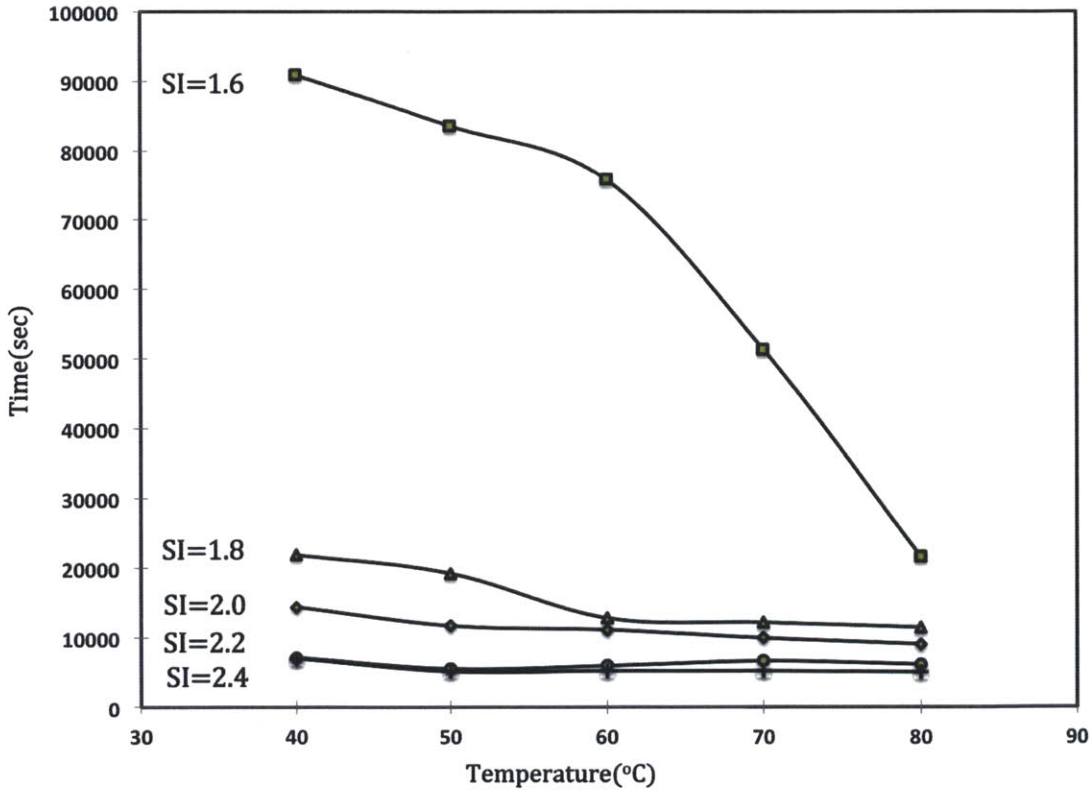

Figure 4.2: Variation of Scale Induction Time with Temperature

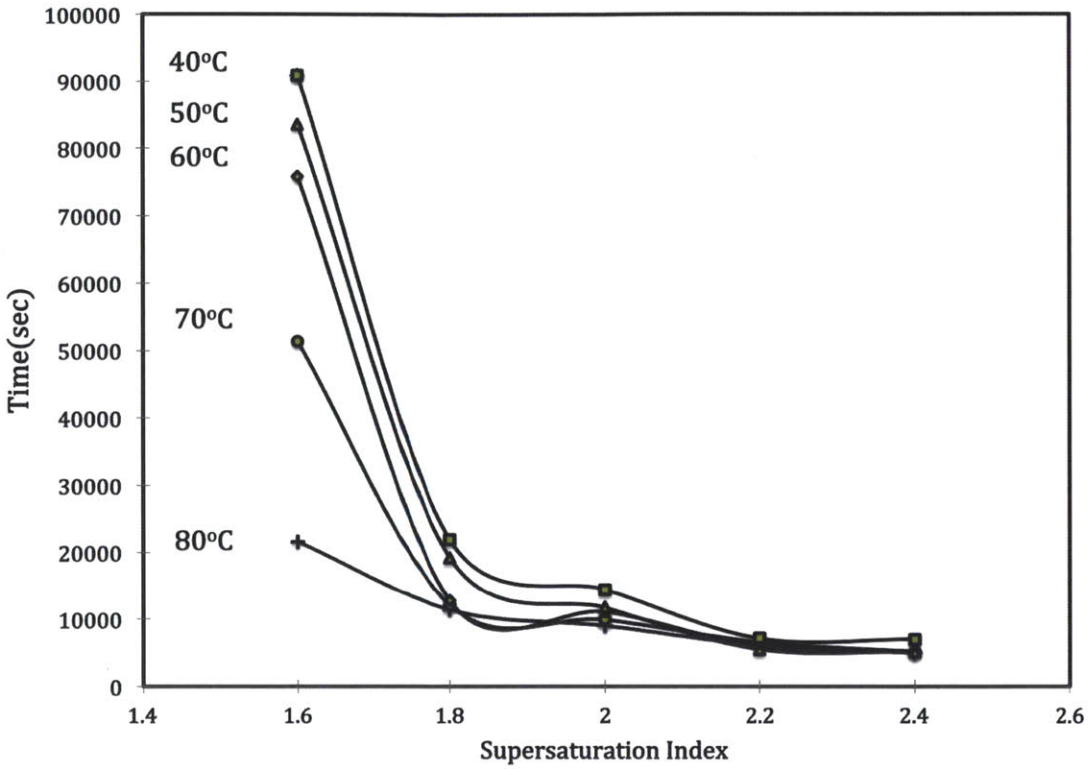

Figure 4.3: Variation of Scale Induction Time with Supersaturation

Several points can be drawn out of the figures.

- Generally, at a given temperature, gypsum scaling is faster at high superaturation indices. When the concentration of the solution increases, there is more potential for crystallization; hence, the time of induction decreases. The potential is enhanced because the driving force for surface reactions increases.

- Generally, at a given supersaturation index, gypsum scaling is faster at high temperatures. At high temperatures, molecules in solution are more agitated and it is more likely for these molecules to bond and undergo a phase change by which they crystallize on the hot surface.

- At high supersaturation indices, the effect of temperature is not significant. The times of induction at a supersaturation index of 2.4 vary from 1hr 23min to 1hr 57min, which

is a much narrower range than that at low supersaturation (6hr 01min to 25hr 15min at an index of 1.6)

- Inspecting results at indices of 2.2 and 2.4 at the temperature range may suggest that there is some index after which the times of induction become fairly constant. The results at 2.2 and 2.4 are very close. However, in a separate test performed at an SI=2.8 and T=80°C, gypsum started to scale on the copper surface after around 20min of operation. It is important to study how the time of induction evolves with even higher supersaturation states.

4.2 SEM Imaging

A scanning electron microscope is used to image samples of the salts collected after experimental runs in order to visualize the differences at a smaller scale. High voltage (5 kV) images are taken at the surface of the crystals. The type of emitted signals employed is BSE or back-scattered electrons signal in which electrons are reflected by elastic scattering to form a focused beam that produces the image.

Samples of salts collected at different temperatures at supersaturation indices of 2.4, 2.0 and 1.8 are scanned using SEM and images are generated at magnification rates of 50, 100, 500 and 1000.

Moreover, energy dispersive X-ray spectroscopy is applied on the samples in order to study their composition. The images produced by SEM and the EDX spectra generated by EDX are shown in the following subsections.

The EDX elemental analysis shows that the produced salts contain calcium, sulfur, and

oxygen. Hydrogen cannot be detected by EDX spectroscopy because the diameter of its orbitals is so small; hence, it is definite that calcium sulfate is formed but it is not certain that it is gypsum in particular.

The SEM images produced gives information about the size and the packing within the samples. More information about crystal orientation could not be retrieved with the used approach. Based on the images, one can safely claim that the crystals are closest to each other at a supersaturation index of 2.0, followed by 2.4 and then 1.8. Whether this claim can be scientifically backed up or not requires more analysis. All the crystals are needle-like; however the size varies and appears to be the smallest (or thinnest) at an index of 2.0.

4.2.1 SEM Images at 80°C

4.2.1.1 SI=2.4

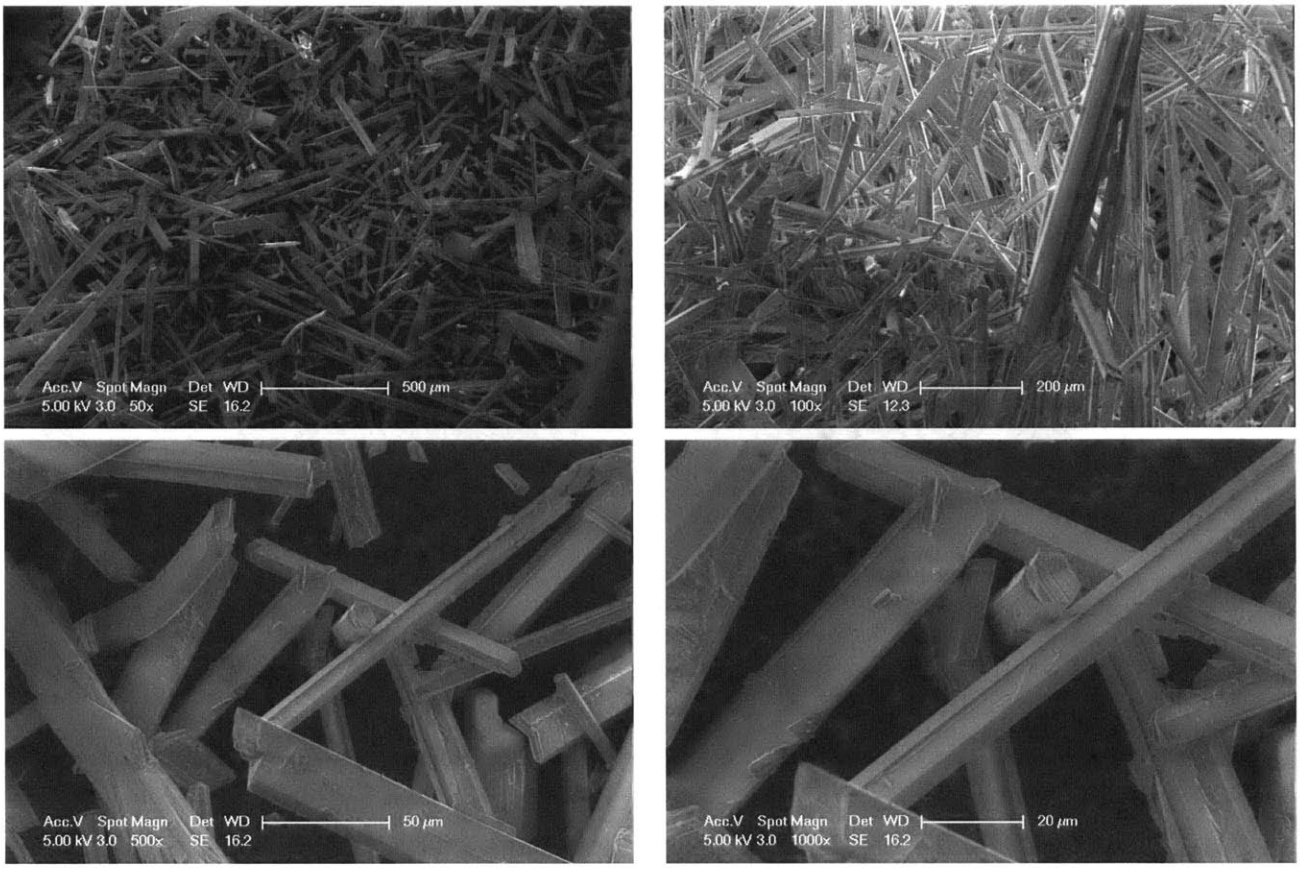

4.2.1.2 SI=2.0

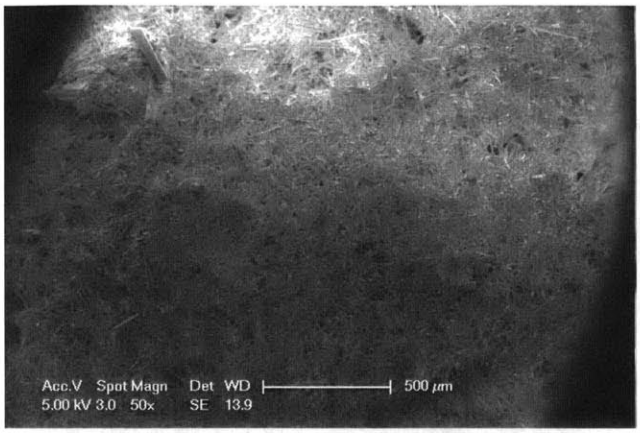
Acc.V Spot Magn Det WD 500 µm
5.00 kV 3.0 50x SE 13.9

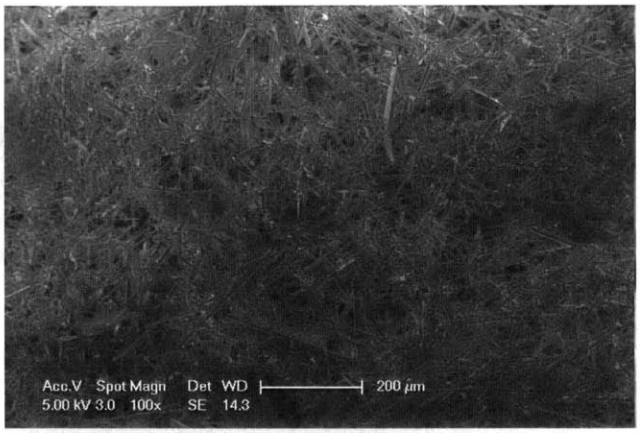
Acc.V Spot Magn Det WD 200 µm
5.00 kV 3.0 100x SE 14.3

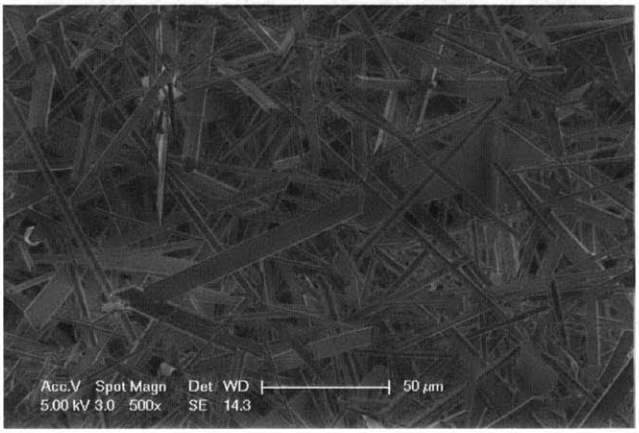
Acc.V Spot Magn Det WD 50 µm
5.00 kV 3.0 500x SE 14.3

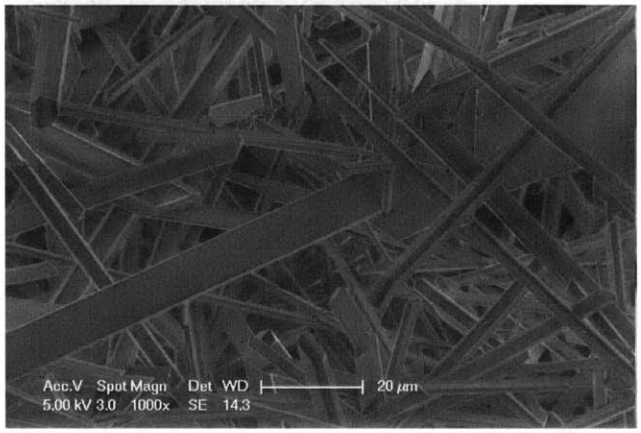
Acc.V Spot Magn Det WD 20 µm
5.00 kV 3.0 1000x SE 14.3

4.2.1.3 SI=1.8

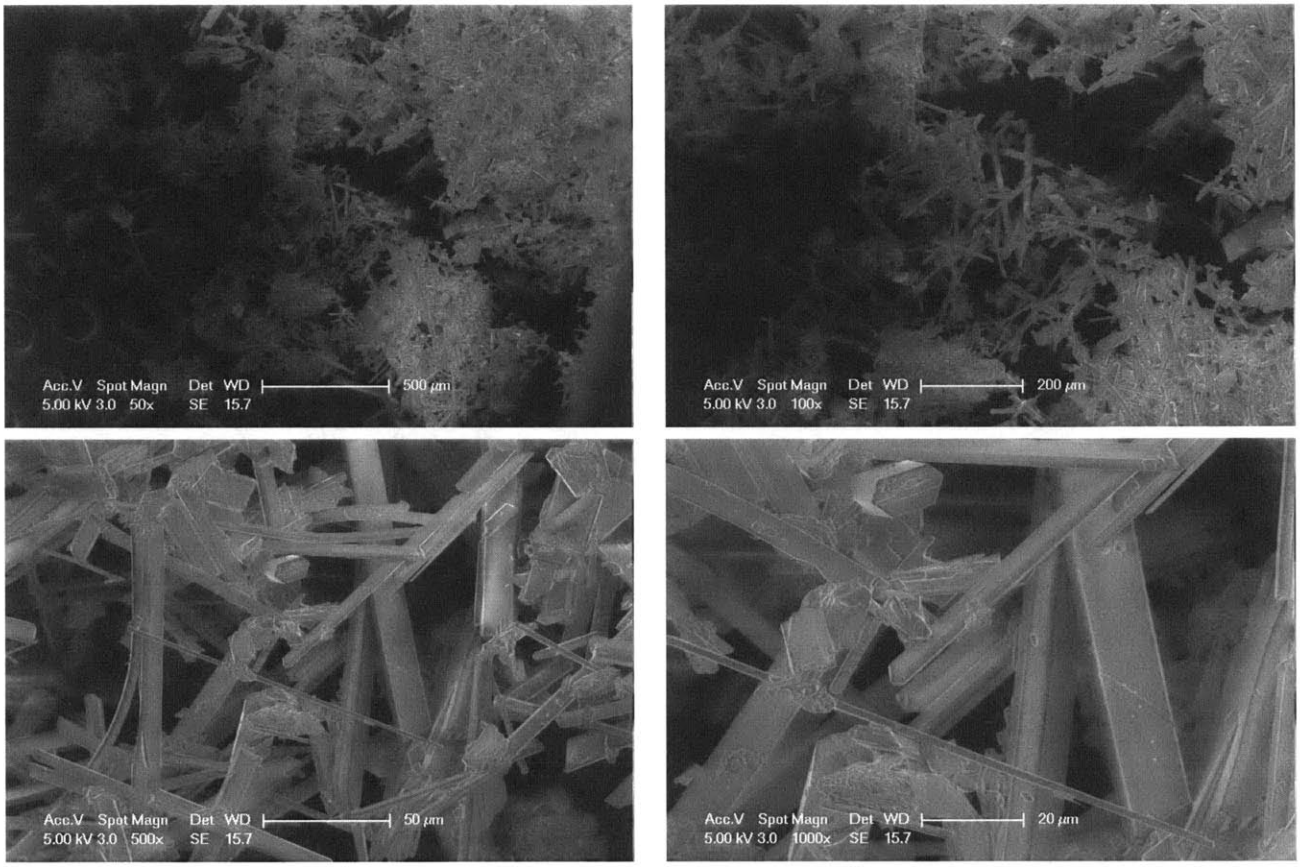
Acc.V Spot Magn Det WD 500 µm
5.00 kV 3.0 50x SE 15.7
Acc.V Spot Magn Det WD 200 µm
5.00 kV 3.0 100x SE 15.7
Acc.V Spot Magn Det WD 50 µm
5.00 kV 3.0 500x SE 15.7
Acc.V Spot Magn Det WD 20 µm
5.00 kV 3.0 1000x SE 15.7

4.2.2 SEM Images at 70°C

4.2.2.1 SI=2.4

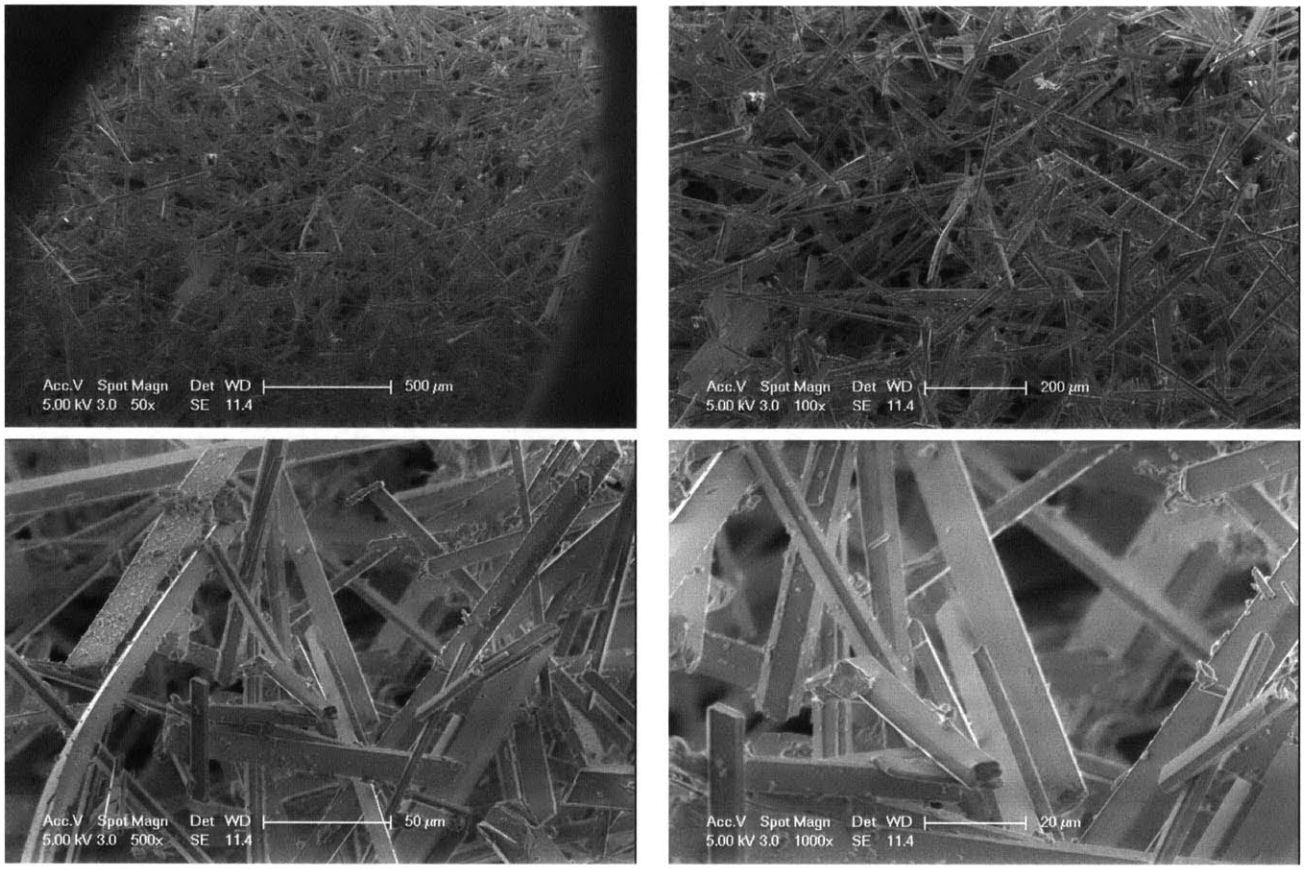

4.2.2.2 SI=2.0

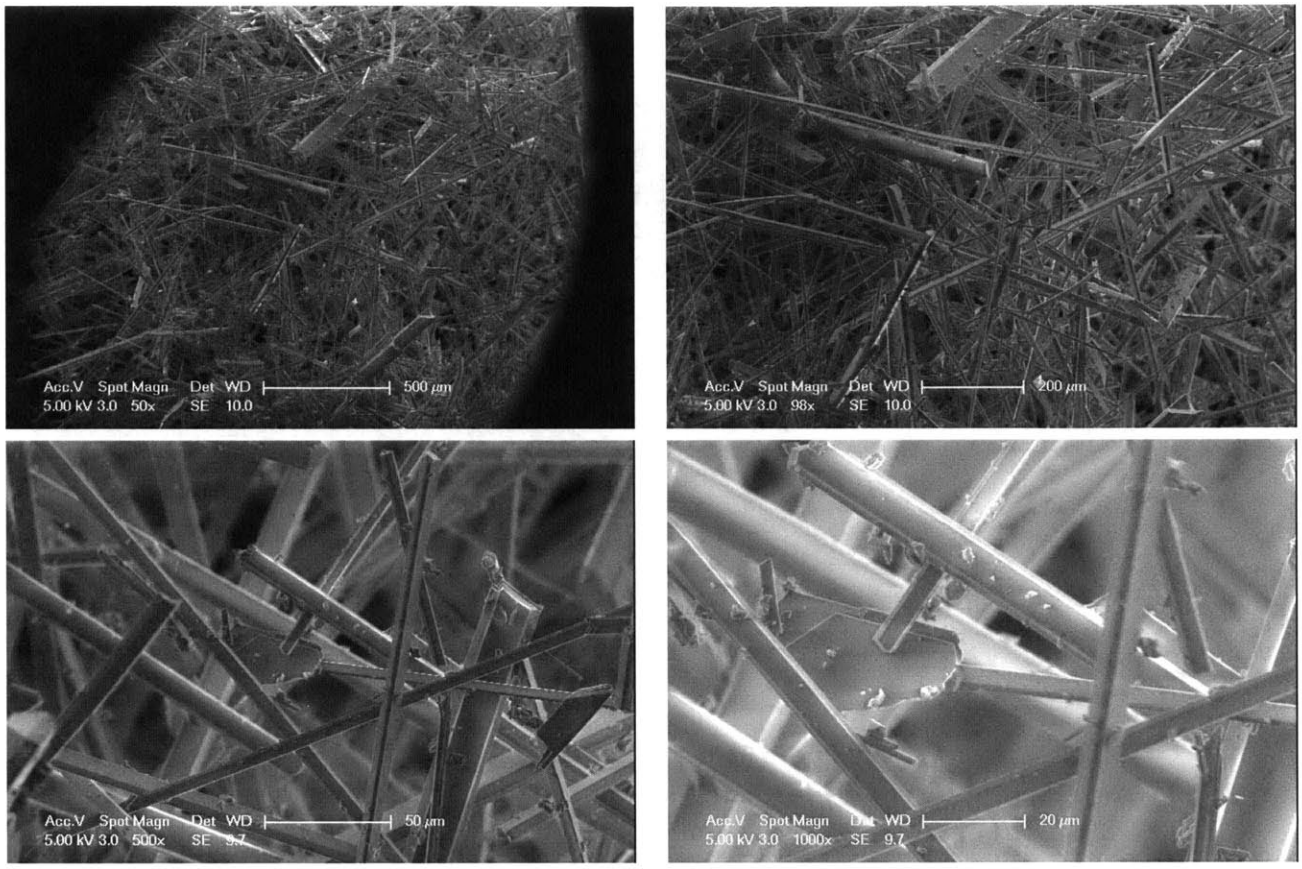
Acc.V Spot Magn Det WD 500 µm
5.00 kV 3.0 50x SE 10.0
Acc.V Spot Magn Det WD 200 µm
5.00 kV 3.0 98x SE 10.0
Acc.V Spot Magn Det WD 50 µm
5.00 kV 3.0 500x SE 9.7
Acc.V Spot Magn Det WD 20 µm
5.00 kV 3.0 1000x SE 9.7

4.2.2.3 SI=1.8

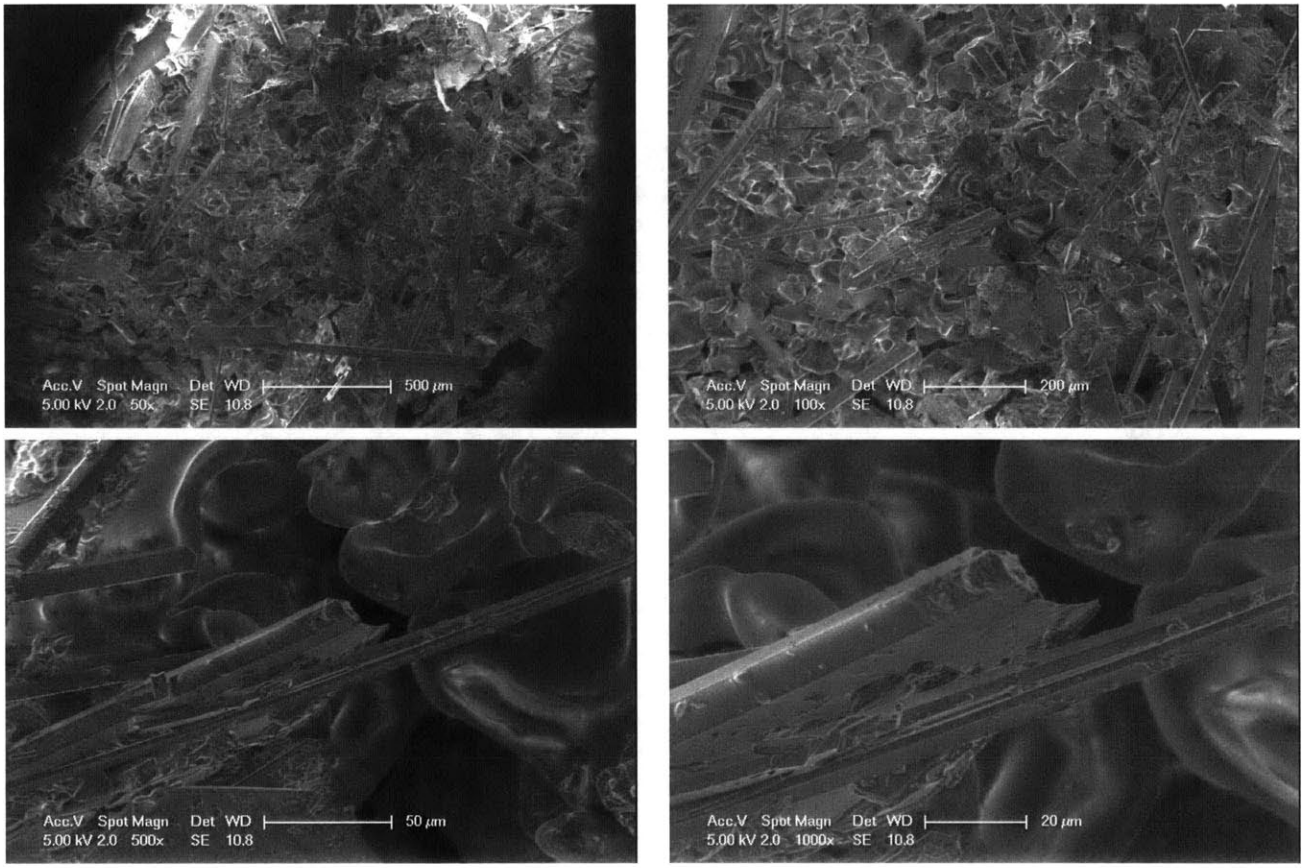
Acc.V Spot Magn Det WD 500 µm
5.00 kV 2.0 50x SE 10.8
Acc.V Spot Magn Det WD 200 µm
5.00 kV 2.0 100x SE 10.8
Acc.V Spot Magn Det WD 50 µm
5.00 kV 2.0 500x SE 10.8
Acc.V Spot Magn Det WD 20 µm
5.00 kV 2.0 1000x SE 10.8

4.2.3 SEM Images at 60°C

4.2.3.1 SI=2.4

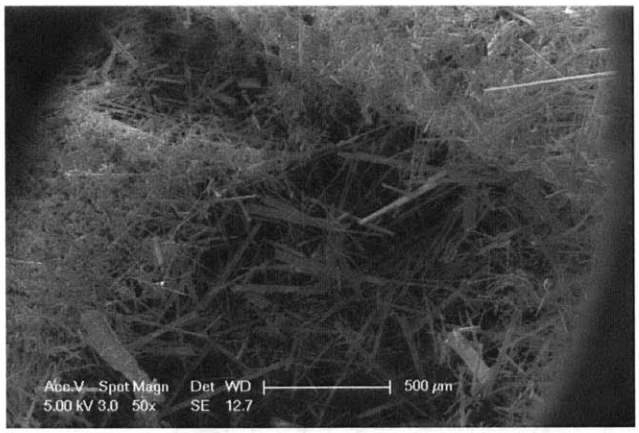

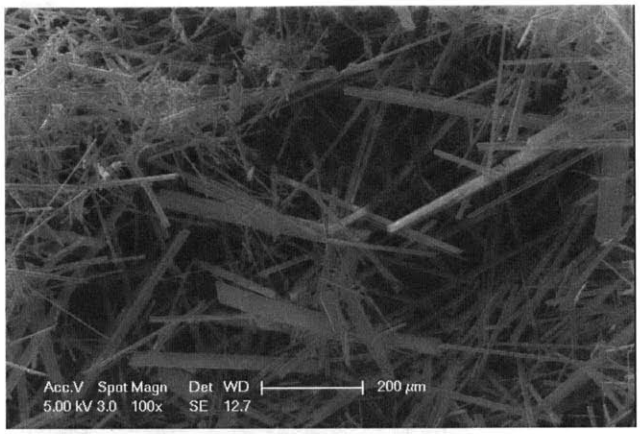

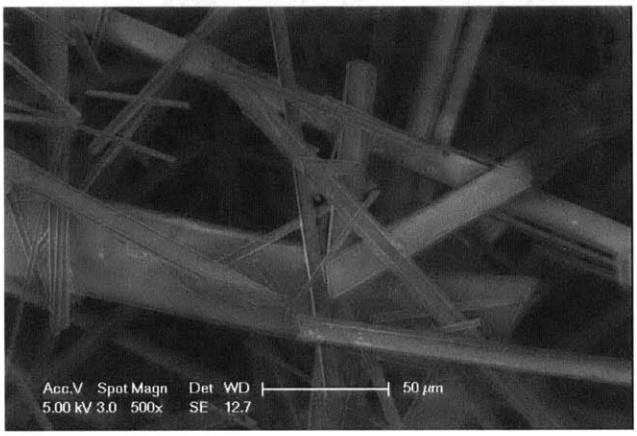

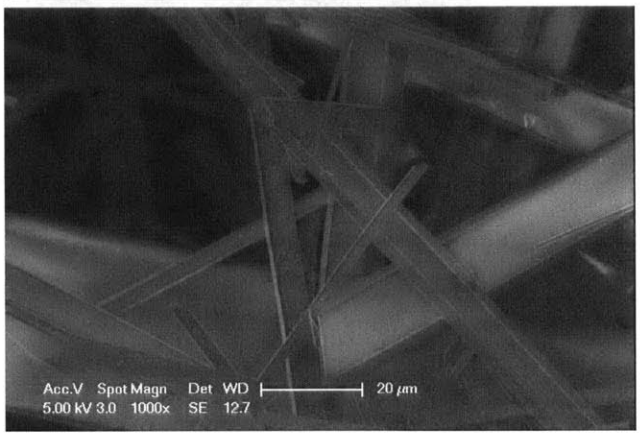

4.2.3.2 SI=2.0

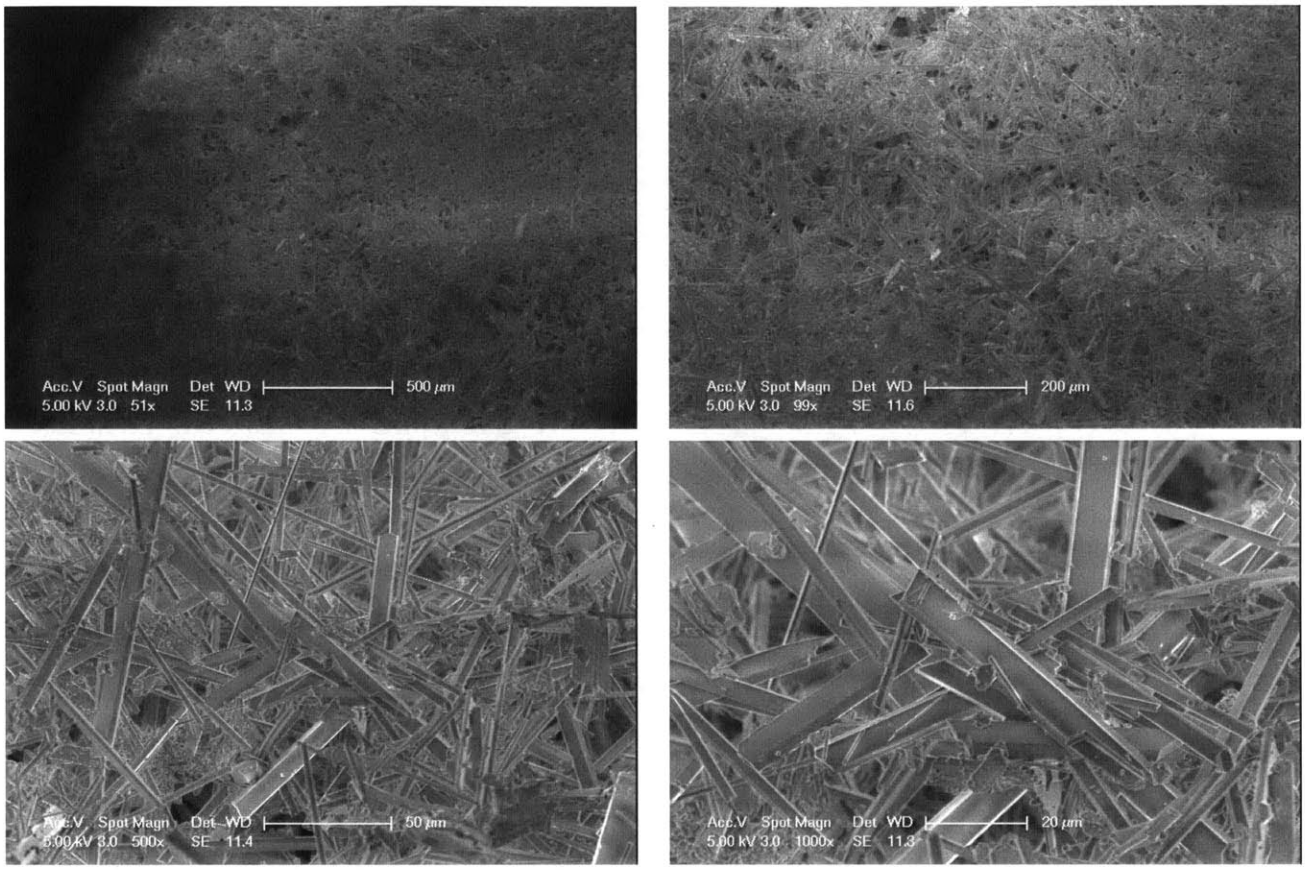
Acc.V Spot Magn Det WD 500 µm
5.00 kV 3.0 51x SE 11.3
Acc.V Spot Magn Det WD 200 µm
5.00 kV 3.0 99x SE 11.6
Acc.V Spot Magn Det WD 50 µm
5.00 kV 3.0 500x SE 11.4
Acc.V Spot Magn Det WD 20 µm
5.00 kV 3.0 1000x SE 11.3

4.2.3.3 SI=1.8

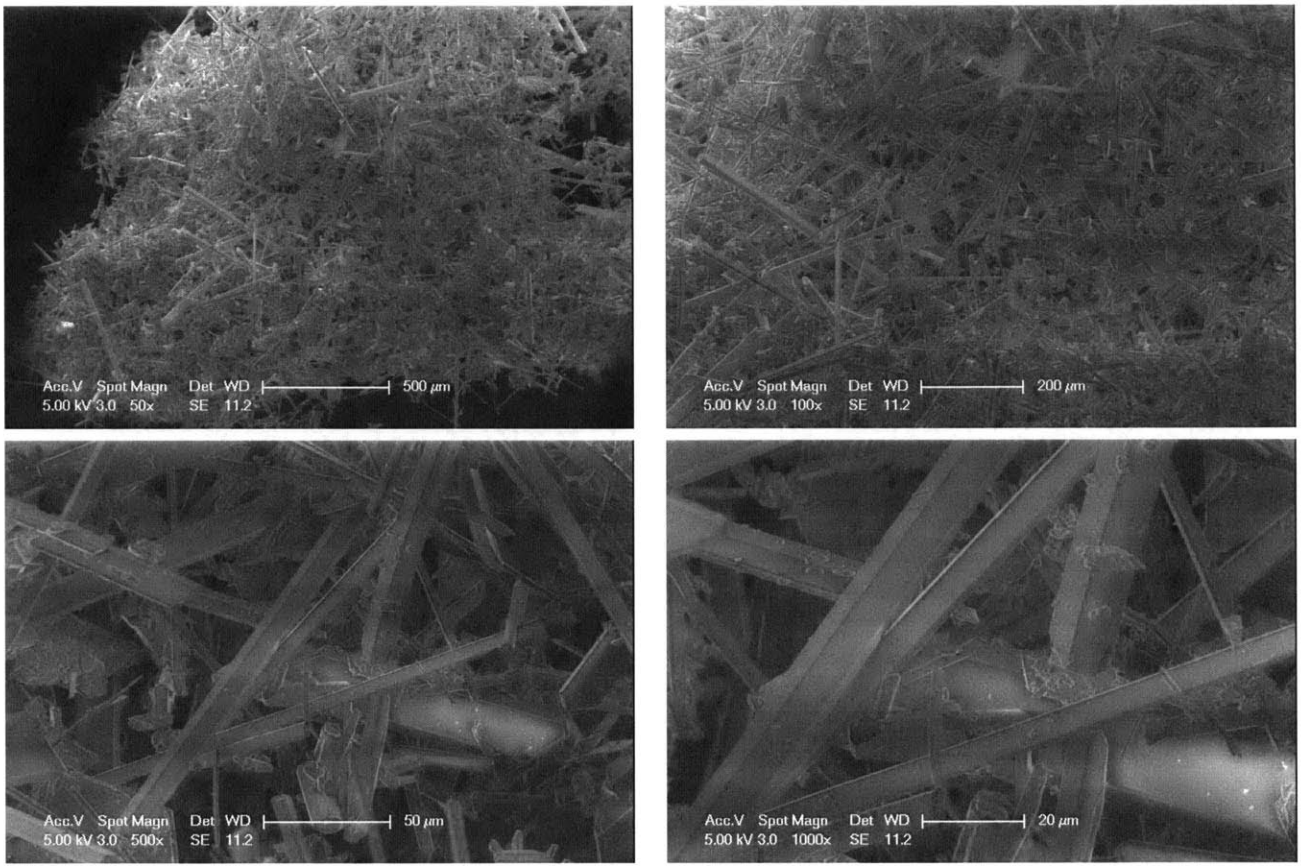
Acc.V Spot Magn Det WD 500 µm
5.00 kV 3.0 50x SE 11.2
Acc.V Spot Magn Det WD 200 µm
5.00 kV 3.0 100x SE 11.2
Acc.V Spot Magn Det WD 50 µm
5.00 kV 3.0 500x SE 11.2
Acc.V Spot Magn Det WD 20 µm
5.00 kV 3.0 1000x SE 11.2

4.2.4 SEM Images at 50°C

4.2.4.1 SI=2.4

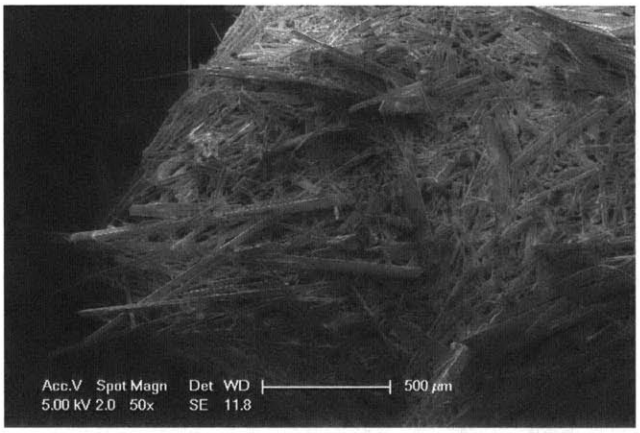

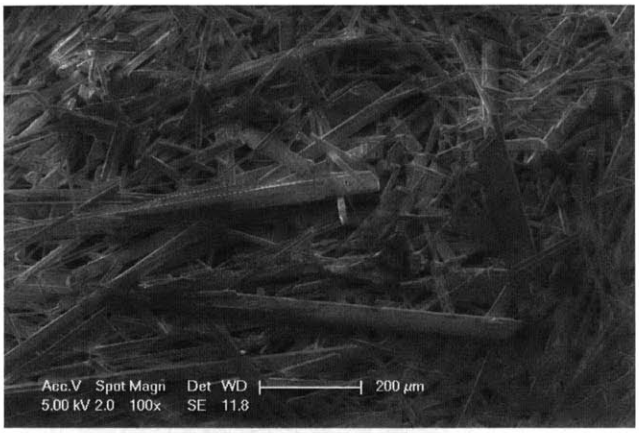

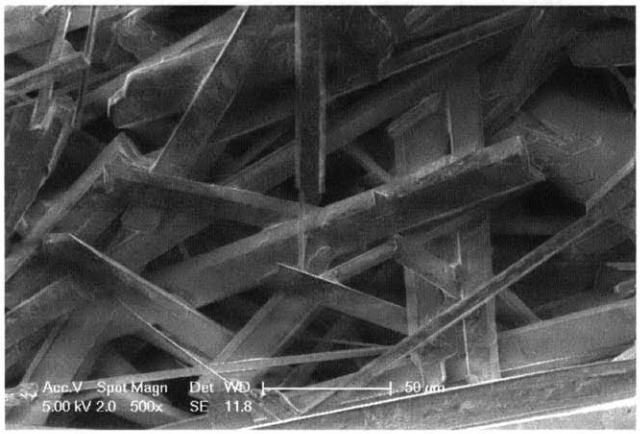

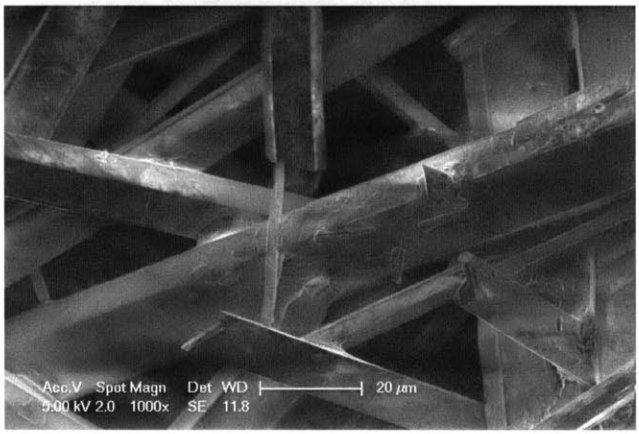

4.2.4.2 SI=2.0

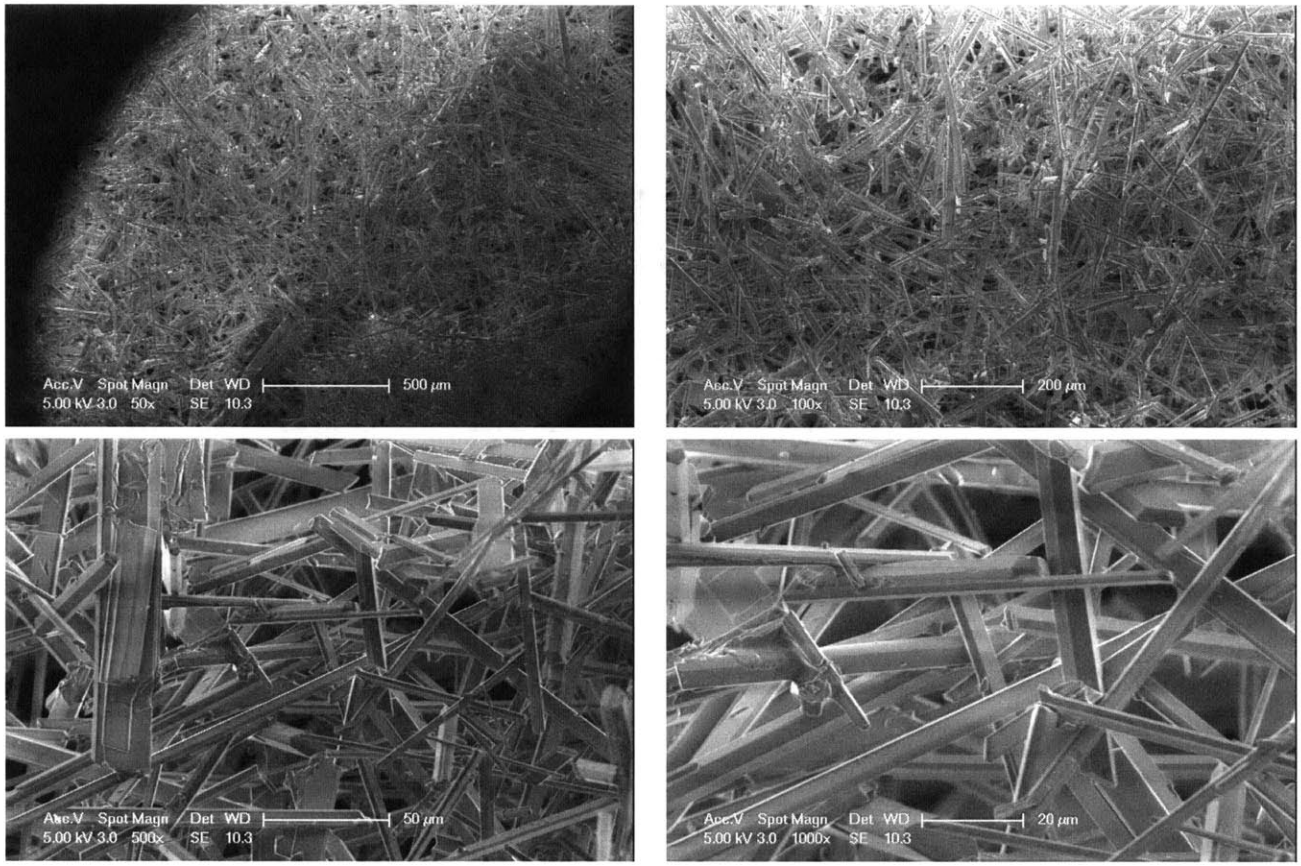
Acc.V Spot Magn Det WD 500 µm
5.00 kV 3.0 50x SE 10.3
Acc.V Spot Magn Det WD 200 µm
5.00 kV 3.0 100x SE 10.3
Acc.V Spot Magn Det WD 50 µm
5.00 kV 3.0 500x SE 10.3
Acc.V Spot Magn Det WD 20 µm
5.00 kV 3.0 1000x SE 10.3

4.2.4.3 SI=1.8

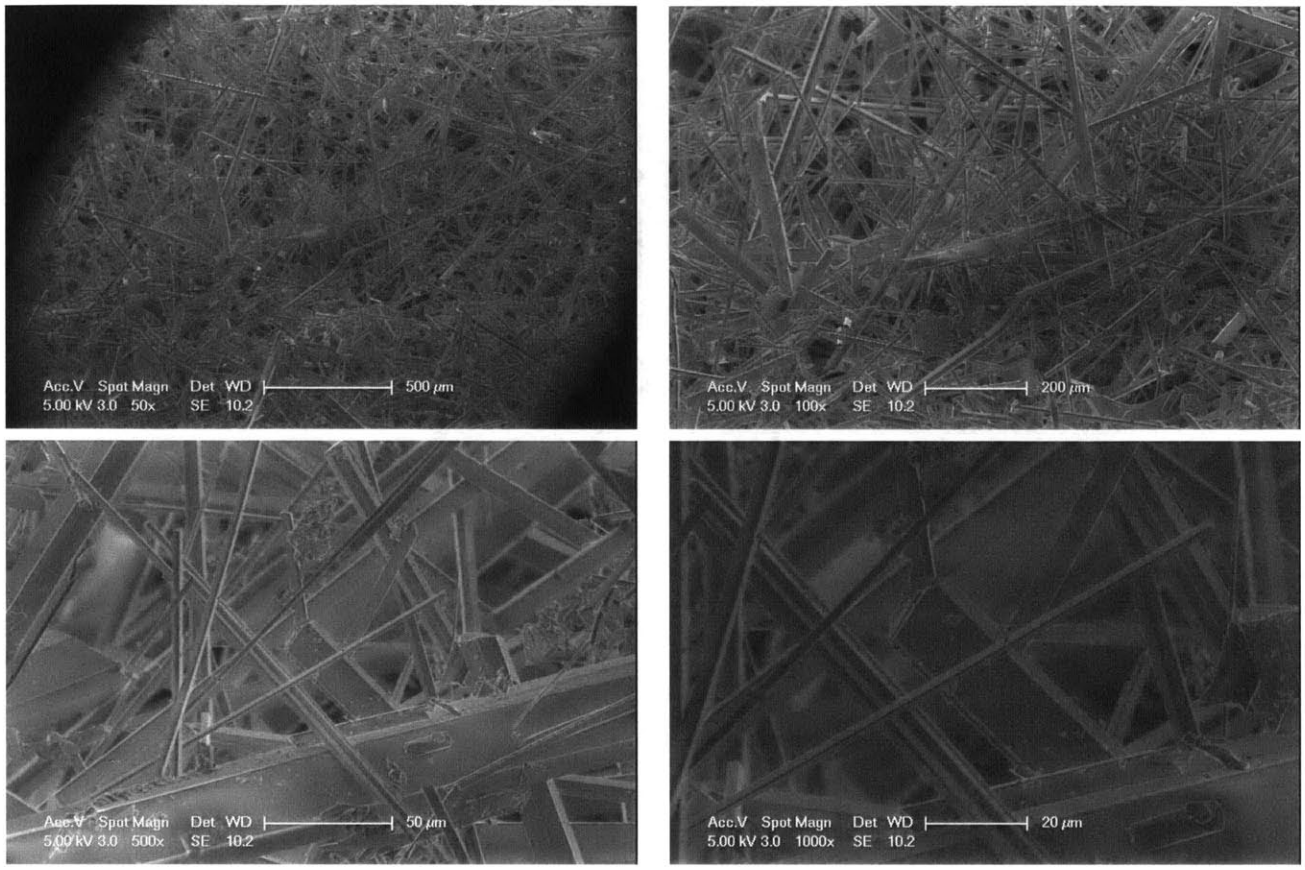
Acc.V Spot Magn Det WD 500 µm
5.00 kV 3.0 50x SE 10.2
Acc.V Spot Magn Det WD 200 µm
5.00 kV 3.0 100x SE 10.2
Acc.V Spot Magn Det WD 50 µm
5.00 kV 3.0 500x SE 10.2
Acc.V Spot Magn Det WD 20 µm
5.00 kV 3.0 1000x SE 10.2

4.2.5 SEM Images at 40°C

4.2.5.1 SI=2.4

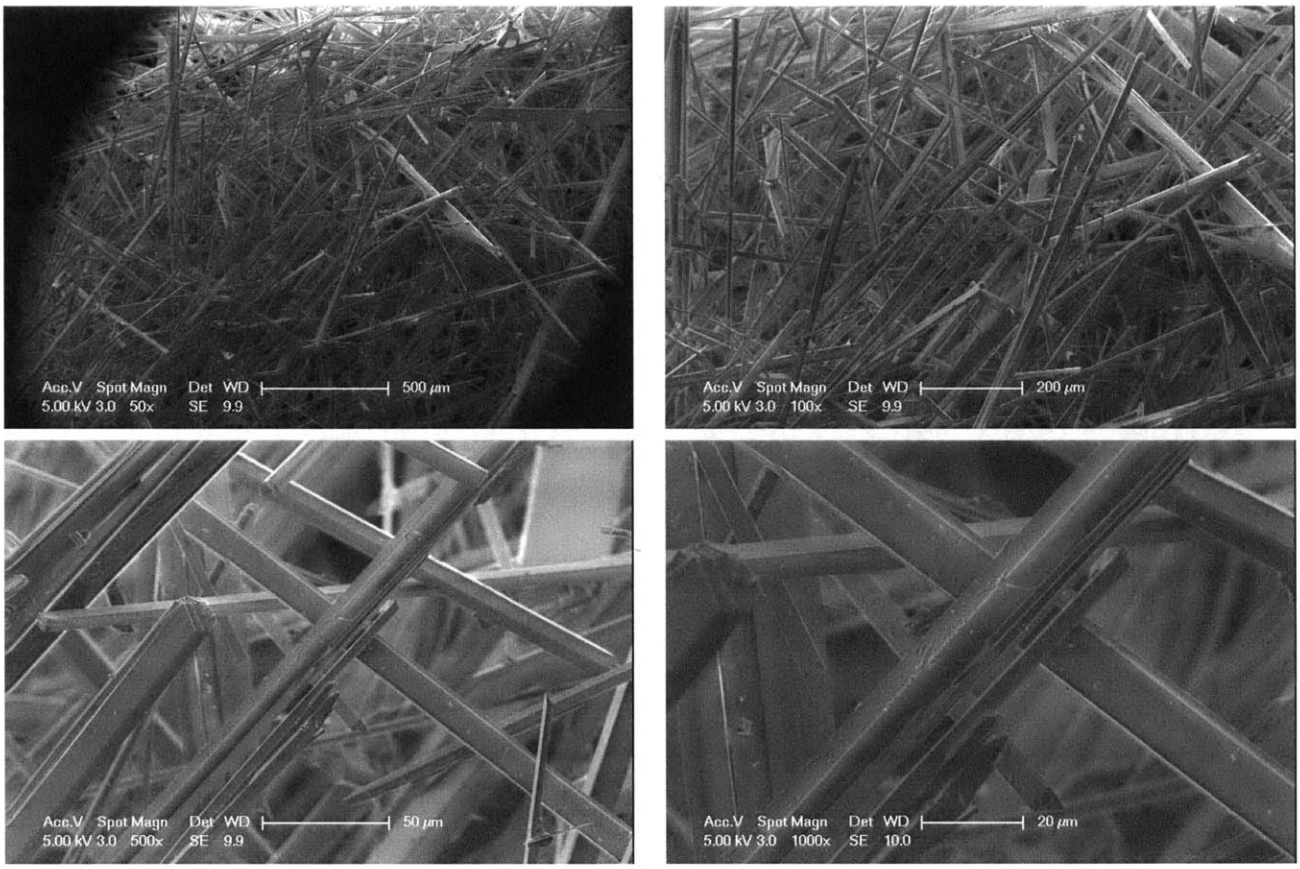

4.2.5.2 SI=2.0

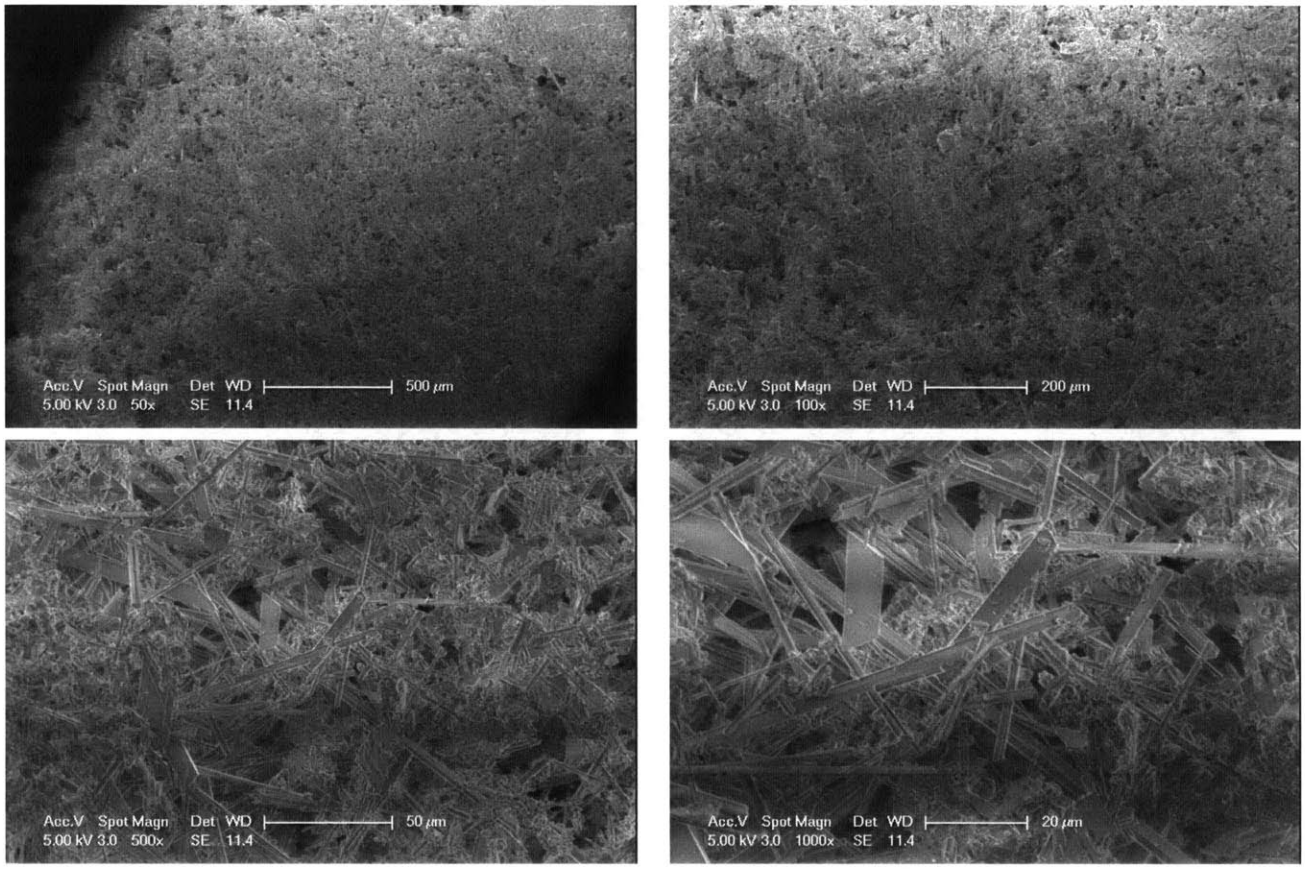
Acc.V Spot Magn Det WD 500 µm
5.00 kV 3.0 50x SE 11.4
Acc.V Spot Magn Det WD 200 µm
5.00 kV 3.0 100x SE 11.4
Acc.V Spot Magn Det WD 50 µm
5.00 kV 3.0 500x SE 11.4
Acc.V Spot Magn Det WD 20 µm
5.00 kV 3.0 1000x SE 11.4

4.2.5.3 SI=1.8

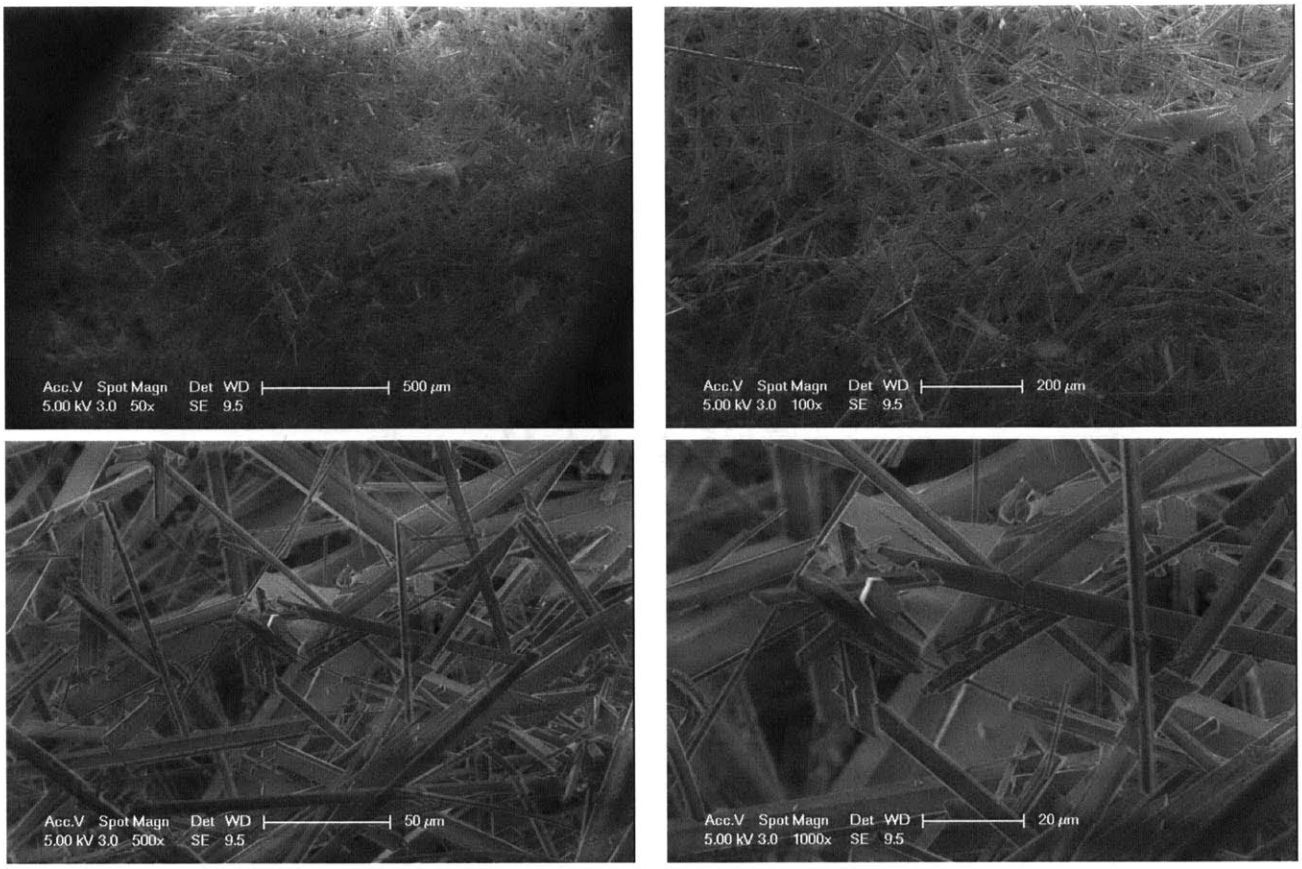
Acc.V Spot Magn Det WD 500 µm
5.00 kV 3.0 50x SE 9.5
Acc.V Spot Magn Det WD 200 µm
5.00 kV 3.0 100x SE 9.5
Acc.V Spot Magn Det WD 50 µm
5.00 kV 3.0 500x SE 9.5
Acc.V Spot Magn Det WD 20 µm
5.00 kV 3.0 1000x SE 9.5

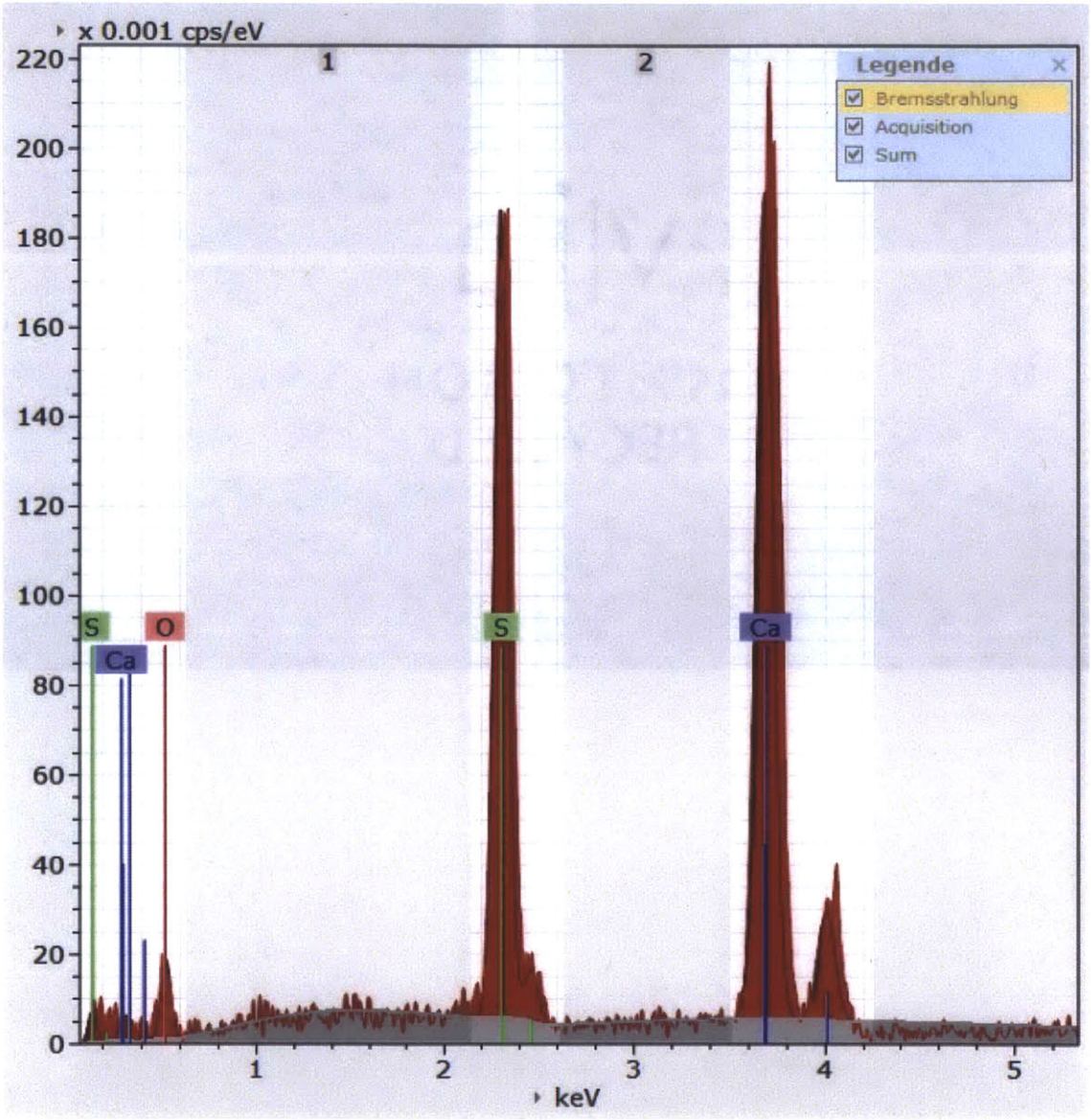

Figure 4.4: EDX Sample Composition at T=80°C and SI=2.4

Chapter 5

Mathematical Modeling of the Time of Induction

The trends in the measured times of scale induction are in line with the reported behavior of gypsum. This chapter explores whether the results are in agreement with the established mathematical analysis of the classical theory of nucleation.

5.1 Classical Nucleation Theory

There exists no general consensus on the mechanism of formation of stable nuclei of salt crystals within a homogeneous fluid or on a surface. Nucleation of molecules is complex by nature as it involves their resistance of the tendency to redissolve as well as their orientation into a fixed lattice. Hence, developing a solid mathematical analysis is very difficult given the lack of understanding of the physical theory.

Crystallization of salts from melts and solutions have been thought of as analogous to condensation of vapor into liquid. The classical theory of nucleation developed from the works

of **Gibbs** [49], **Volmer** [50] and others is based on this premise.

The model is based on Gibbs free energy considerations. The main assumption is that the existing droplets and formed clusters are all spherical and the clusters are described by macroscopic thermal parameters.

Gibbs outlined the nucleation theory for crystallization of solids within a homogeneous fluid [49] . Each particle is a sphere of radius r. The overall excess free energy between the solid sphere and the solute in solution is given by

$$\Delta G = \Delta G_S + \Delta G_V = 4\pi r^2 \gamma + \frac{4}{3}\pi r^3 \Delta G_v \tag{5.1}$$

where ΔG_S is the excess free energy between the particle's surface and bulk, ΔG_V is the excess free energy between a very large particle and the solute in solution, γ is the interfacial tension between the developing crystal and the solution, and ΔG_v is the free energy change of transformation per unit volume. ΔG has a global maximum, ΔG_{crit} obtained by maximizing ΔG

$$\Delta G_{crit} = \frac{4\pi\gamma r_c^2}{3} \tag{5.2}$$

r_c is the minimum radius for a stable nucleus. Particles smaller than r_c will dissolve or evaporate. Particles larger than r_c will continue to grow.

The rate of nucleation or the number of nuclei formed per unit volume is defined using an **Arrhenius** relation, commonly used for thermally activated processes.

$$J = A \exp(-\frac{\Delta G}{kT}) \tag{5.3}$$

where k is the Boltzmann constant (1.3805×10^{-23} J/K)

Based on Gibbs-Thomson relationship for non-electrolytes, the rate of nucleation is expressed as

$$J = A \exp[-\frac{16\pi\gamma^3 v_m^2}{3n^2 N_A^2 k^3 T^3 (\ln S)^2}] \tag{5.4}$$

where A is a frequency factor, v_m is the molecular volume of the formed crystals and S is the supersaturation index defined as the ratio of the solute concentration at temperature T to the concentration corresponding to a saturated solution at the same temperature. In the case of non-spherical nuclei, the shape factor $16\pi/3$ has to be replaced with an appropriate value corresponding to the geometry of the molecules.

This equation suggests that the rate of nucleation is mainly governed by three variables: absolute temperature, index of supersaturation and surface energy. The relative significance of each is discussed later. Mullin [51] suggests that the induction time τ_D is inversely proportional to the nucleation rate such that

$$\tau_D = \frac{B}{J} \tag{5.5}$$

Hence,

$$\ln \tau_D = \ln \frac{B}{A} + \frac{K}{(\ln S)^2} \tag{5.6}$$

in which

$$K = \frac{16\pi\gamma_{eff}^3 v_m^2}{3n^2 N_A^2 k^3 T^3} \tag{5.7}$$

Since the model developed by Mullin is designed to mathematically explain homogeneous nucleation that is a prerequisite of bulk crystal growth, Volmer et al. suggested a correction for heterogeneous nucleation [52]. The correction stems from the fact that in the presence of nucleation accelerators or a sympathetic surface, the formation of nuclei with a critical radius requires an overall free energy change that is less than that associated with homogeneous nucleation. Hence, γ is replaced with γ_{eff} to account for heterogeneous nucleation.

According to Volmer, γ_{eff} is given by

$$\gamma_{eff} = \gamma\phi^{1/3} \tag{5.8}$$

where the correction parameter ϕ is equal to 1 in case of homogeneous nucleation and is less than 1 for heterogeneous nucleation. In cases of heterogeneous nucleation, each situation must be considered separately as there is no general governing rule. However, ϕ may be given as a function of a contact angle θ as follows:

$$\phi = \frac{(2 + \cos\theta)(1 - \cos\theta)^2}{4} \tag{5.9}$$

The angle θ is the angle between the crystalline deposit and the foreign solid surface. It is equivalent to the wetting angle in liquid-solid systems. Since the interfacial tension is a significant parameter influencing nucleation, the contact angle plays an important role. Figure 4.1 reproduced from Mullin, shows the interfacial energy diagram for the three phases at nucleation on the surface: two solids and a liquid. In the figure, γ_{sl} is the interfacial tension between the surface and the liquid, γ_{cs} is the one between the forming crystals and the surface and γ_{cl} is the one between the crystal and the liquid. θ is shown as the angle between γ_{cs} and γ_{cl}, where $\cos\theta = \frac{\gamma_{sl}-\gamma_{cs}}{\gamma_{cl}}$

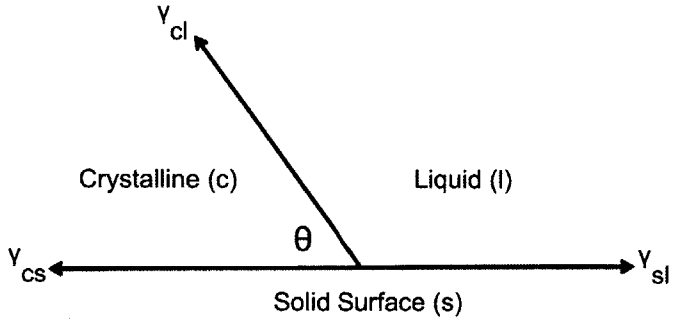

Figure 5.1: Interfacial Energy Diagram

The values taken by θ range from 0 to 180°. The variation of the factor ϕ in this range is shown in Fig 5.2.

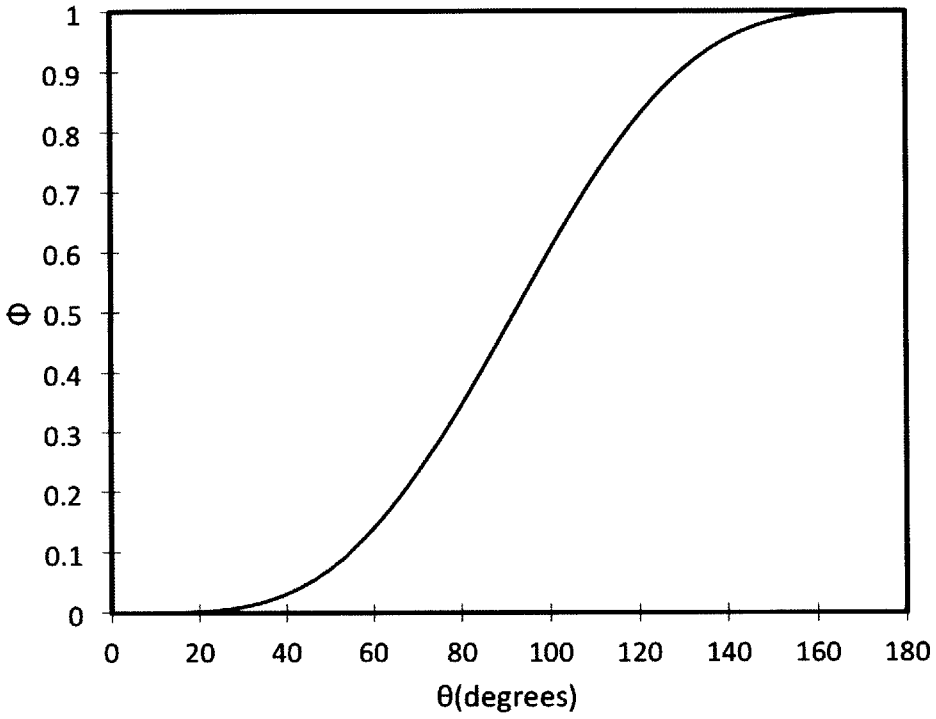

Figure 5.2: Heterogeneous Nucleation Correction Factor vs Contact Angle

According to this model, $\ln \tau_D$ has a linear relationship with $\frac{1}{(\ln S)^2}$. Hence a plot of $\ln \tau_D$ versus $\frac{1}{(\ln S)^2}$ is a straight line with slope K. Applying the Mullin model of classical nucleation [51] to the experimental results discussed in the previous chapter reveals that the results are in accordance with the analytical model. Plots at various surface temperatures are shown below.

Values used throughout the model for the gypsum solution are summarized in the following table.

Table 5.1: Model Parameters at Different Temperatures

Symbol	Parameter	Value	Unit
N_A	Avogadro's number	6.022×10^{23}	mol^{-1}
n	number of crystallizing ions	2	-
v_m	molar volume of the crystalline phase	7.445×10^{-5}	m^3/mol
k	Boltzmann constant	1.38×10^{-23}	J/K
T	absolute temperature	[40,50,60,70,80]	°C
SI	supersaturation index	[1.4,1.6,1.8,2.0,2.2,2.4]	-
θ	contact angle	$0 \leq \theta \leq 180$	degrees

5.1.1 Modeling Results at 80°C

Figure 4.3 shows the data points collected at 80° C. A linear fit of the results is expressed by

$$\ln \tau_D = 8.0429 + \frac{0.4385}{(\ln S)^2}$$

By comparison with the model suggested by Mullin, $K_{80} = 0.4385$. The corresponding

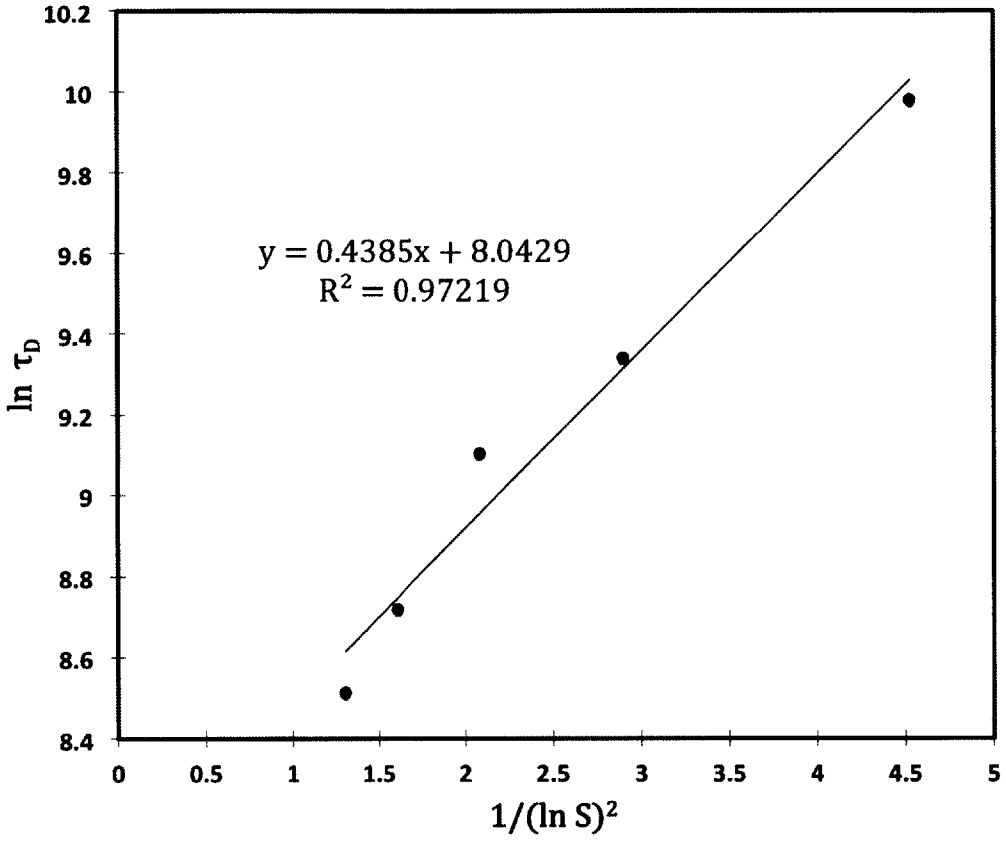

Figure 5.3: Classical Nucleation Theory Model of Results at 80°C

interfacial tension is

$$\gamma_{80} = \left(\frac{3K_{80}}{16\pi n^2 N_A^2 v_m^2 \phi}\right)^{1/3}(kT)$$

where ϕ varies with the contact angle as described before. The values taken by the interfacial tension at 80°C as a function of the change in the contact angle is shown in Fig. 5.4.

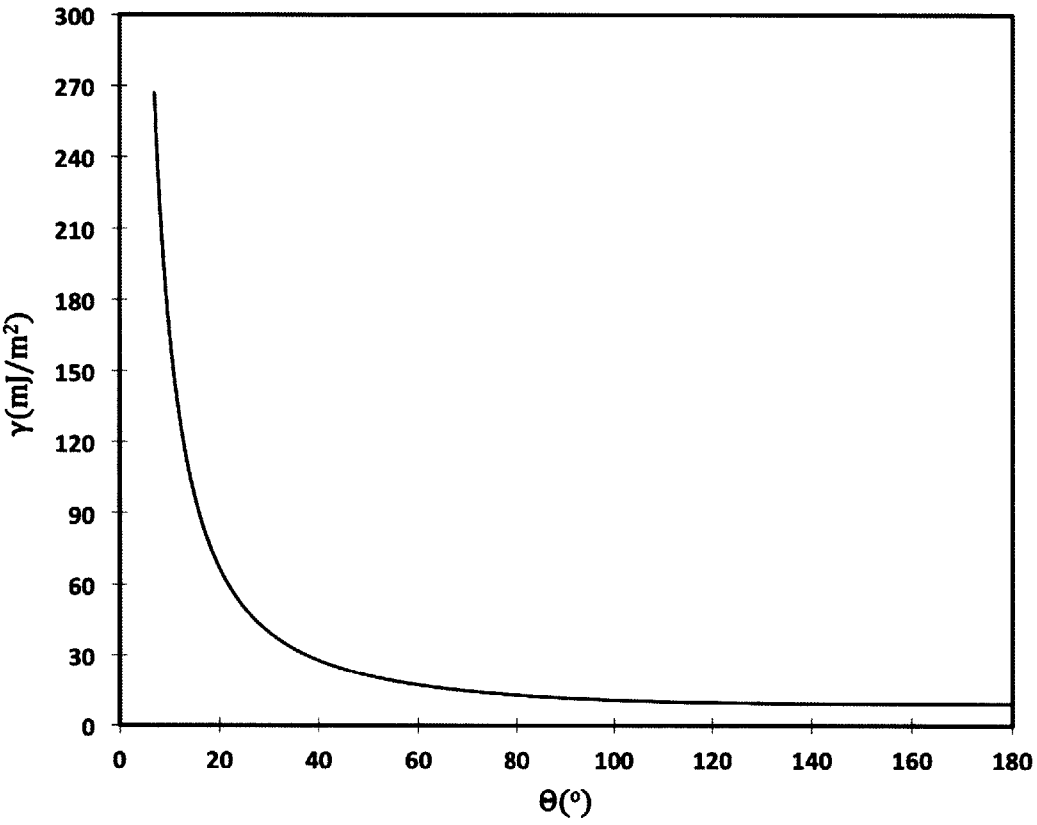

Figure 5.4: Interfacial Tension at 80°C as a function of contact angle

5.1.2 Modeling Results at 70°C

Figure 5.5 shows the data points collected at 70° C. A linear fit of the results is expressed by

$$\ln \tau_D = 7.6548 + \frac{0.6861}{(\ln S)^2}$$

By comparison with the model suggested by Mullin, $K_{70} = 0.6861$. The corresponding

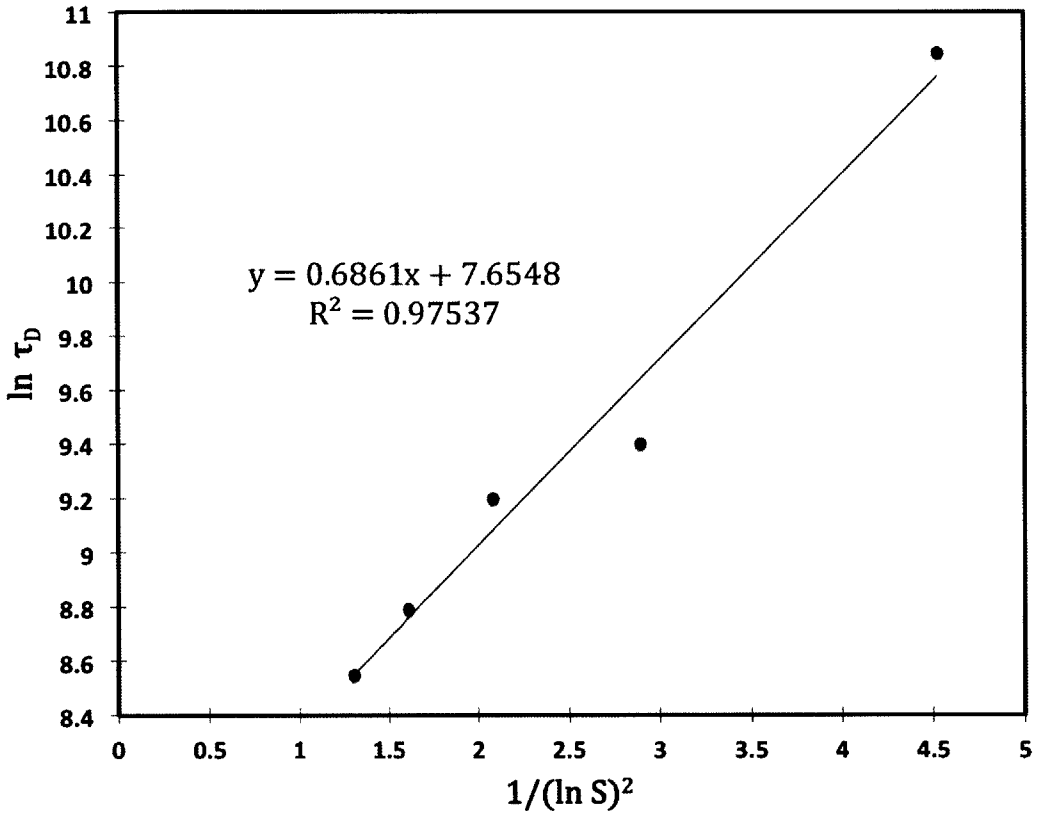

Figure 5.5: Classical Nucleation Theory Model of Results at 70°C

interfacial tension is

$$\gamma_{70} = (\frac{3K_{70}}{16\pi n^2 N_A^2 v_m^2 \phi})^{1/3}(kT)$$

The values taken by the interfacial tension at 70°C as a function of the change in the contact angle is shown in Fig. 5.6.

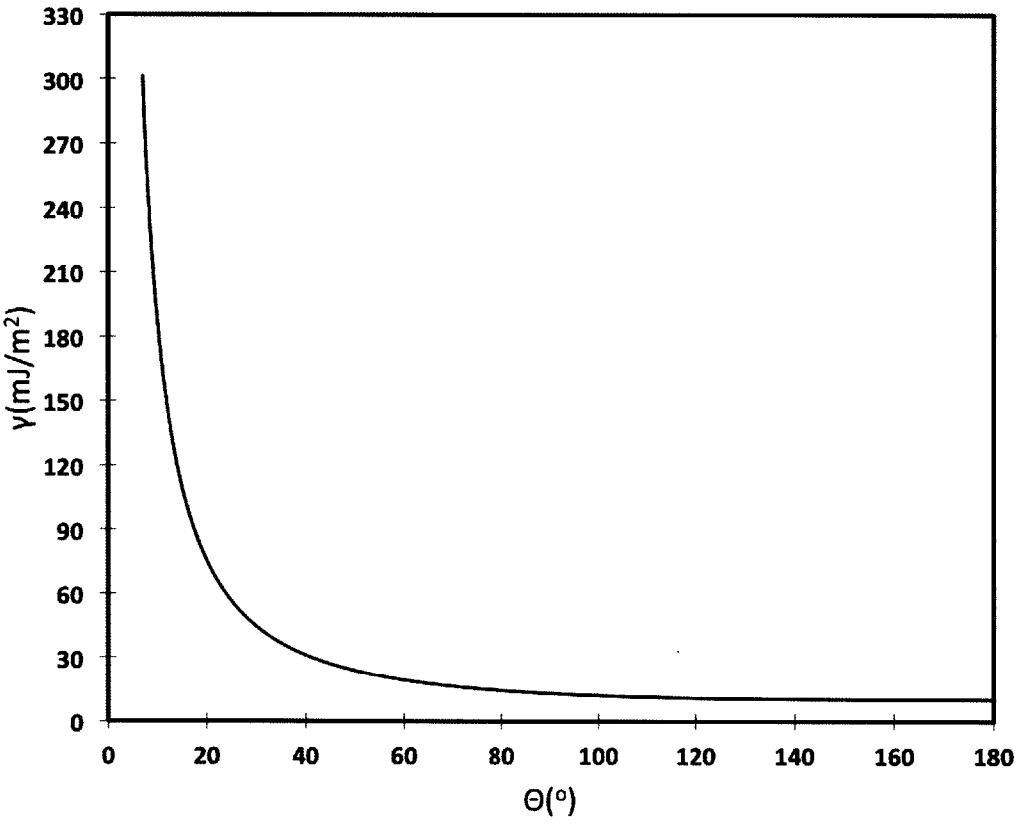

Figure 5.6: Interfacial Tension at 70°C as a function of contact angle

5.1.3 Modeling Results at 60°C

Figure 5.7 shows the data points collected at 60° C. A linear fit of the results is expressed by

$$\ln \tau_D = 7.4303 + \frac{0.8139}{(\ln S)^2}$$

By comparison with the model suggested by Mullin, $K_{60} = 0.8139$. The corresponding

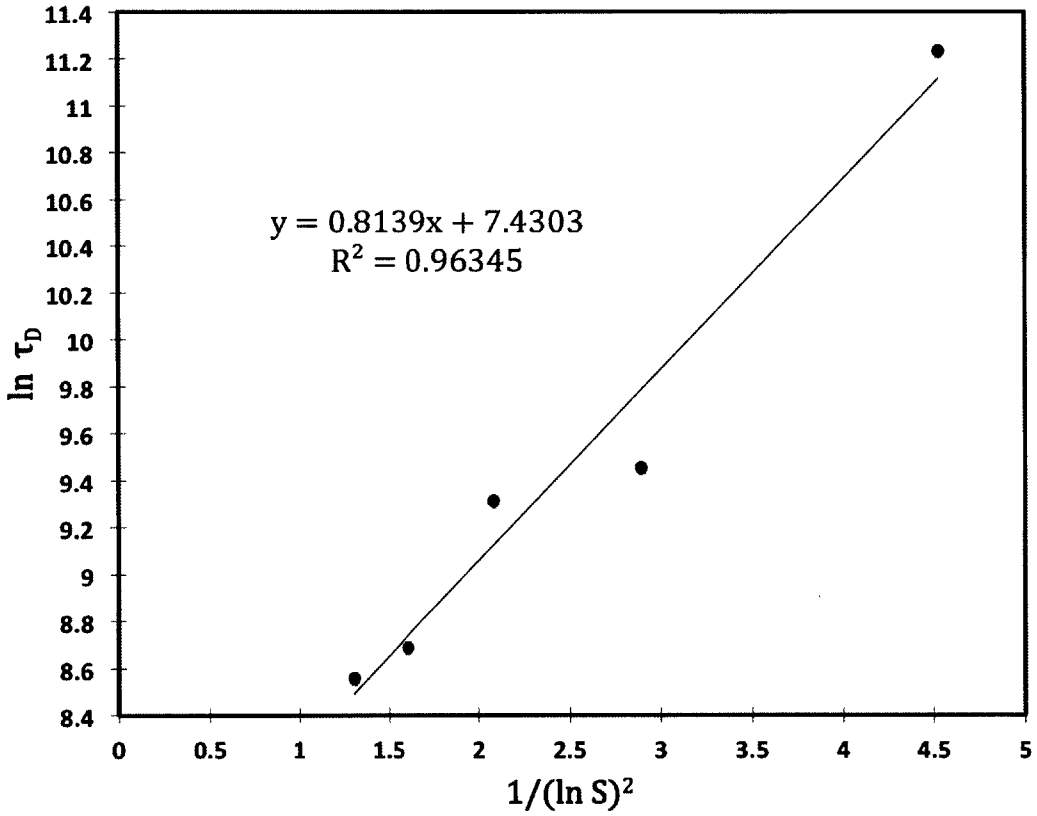

Figure 5.7: Classical Nucleation Theory Model of Results at 60°C

interfacial tension is

$$\gamma_{60} = (\frac{3K_{60}}{16\pi n^2 N_A^2 v_m^2 \phi})^{1/3}(kT)$$

The values taken by the interfacial tension at 60°C as a function of the change in the contact angle is shown in Fig. 5.8.

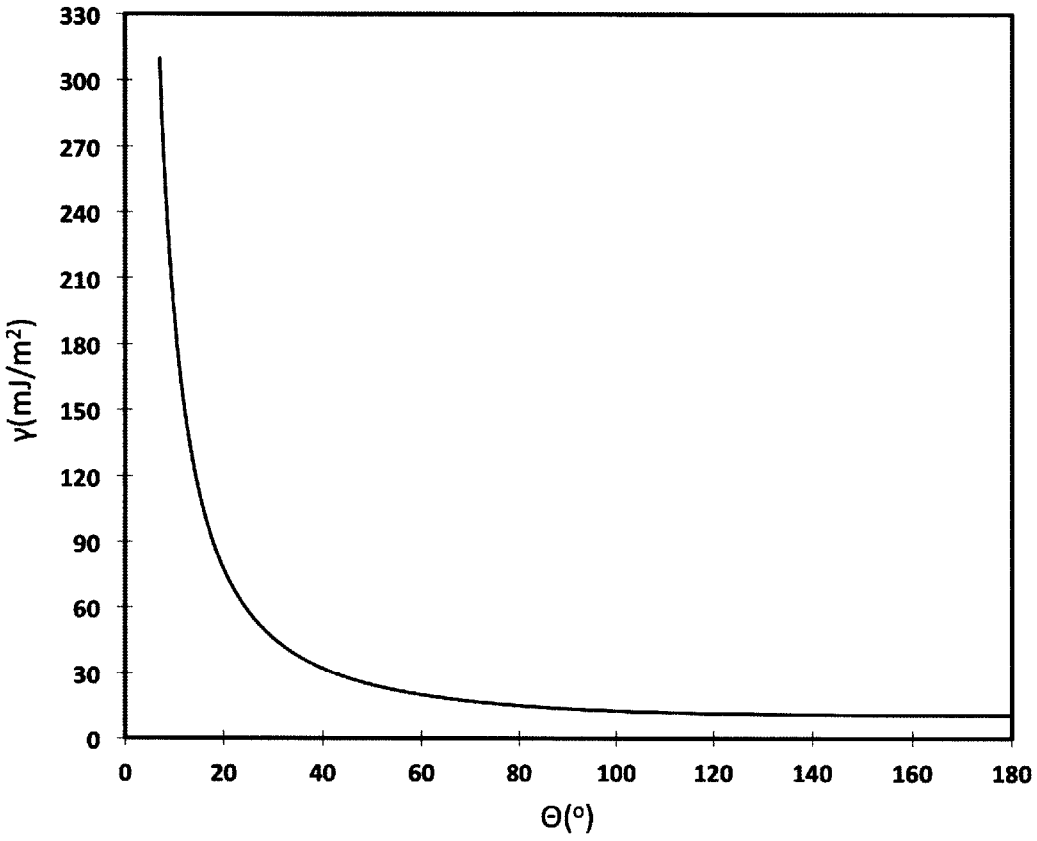

Figure 5.8: Interfacial Tension at 60°C as a function of contact angle

5.1.4 Modeling Results at 50°C

Figure 5.9 shows the data points collected at 50° C. A linear fit of the results is expressed by

$$\ln \tau_D = 7.3671 + \frac{0.8773}{(\ln S)^2}$$

By comparison with the model suggested by Mullin, $K_{50} = 0.8773$. The values taken by the

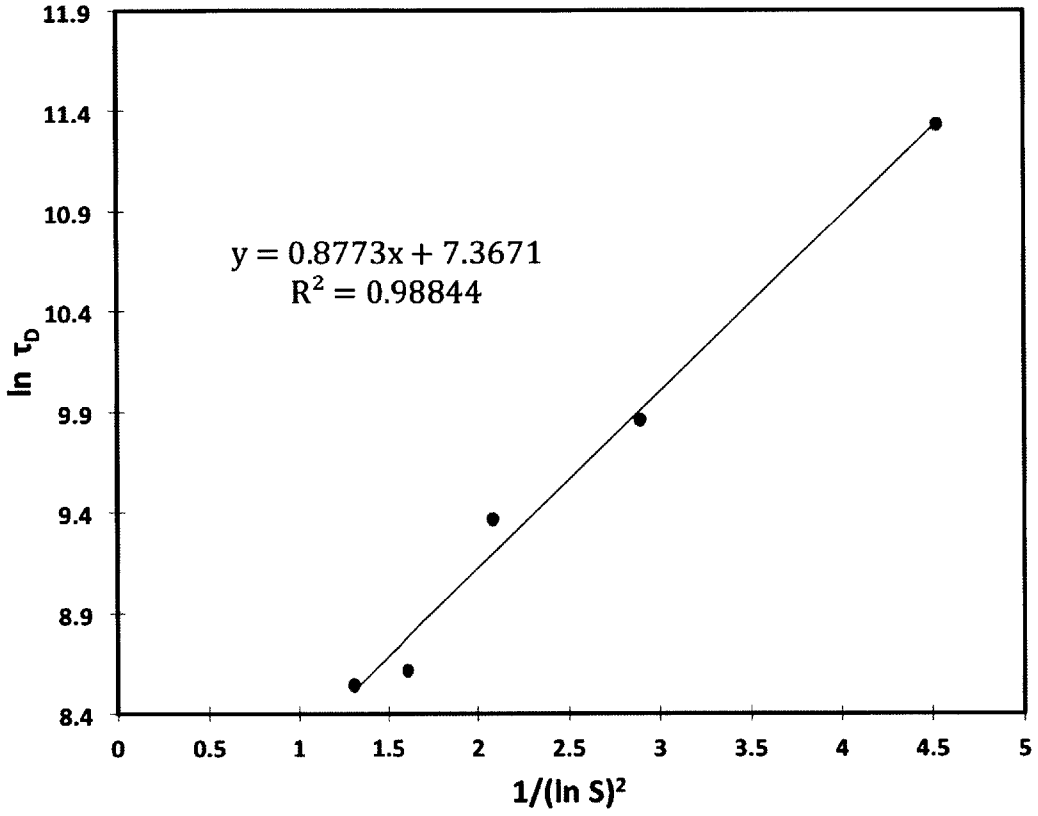

Figure 5.9: Classical Nucleation Theory Model of Results at 50°C

interfacial tension at 50°C as a function of the change in the contact angle is shown in Fig. 5.10.

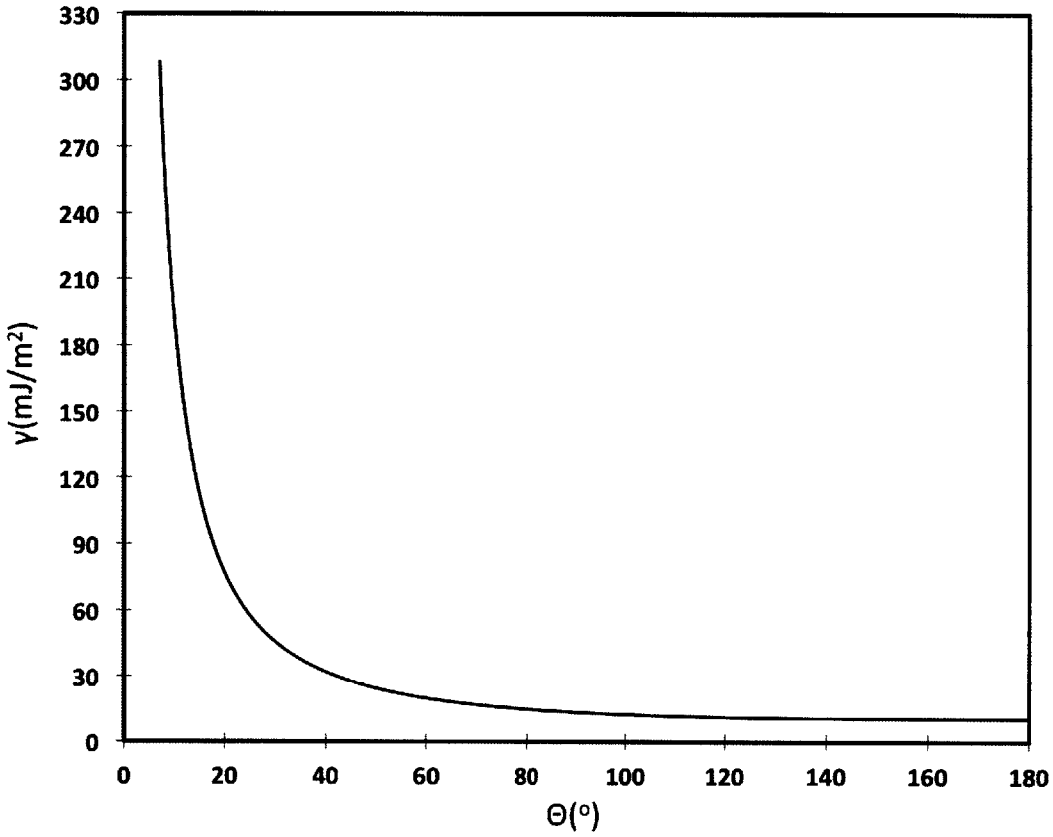

Figure 5.10: Interfacial Tension at 50°C as a function of contact angle

5.1.5 Modeling Results at 40°C

Figure 5.11 shows the data points collected at 40° C. A linear fit of the results is expressed by

$$\ln \tau_D = 7.7309 + \frac{0.8104}{(\ln S)^2}$$

By comparison with the model suggested by Mullin, $K_{40} = 0.8104$. The values taken by the

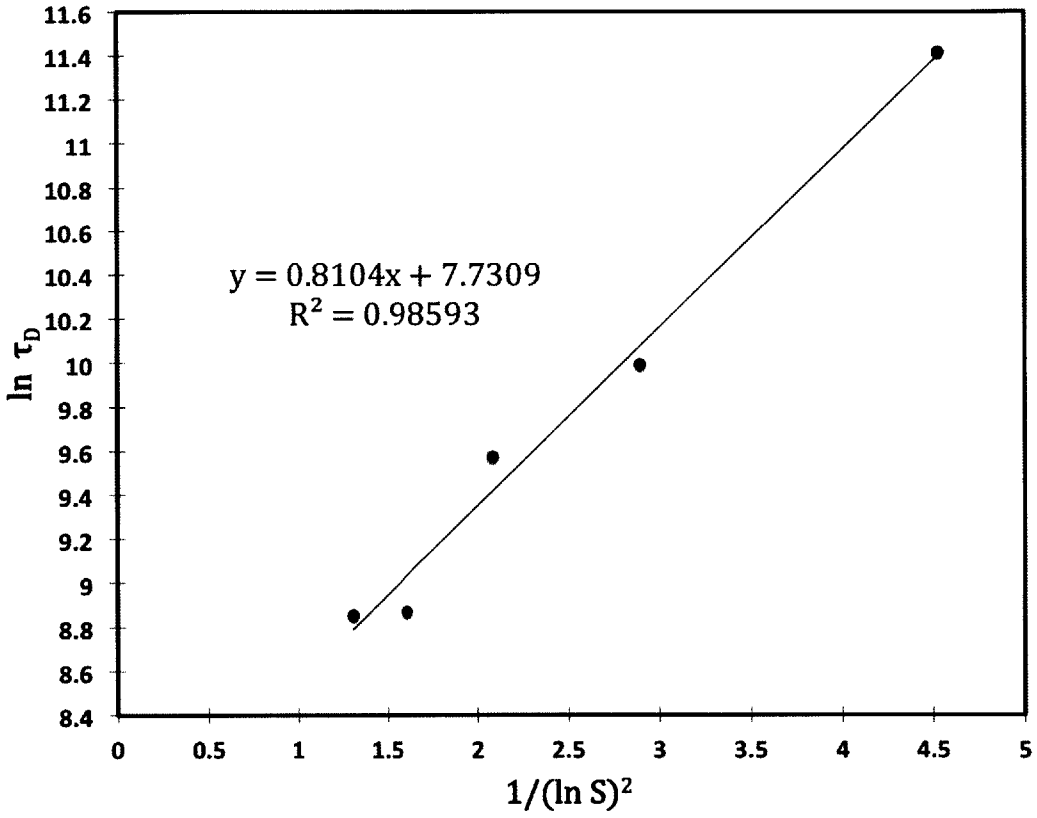

Figure 5.11: Classical Nucleation Theory Model of Results at 40°C

interfacial tension at 40°C as a function of the change in the contact angle is shown in Fig. 5.12.

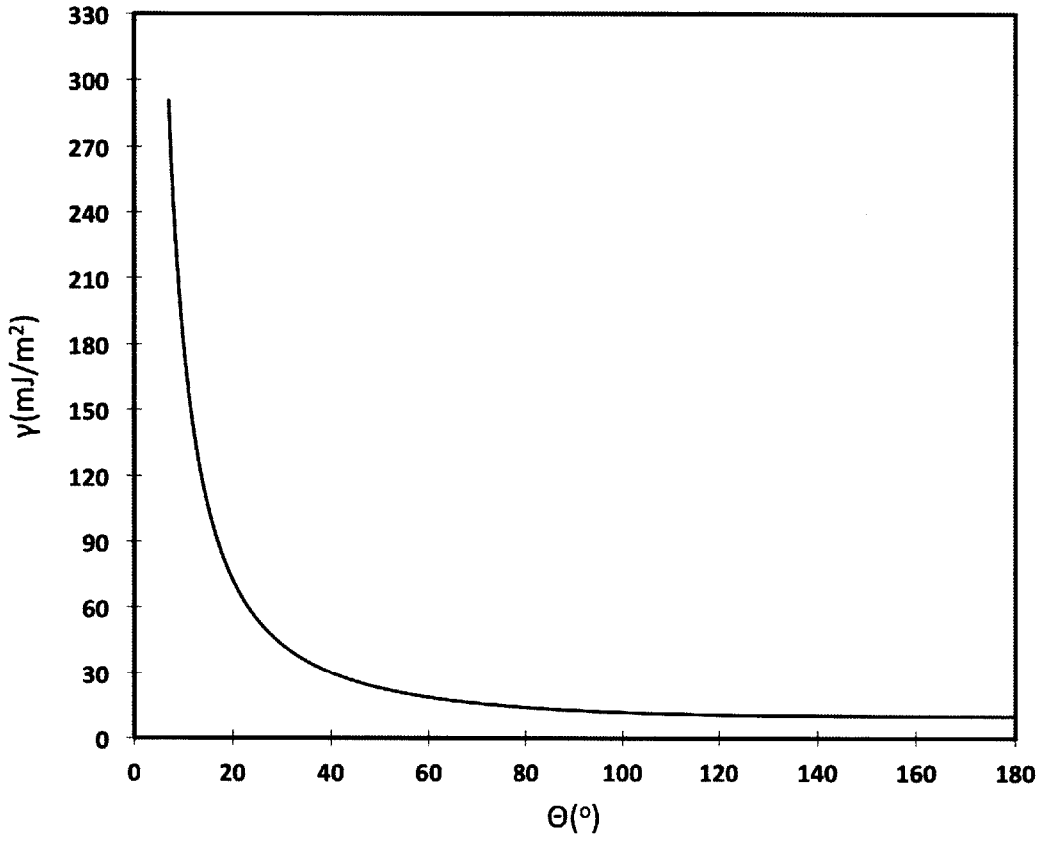

Figure 5.12: Interfacial Tension at 40°C as a function of contact angle

5.1.6 Comments on the Results

The results obtained for the linear fit of the data points are summarized in the following table.

Table 5.2: Model Parameters at Different Temperatures

Temperature (°C)	Coefficient of Determination	K
80	0.97219	0.4385
70	0.97537	0.6861
60	0.96345	0.8139
50	0.98844	0.8773
40	0.98593	0.8104

Using the coefficient of determination or R-squared as a measure of how well the data points are replicated in the model, it is obvious that the results fit the classical nucleation theory model of Mullin very well at the different test temperatures (R^2 is very close to 1). The slope K that is directly proportional to the third power of the effective interfacial tension and inversely proportional to the third power of temperature generally decreases with temperature, which is reflected in a slight decrease in interfacial tension. The value at 40°C does not fit the trend. 40°C is the maximum of the gypsum solubility curve, after which gypsum starts to exhibit a retrograde solubility behaviour. Whether this influences the K value or it is due to experimental variation cannot be inferred from this information.

Fig 5.13 shows a plot of the slope K versus T. A fourth degree polynomial fit suggests K is a function of T^4. Based on Eq. 5.7, in case the results at 40°C are not due to experimental error, this suggests that γ_{eff} is a function of $T^{2/3}$.

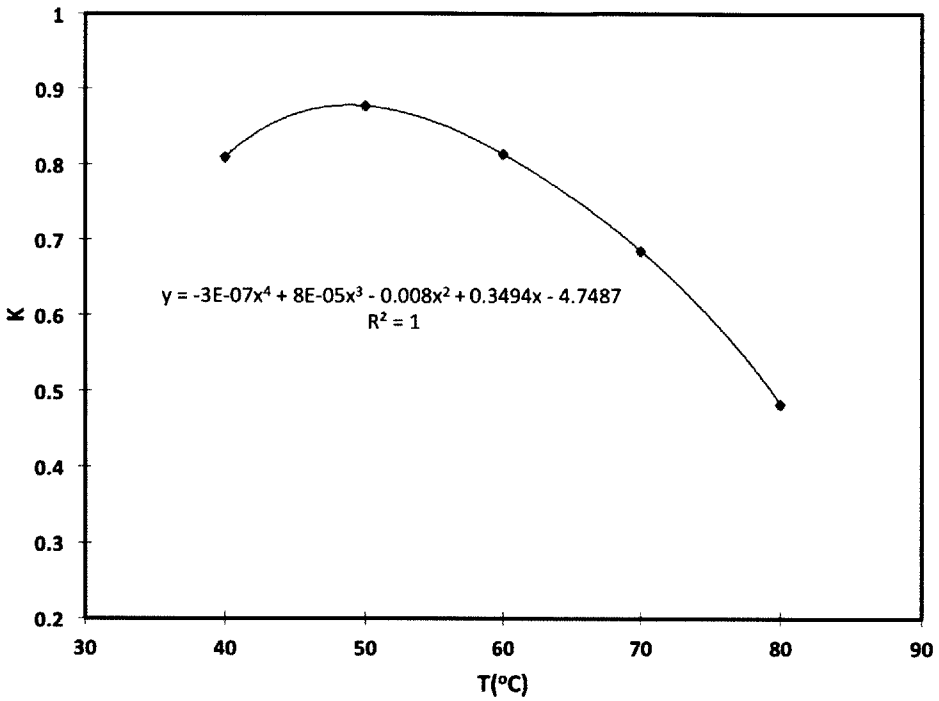

Figure 5.13: Change of Slope with Temperature

The linear plots are all shown in Figure 5.14. The lines get further with decreasing supersaturation. This is mainly because the effect of temperature on the time of induction is more significant at lower supersaturation indices. Values of interfacial tension calculated from the slopes of the linear fits are also plotted in Fig. 5.15. There is a very slight change in the values with temperature. Hence, temperature variation is not very significant.

The values of the interfacial tension calculated based on the model are within the ranges reported in literature. For surface nucleation, values of 7.9 and 14.6 mJ/m^2 have been reported by Linnikov et al. for laminar flow on a metal surface [53] and by Hasson et al. on a polymeric membrane surface [54]. Fahiminia et al. reported interfacial energy of a range 8-50mJ/m^2 for $CaSO_4$ crystallization under sensible heating conditions. [55]

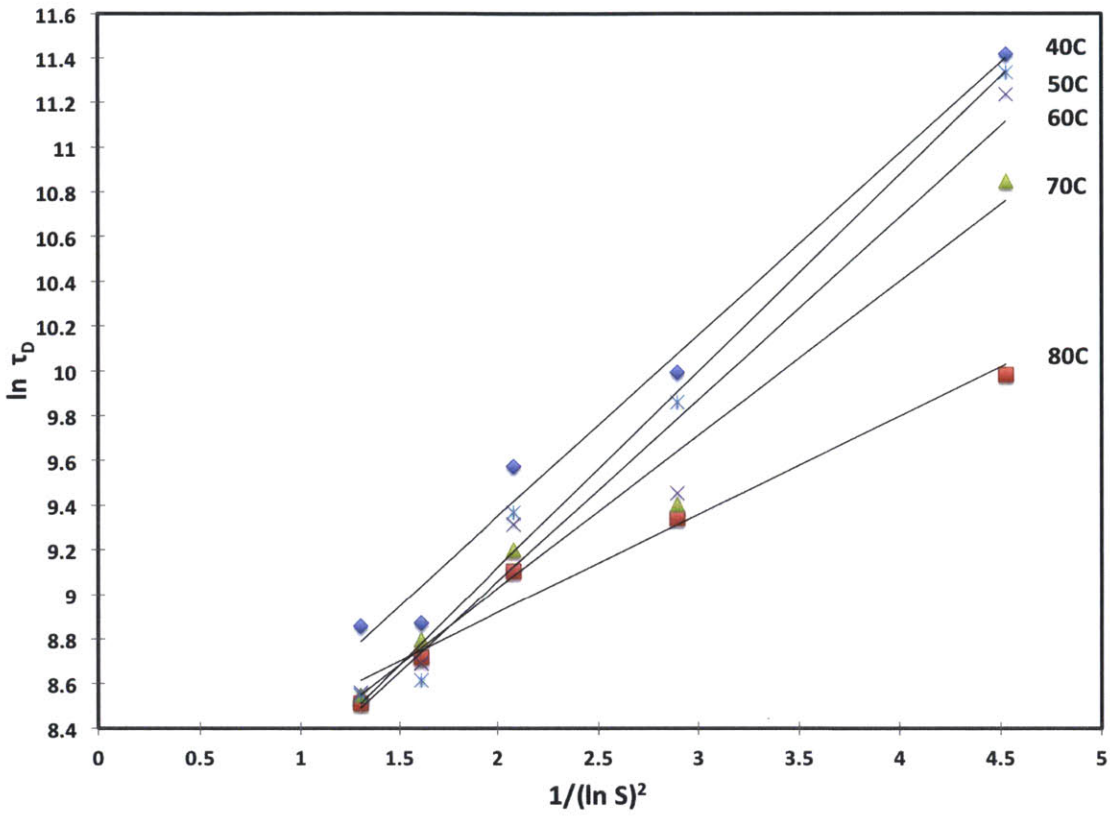

Figure 5.14: Classical Nucleation Theory Model of Results

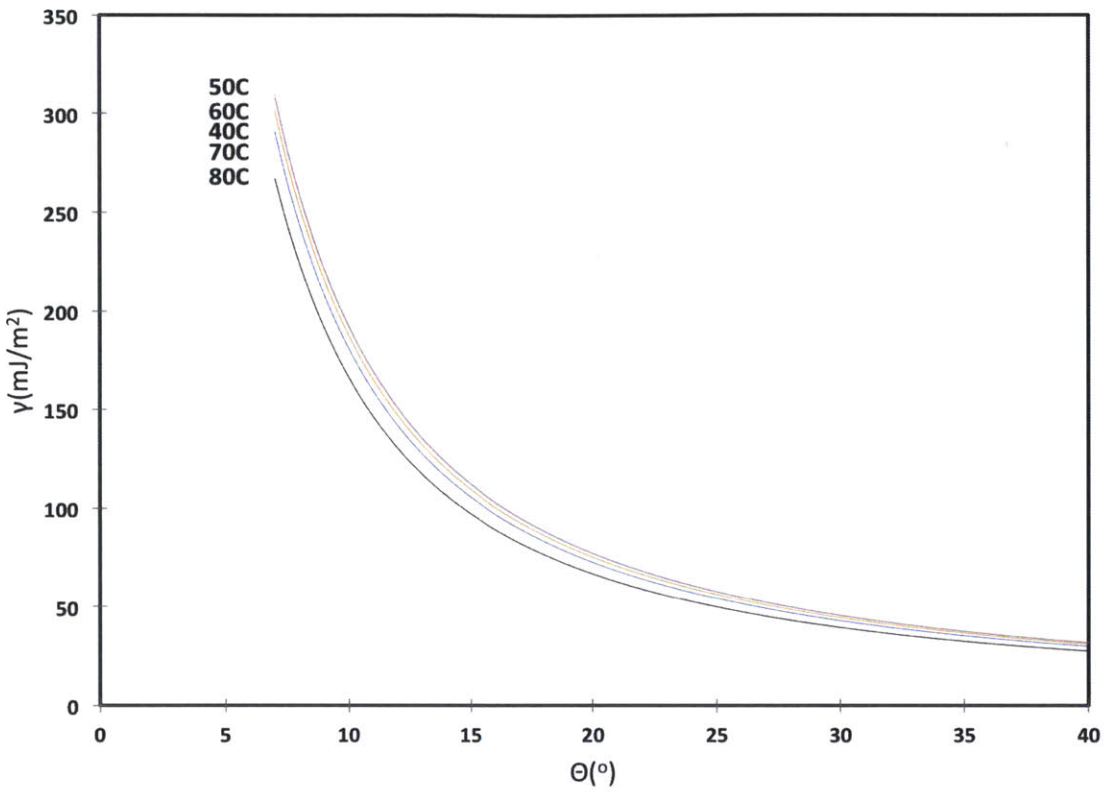

Figure 5.15: Interfacial Tension at Different Temperatures

5.2 Inferences for the Case SI=1.4

5.2.1 Mullin Model Extrapolation

Extrapolation of the linear fits as per the classical nucleation theory model suggested by Mullin reveals the following times of induction of gypsum for a supersaturation index of 1.4

Table 5.3: Expected Waiting Time at SI=1.4

Temperature ($°C$)	Expected Wait
80	41hr 34min ≈1.7 days
70	251hr 13min ≈10.5 days
60	620hr 36min ≈25.8 days
50	1019hr 55min ≈42.5 days
40	812hr 42min ≈33.8 days

To test the validity of the extrapolation, the experiment at 80°C was allowed 48 hours. At the end of the experiment, few crystals were visible on the surface of the plate. Given surface coverage considerations, the numerous crystals do not form what may be called a scale layer. Hence, at SI=1.4 even if the experiment is allowed enough time for crystallization to take place, the scaling rate is definitely lower than the one observed at higher temperatures.

One of the hypotheses that can be thought of to explain such behavior at relatively low temperatures is thermophoresis.

5.2.2 What is Thermophoresis?

Thermophoresis, also known as thermodiffusion or thermomigration is a phenomenon observed in a medium containing mobile particles that exhibit different reactions to a driving thermal potential. A visible example of thermophoresis is the migration of tobacco smoke aerosols down the temperature gradiant as they are attracted away from a hot cylindrical rod. Thermophoresis is labeled positive when particles move from a hot to a cold region and negative when the opposite takes place. The force associated with the phenomenon is called the thermophoretic force and it quantifies the presence of a temperature gradient.

5.2.3 Thermophoresis in the Scaling Context

In surface crystallization experiments, thermophoresis can be thought of as the phenomenon which is driving particles in the hot vicinity of the plate to migrate into a cooler region. As these particles depart away from the plate surface, they move from a region where their concentration is in a supersaturation regime to a region where they are in a subsaturation phase. This causes the crystals that form in the vicinity of the plate to redissolve into solution. After a while they rediffuse again to the hot region and thermophoresis continues to

occur. The forming crystals are not given enough time to stick to the surface. Therefore, a supersaturation region within the hydrodynamic (also thermal in the case of natural convection) boundary layer can be defined. In this sense, one can think of a supersaturation boundary layer.

A sample case at T=80°C and SI=2.0 is considered here and a plot displaying the supersaturation region within which a thermophoretic force drives particles out the hot vicinity is shown in Fig 5.16. The supersaturation region is colored in red.

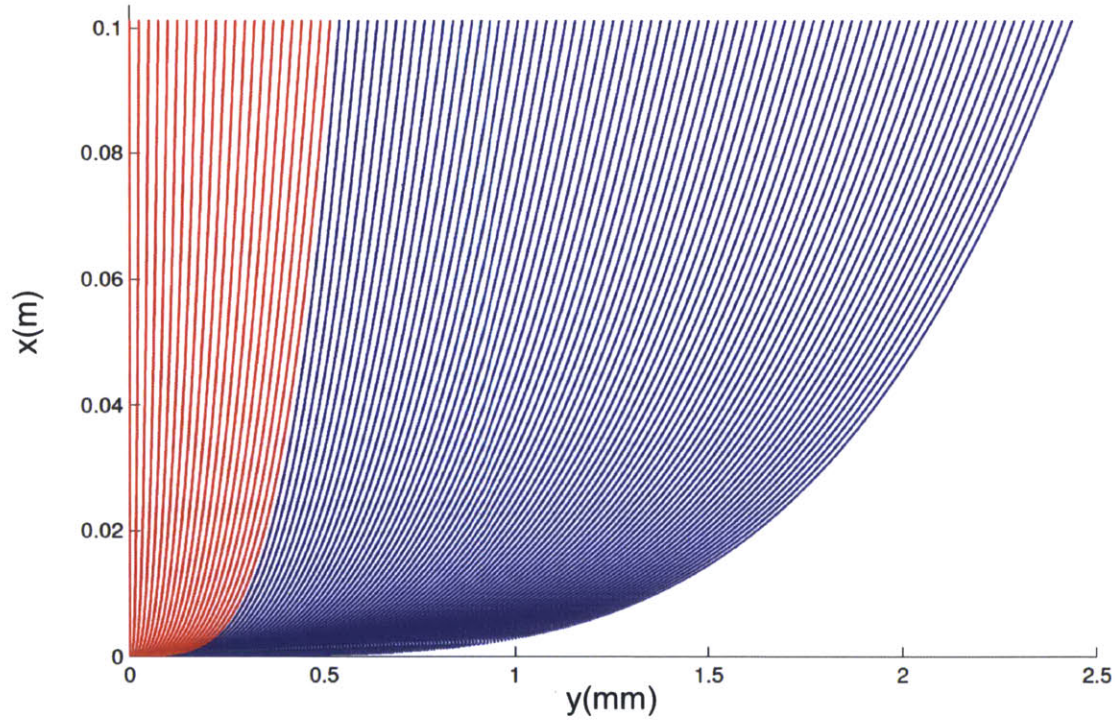

Figure 5.16: Supersaturation Boundary Layer at 80°C and SI=2.0

In order to define the two regions, the solution within the hydrodynamic boundary layer is depicted as a matrix of points. The thermal profile as per the integral method solution of natural convection is then found. The concentration at each point of the matrix is calculated based on a fit for the equilibrium solubility-temperature curve of gypsum.The used parabolic

fit is shown in the equation below.

$$C(i,j) = (-0.0602986T(i,j)^2 + 5.65504T(i,j) + 507.332) \times \frac{M_{\mathrm{CaSO_4}}}{M_{Ca}} \qquad (5.10)$$

where i and j represent the coordinates of the point in the matrix, C stands for concentration and T stands for temperature.

Finally, The calculated concentration is compared to the prepared concentration of the global solution. If the former is greater, the point is said to lie in a supersaturation region.

Chapter 6

Conclusions

The parametric study performed to measure the time of induction of gypsum scale on a heated copper plate emphasizes some established observations. Nucleation is promoted with higher surface temperatures and higher degrees of supersaturation. However, these two governing parameters are not independent in effect. This is because it was experimentallys shown that the impact of surface temperature becomes less significant with the increase of supersaturation i.e. when the solution becomes more saline. In this context, temperature does not have a singinifact effect on scaling that takes place in applications such as produced water or flowback water remediation.

Since the variation of the time of scale induction is in line with the reported trends at various flow conditions, it is important to conclude that behavior of calcium sulfate is not completely different in the case of natural convection conditions.

Mullin's classical nucleation theory provides an excellent model fit for the experimental results since $\ln \tau_D$ is a first order function of $1/(\ln SI)^2$. The slopes at different temperatures are used to calculate the interfacial energies between crystalline gypsum and the copper

surface. Values computed lie within the reported ranges. The interfacial energy is a strong function of the contact angle for which there is no direct way to compute.

Fouling analysis and model improvement has to stay in progress due to the complex nature of deposit formation and lack of reproducible measurement of fouling resistance. Many assumptions simplify the existing models, thereby not depicting very accurate approximations. Some of these assumptions are neglecting surface roughness (a perfectly smooth surface simply does not exist), neglecting the change in roughness with crystal formation (this certainly affects the rate at which other deposits form), neglecting any change in the working fluid's physical properties, neglecting any change in flow velocity conditions with change of contact area, assuming spherical molecules and neglecting the shape of deposits. Moreover, all the existing models account for one fouling mechanism.

Hence, more research has to be done in order to outline a model that accounts for changes in different properties at the surface as well as in the working fluid. Better understanding of coprecipitation of various salts is also important in order to be able to improve fouling mitigation in multiple salt applications. Moreover, while most of the research done in the field focuses on scale induction time, it is necessary to develop the technology that would assist in evaluating the initial and roughness delay times because nucleation starts then.

The adversity of the problem of scaling is reflected in both system heat transfer capacity and cost. The increase in cost is divided into increased capital expenditure, energy costs, maintenance costs, cost of production loss, and extra environmental management cost. In 1982, fouling costs accounted for 0.12-0.22% of the GNP of the USA (3680-7000 million dollars out of 3634000 million dollars) and 0.20% of the GNP of the total industrial world [5]. With the pressing need for more robust water remediation technologies and the increased usage of heat exchanger applications, the problem of fouling will exert more financial stress

on operators. Therefore, fouling mitigation has to be one of the most important focuses of energy research with the hopes that fouling gets demoted from its position as one of the unsolved heat transfer problems.

Appendix A

Scaling Experiment Photos

This section contains some images taken at different stages and conditions of experimentation.

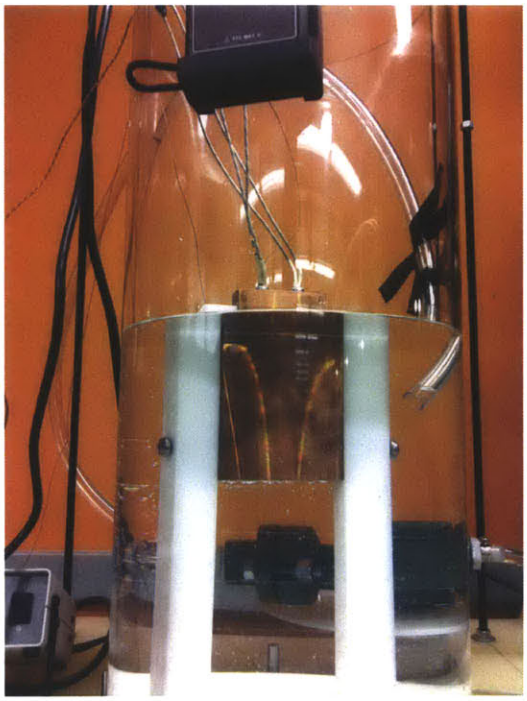

Figure A.1: Copper Plate Component System

Figure A.2: Recirculation Pump Component System

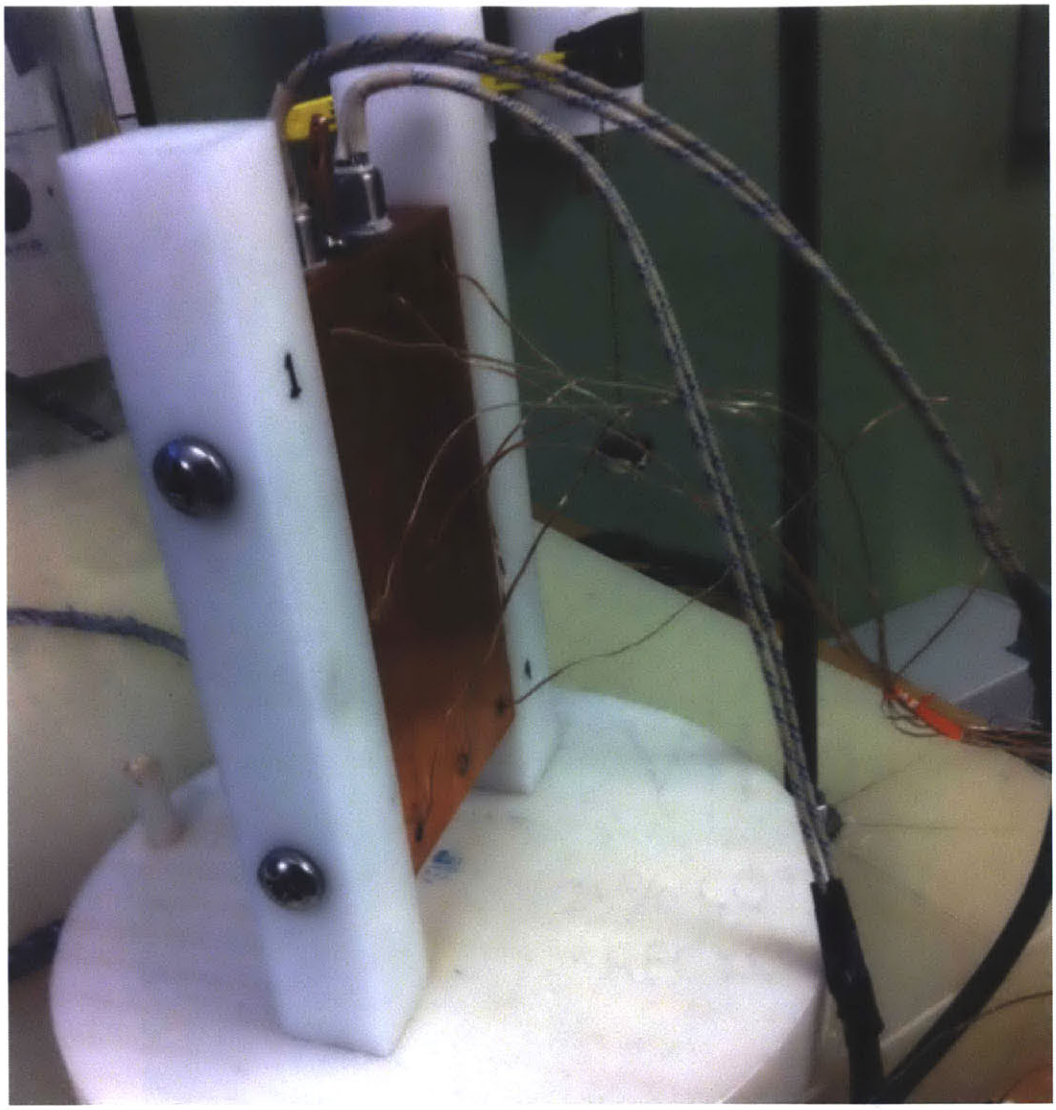

Figure A.3: Thermocouples and Cartridge Heaters

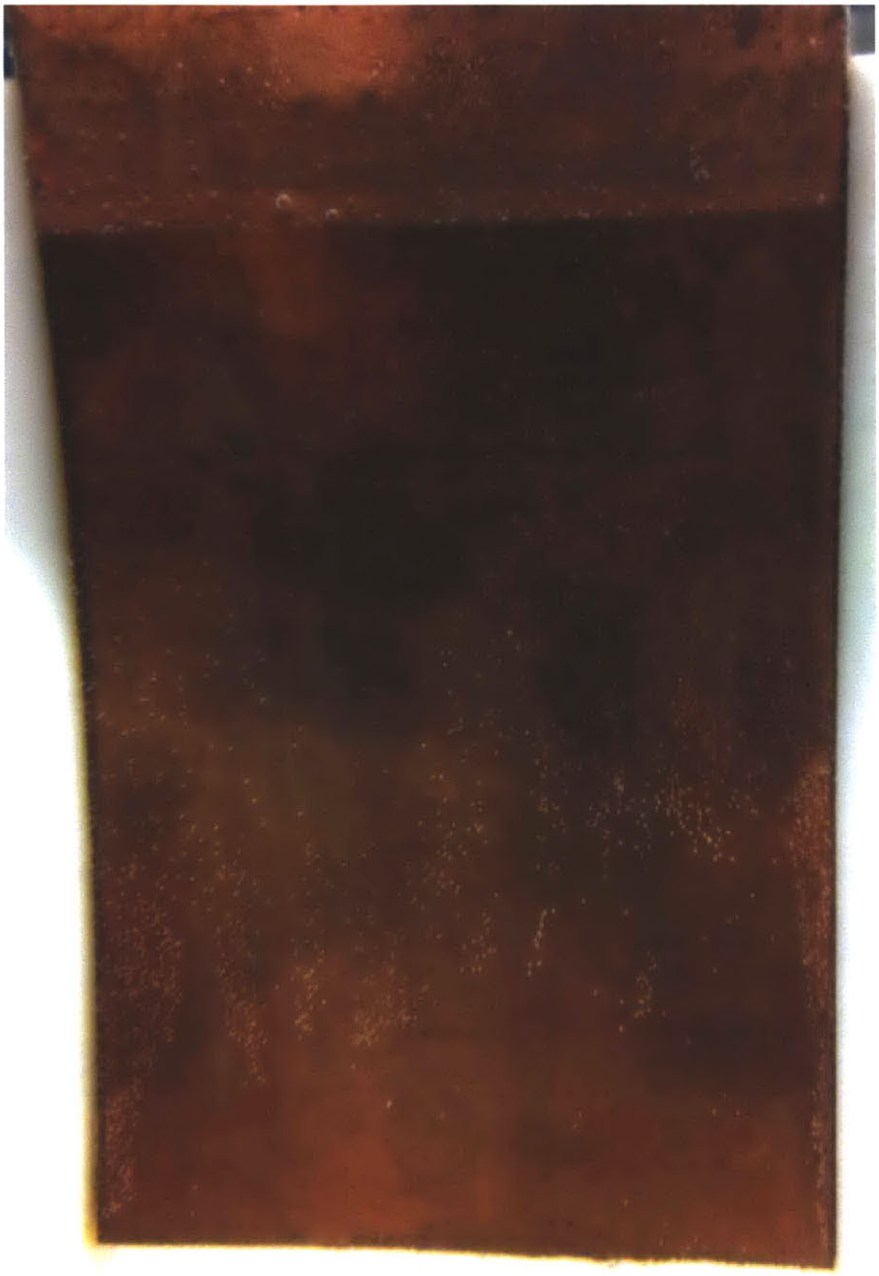

Figure A.4: Copper Surface at t=0

Figure A.5: Gypsum Inception Layer at T=80°C

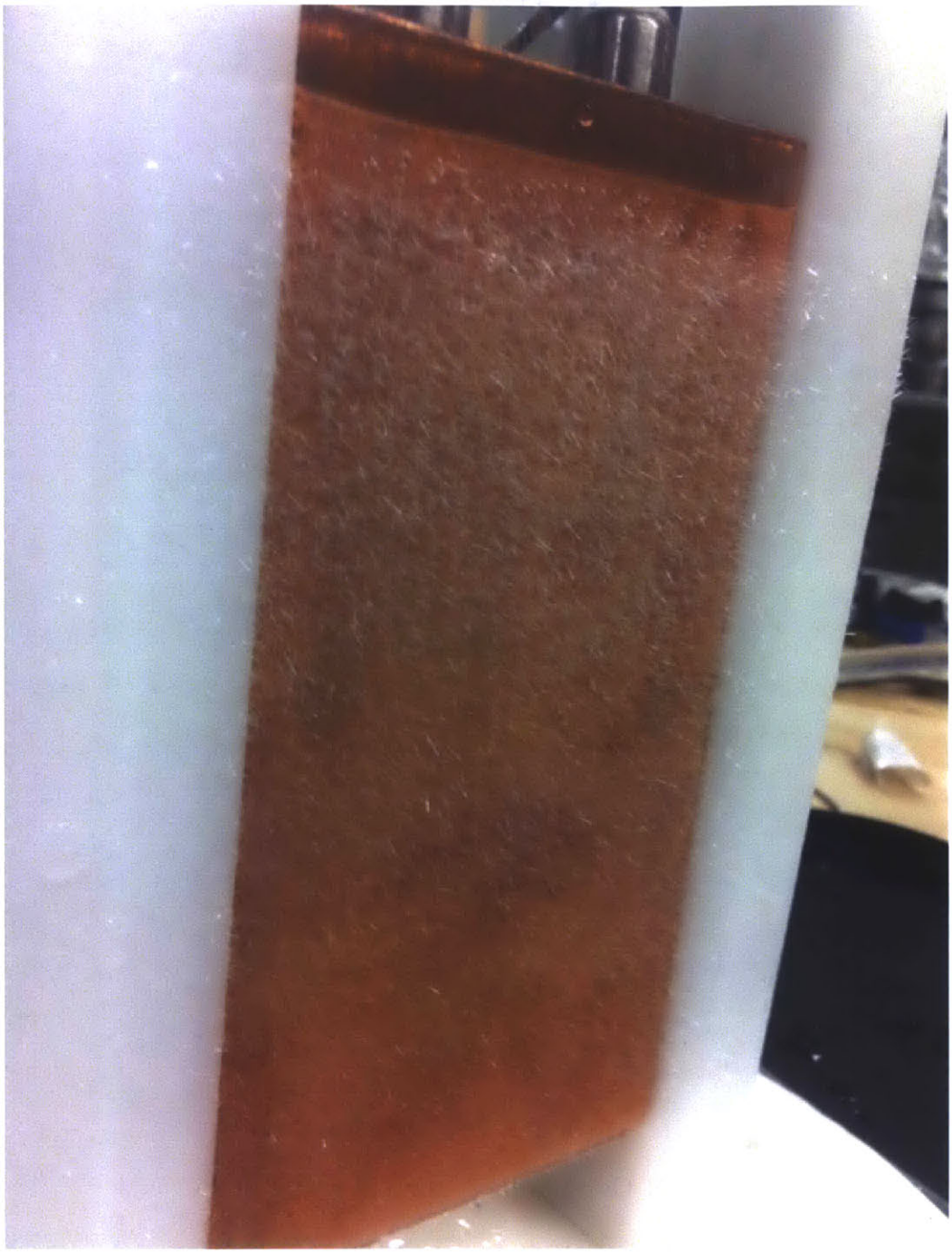

Figure A.6: Gypsum Inception Layer at T=70°C

Figure A.7: Gypsum Scale Layer at T=40°C and SI=2.4

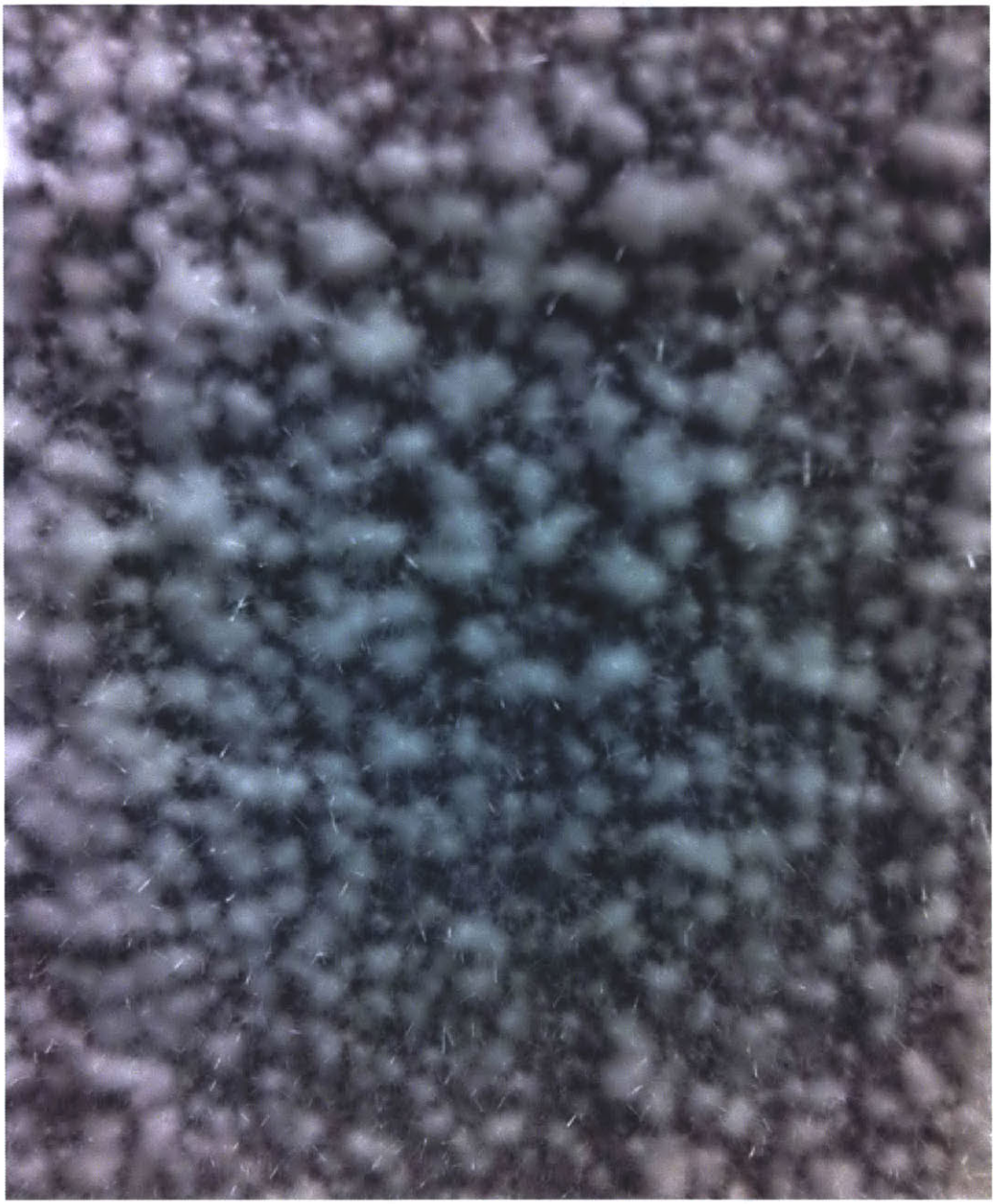

Figure A.8: Gypsum Scale Layer at T=50°C and SI=2.4

Figure A.9: Gypsum Scale Layer at T=60°C and SI=2.0

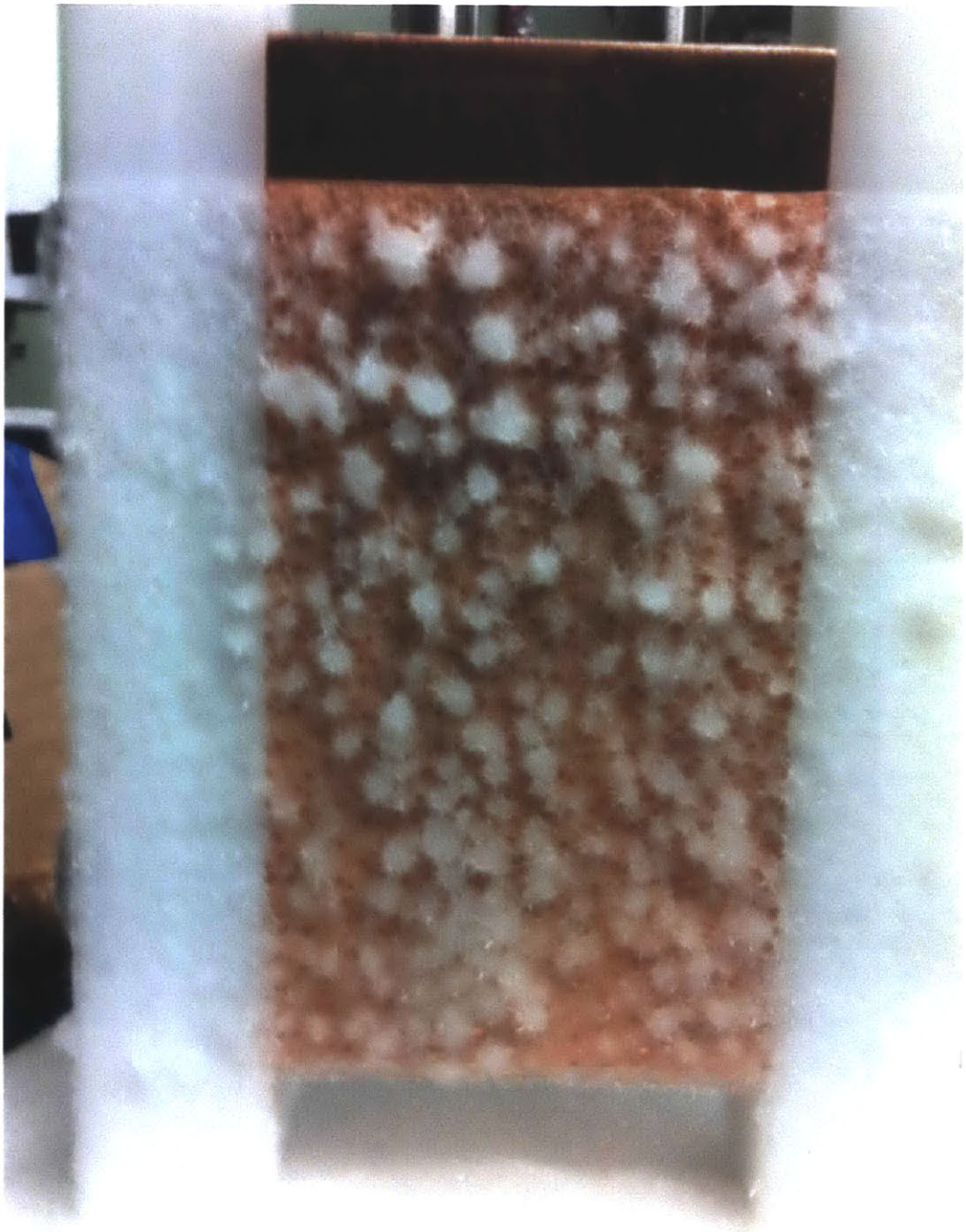

Figure A.10: Gypsum Scale Layer at T=70°C and SI=1.8

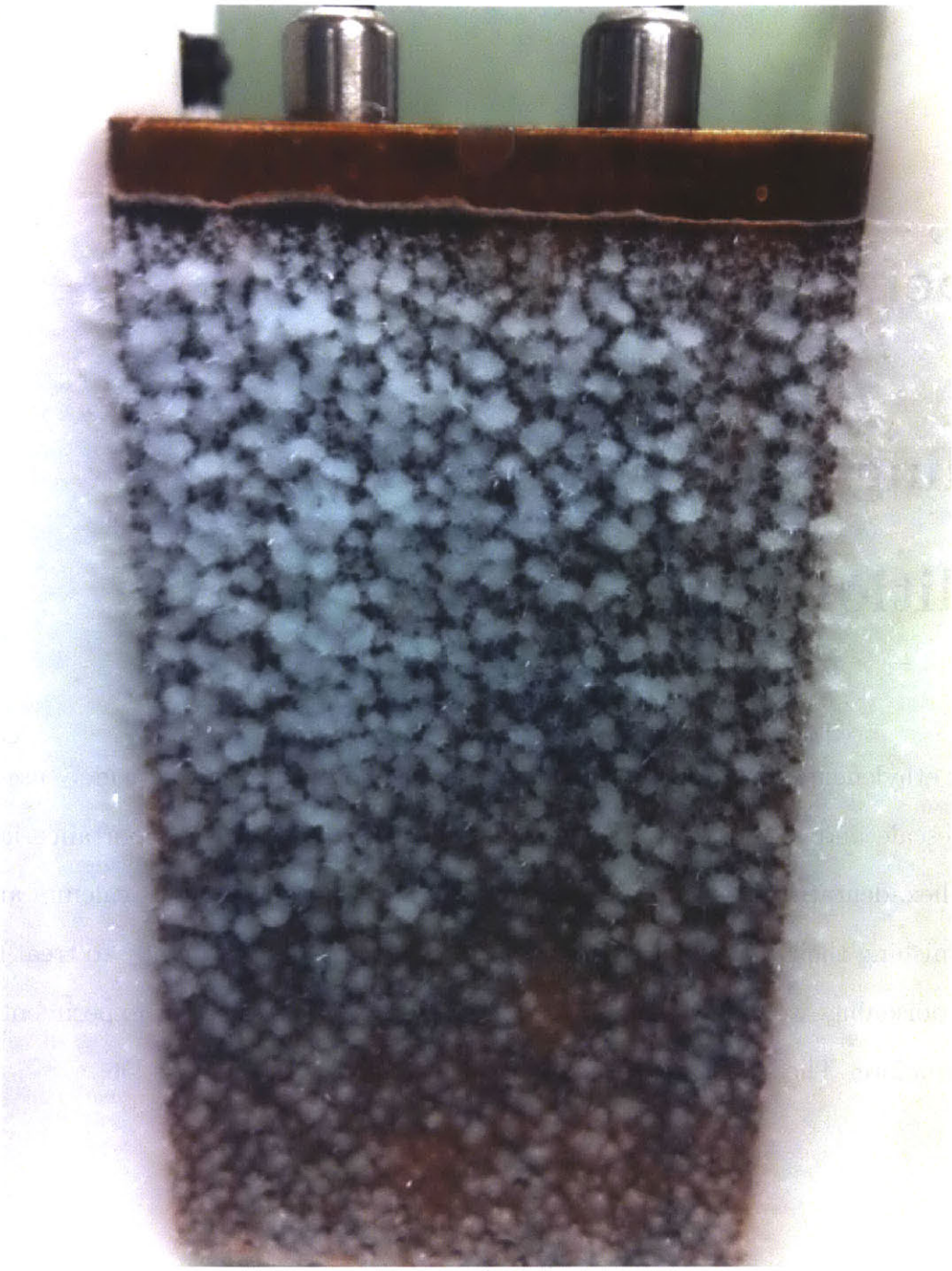

Figure A.11: Gypsum Scale Layer at T=80°C and SI=1.6

Appendix B

Scaling Mitigation with EDTA Addition

EDTA or ethylenediaminetetraacetic acid is a polyamino carboxylic acid widely used to dissolve limescale and as a chelating agent for medical treatment. Its importance lies in its role as a hexadentate ligand by which it can sequester metal ions such as calcium and ferric ions diminishing their reactivity. Analagous to its use in chelation therapy to treat mercury and lead poisoning, we used EDTA to delay gypsum scaling in the same experimental setup described before. The structural formula of EDTA is shown in Fig. A.1 [56].

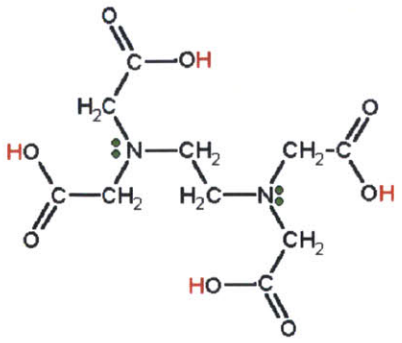

Figure B.1: EDTA Complex

Calcium ions that can precipitate from solution to produce gypsum scale are sequestered by the addition of EDTA. The multi-dentate ligand of EDTA bonds with calcium to form a non-scaling ionic complex. Hence, calcium ions stay in solution.

The experiment was performed at T=80°C and SI=4. Without adding any EDTA, scaling started forming only 10 min after starting the experimental run. However, with the addition of EDTA no scale formed even after 30 hours of operation.

This simple run shows that the usage of EDTA is a very promising technique for fouling mitigation especially that EDTA recovery is possible through pH adjustments. Fig. B.2 and B.3 show the copper plate without and with EDTA addition respectively. Fig. B.4 shows a blue color solution that resulted from EDTA ion confinement.

Figure B.2: Gypsum Scale Layer at T=80°C and SI=4.0 without EDTA

Figure B.3: Gypsum Scale Layer at T=80°C and SI=4.0 with EDTA

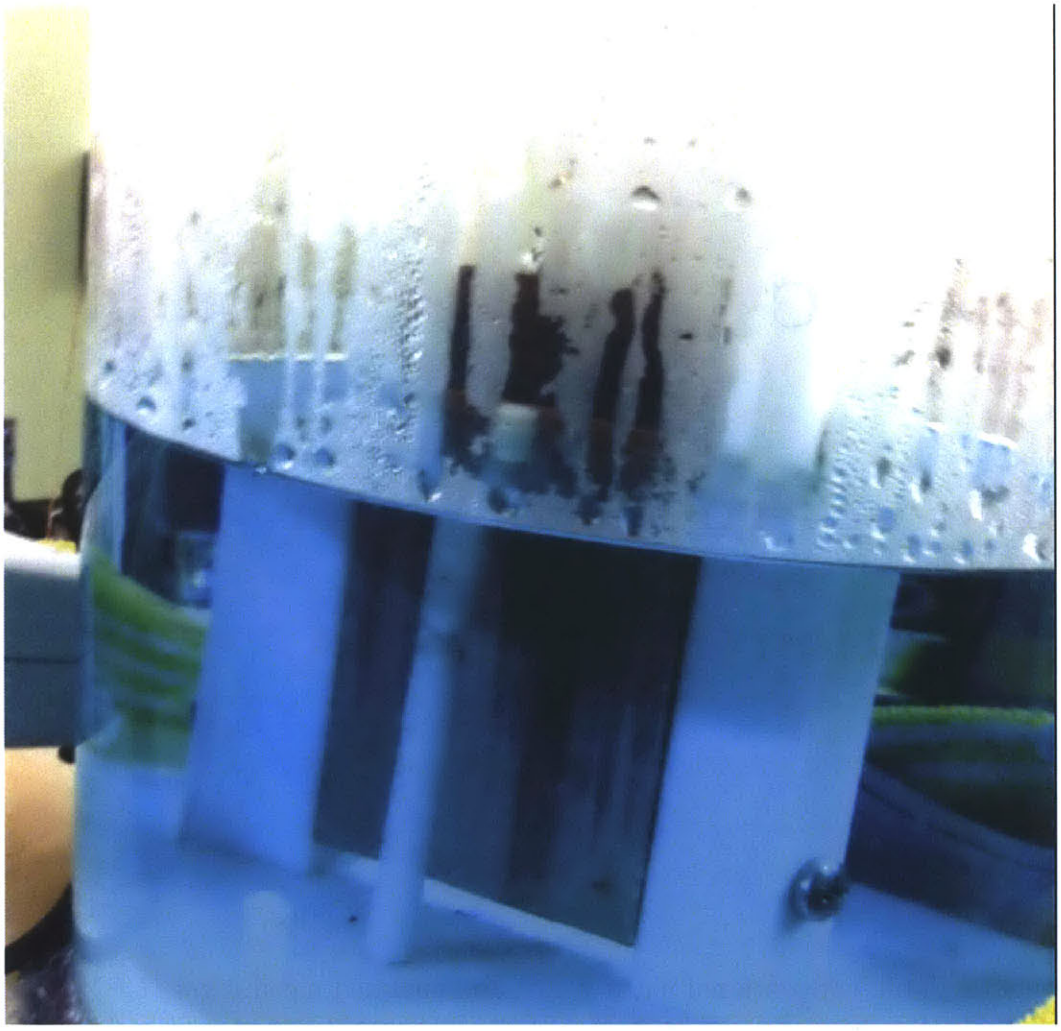

Figure B.4: Solution Resulting from EDTA Ion Caging

Appendix C

Review of Produced Water Remediation Technologies

C.1 Abstract

The production of oil, conventional natural gas, and coal bed natural gas (CBNG) results in the co-generation of substantial flows of water from the hydrocarbon-bearing formation [57]. Produced water constitutes the largest volume of waste streams associated with oil and gas extraction techniques. Produced water is generally a mixture of dissolved and dispersed oil compounds, dissolved solids, toxicity, organic and inorganic compounds, along with some radioactive material. Proper remediation of produced water faces a number of challenges, chief among which are efficient oil-water separation and coping with highly saline water. In fact, due to the increasing waste volume worldwide, the issue of produced water has lately developed as a critical environmental concern especially with the notorious image oil companies have encountered when it comes to public reception and international missions of ensuring affordable and abundant energy supplies. Historically, produced water was disposed in evaporation ponds, but this is no longer acceptable environmentally and socially.

Discharging produced water has to meet very strict local or international standards due to the abundance of toxic compounds. This study presents other produced water treatment options through some stand-alone technologies as well as other hybrid systems.

C.2 Definition

Different definitions have been associated with the term 'produced water'. The US Environmental Protection Energy (EPA 1976) defined produced water as all waters and particulate matter associated with oil and gas producing formations [58]. According to the US Department of Energy (DOE) the term 'produced water' has been assigned to water trapped in underground formations, and brought to the surface along with gas or oil [58].

To understand other definitions, a new term has been defined in gas extraction industries, which is "flowback water". Flowback water is the murky salty water produced as a result of hydrofracking-the propagation of fractures in a rock layer caused by a pressurized fluid- in natural gas wells. Flowback water is a mixture of both the frac load recovery that returns to the surface and the produced water. According to Horn et al. [59], when the flowback volume reaches 100% of the fracturing fluid volume it is then subsequently referred to as produced water.

FakhrulRazi et al. [60] describes three origins of saline water that are (1) from above or below the hydrocarbon-bearing strata, (2) from within this zone, and (3) from the injected additives during production activities. This last category is called the formation water and is termed produced water when saline water mixed with hydrocarbons comes to the surface [61].

There are several factors that can be used in order to label water as being "flowback" or "produced". First, it appears that financial reasons are the most widely used to make the distinction. According to this rationale, water produced during well completion stages is called flowback water and the well completion budget should cover the associated costs. In times of under production, the water is called produced and the associated costs are nothing but operating costs. Second, some gas production companies use a time factor. For example

30 days can be used as a demarcation period. During this period the flow rate typically drops off. Third, some producers use volume considerations or how much they are getting back as a proportion of the amount of fracturing fluid being injected. It may be 100% as per the definition presented by Horn et al. [59].

C.3 Produced Water Characteristics

Produced water is a mixture of tens of different compounds rather than a single commodity. Hence, the properties of a sample of produced water are to vary considerably. Some of the factors that influence the physical, chemical, and biological properties of this water are:

- Geographic location of the well: geography affects the properties of produced water at different levels. One of the major sources of water that leaks to underground rock layers is meteoric, which is represented by rainfall. Rainfall varies in chemistry and volume relative to geographic location; thereby variably influencing properties of water produced during well completion stages.

- Geological formation with which the produced water has been in contact for thousands of years [62]: Produced water forms in the zones within and around the hydrocarbon bearing layers. The properties of these layers vary with different geological formations shaped with years.

- Type of hydrocarbon being produced: properties of produced water associated with extraction of crude oil are significantly different from those associated with production of natural gas. Moreover, within the same category the molecular weight of hydrocarbons being extracted is of chief importance.

- Age of reservoir: as oil fields age, water production increases. This explains the high water to oil ratio of the US.

- Water injection: water flooding, during production processes, into the formation layers as part of enhanced oil recovery, dramatically impacts the properties of produced water.
- Well development procedures: companies depend on a host of activities engaged within well development and maintenance procedures, all making the variation in composition of produced water expected.

It is worth mentioning that proper depiction of the characteristics of produced water in certain field will help optimize production. Breit et al. states that well-rounded understanding of produced water constituents greatly helps decide on what kind of scale inhibitors or treatment chemicals are optimal for a certain reservoir [63], and as well can help detect potential problem areas. At another level, constituents of the produced water have to be understood for regulatory compliance.

C.4 Produced Water Chemistry

Produced waters are highly varied in composition [57]. Selecting water management or disposal options is highly dependent on the type of components present in the water. Different onshore and offshore activities give the most attention to oil and grease (O&G) as the most common constituent in produced water. Salt content or salinity, expressed as TDS (Total Dissolved Solids) is a primary constituent of produced water in onshore production [62]. Generally, constituents can be divided to whether they are organic or inorganic, which in turn are categorized into soluble (scale, grit, colloids) or insoluble (cations and anions). Produced water is usually circum-neutral with pH values between 6 and 8; buffering is provided through the presence of bicarbonate [57] (Produced water from gas production are more acidic, pH=3.6) Acids or caustics added as part of chemical treatment will definitely shift the pH values. Also, most produced waters are much more saline than seawater.

In the production of crude oil, produced water is mainly a mixture of organic and inorganic compounds. Tibbets et al. states that in offshore wells, at the time of discharge, these compounds can be at different physical states, like solution, emulsion, adsorption, or suspension [64]. Solids, bacteria, seawater added to maintain reservoir pressure, chemical additives, and drilling cuttings are all potential constituents. Some of the treatment chemicals are scale and corrosion inhibitors, emulsion breakers, biocides, coagulants, flocculants, oxygen scavengers, clarifiers, and solvents to reduce paraffin deposits (Cline 1998)

In gas production wells, produced water is separated from gas during production activities and water injection is not used. Hence, the produced water that comes to the surface is a mixture of condensed water and formation water. Toxicity is represented by a high content of low-weight aromatic hydrocarbons like benzene, toluene, ethylbenzene, and xylene (BTEX). This toxicity is much higher than that produced in oil production wells. Jacobs et al. shows that water produced from gas/condensate platforms is 10 times more toxic than that produced from oil platforms [65]. Well stimulation, gas processing, and treatment chemicals include dehydration chemicals and H_2S removal helpers that might leave brines and mineral acids in produced water.

C.5 Constituents of Produced Water from Conventional Oil and Gas Wells

The major compounds of produced water include:

- Dissolved and dispersed oil compounds: the amount of oil present in produced water before treatment is a function of composition, pH, salinity, temperature, oil to water ratio, type of oilfield chemicals, and quantity of various stability compounds like waxes and fine solids [66]. Oil is a mixture of hydrocarbons like BTEX, polyaromatic hydro-

carbons (PAHs), naphthalene, dibenzothiophene (NPD) and phenols. These are not all dissolved in water.

⋆Dissolved oil: Polar compounds of the oil mixture are water soluble. BTEX and phenols are the most soluble in water [67]. Aliphatic hydrocarbons, carboxylic acids, organic acids such as formic and propionic are typically counted in soluble oil compounds [68].

⋆Dispersed oil: This includes small suspended oil droplets, whose volume depends on the shear history of the droplets, interfacial tension between oil and water [68] and oil density. Examples are PAHs and heavier alkyl phenols.

- Dissolved Formation Minerals: These are all inorganic compounds like

⋆Cations and Anions: Some Cations are monovalent like sodium Na^+, potassium K^+; others are multivalent like calcium Ca_2^+, magnesium Mg_2^+, barium Ba_2^+, and iron(II) Fe_2^+. Examples of anions include chloride Cl^- , sulfate SO_4^{2-}, and carbonate CO_3^{2-}. These ions influence salinity, buffering capacity and scale potential [66].

⋆Heavy metals such as Cadmium, Chromium, Copper, Lead, Mercury, Nickel, Silver, and Zinc.

⋆Naturally Occurring Radioactive Material (NORM): the primary radioactivity source in water is the radioactive ions of radium that co-precipitate with other types of scale, the most common of which is Barium Sulfate. 226Ra and 228Ra are the most abundant NORM in produced water [69]. In the North Sea, concentrations range from 0.3 to 21 Bq/L [70].

- Production Chemical Compounds:

⋆These are the chemicals added to the well for different reasons, like enhanced recovery, pressure maintenance, scale inhibition, flocculation enhancement, gas processing, or well simulation. Examples are biocides, antifoam, asphaltenes, waxes, emulsion

breakers, alkylbenzen sulfonate, and alkyldimethylbenzenylamonium. Concentration is as low as 0.1ppm [62].

- Production Solids: These include a wide spectrum of solids that appear in water throughout production and extraction. Examples are precipitating solids, like sand and silt, carbonates, proppants, and corrosion products. Concentrations range from insignificant to a solids slurry and oily sludge is sometimes formed in production equipment, case in which maintenance is required [62].

- Scales: Scale is formed when ions in the supersaturated water react to form precipitates. Examples include calcium carbonate, barium sulfate, calcium carbonate, iron sulfate, and strontium sulfate. The disadvantage of scale lies with clogging flow lines, and forming emulsions that need be broken.

- Bacteria and BOD: Bacteria can clog lines and produce H_2S which is corrosive. Biological analysis indicates that there are 50-100 cells of microorganisms per mL [71].

- Sulfates: Sulfates control the solubility of other ions such as calcium.

- Dissolved gases: Carbon Dioxide, Oxygen, and Hydrogen Sulfide are common gases in produced water.

C.6 Volume of Produced Water

Produced water volumes increase as oil wells get more mature. That's why the water-to-oil ratio has significantly increased recently. Studies associated with global water production onshore and offshore, have estimated water production at 250 million barrels per day compared to 80 million barrels per day of oil. This represents a water-to-oil ratio of 3:1, i.e. a 70% water cut. This water cut is continuously increasing, driven up by maturity of wells [72].

In the US, this ratio is estimated to an average of 7:1, and in some very old wells, it is 50:1. Offshore and onshore production of water is shown in Fig C.1 [72].

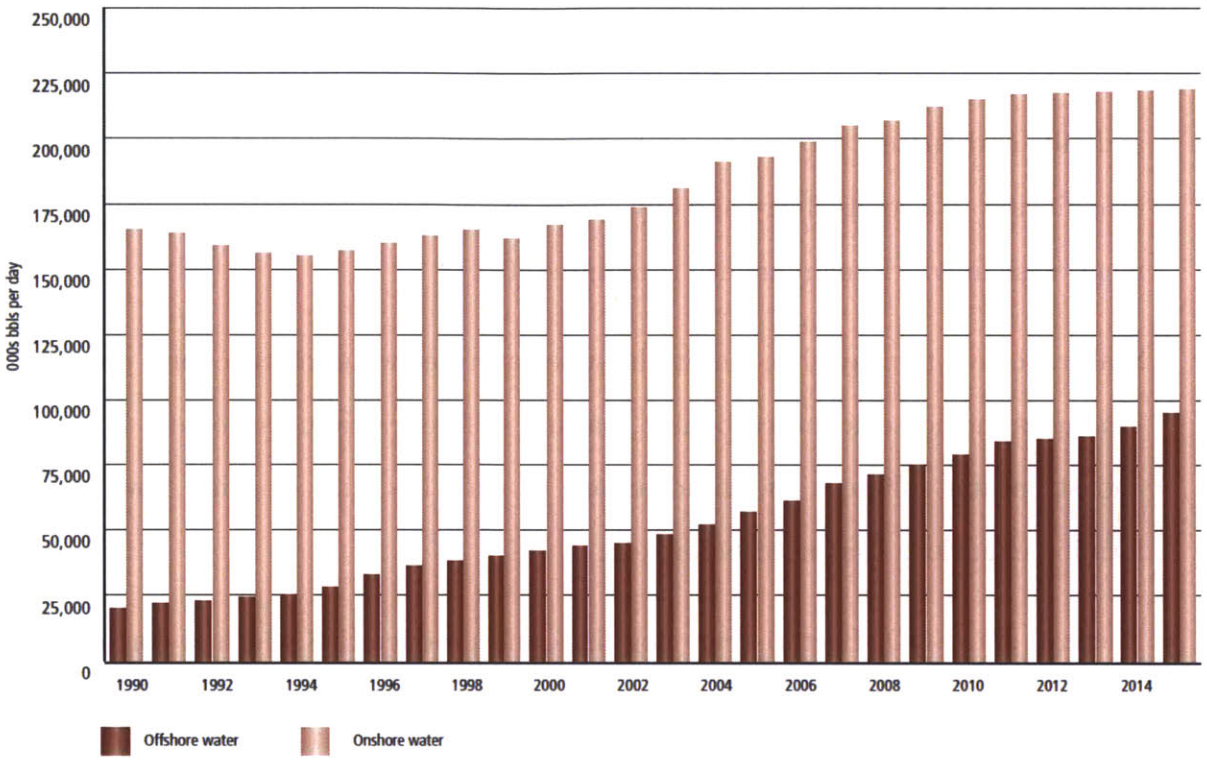

Figure C.1: Onshore and Offshore Water Production

C.7 Factors Affecting Volume of Produced Water

The volume of produced water is a function of a number of factors of different natures. These factors were all presented in Reynolds et al. [73]:

- Method of well drilling: produced water is generated at higher rate in horizontal wells than vertical ones, at a similar drawdown.
- Location of well within homogeneous or heterogeneous reservoirs
- Type of completion: open hole method avoids drilling into water, while perforated completion method offers a higher degree of control

- Type of water separation technology: different methods are used to reduce the volume produced and reduce lifting costs, such as using gelled polymers, and reducing beam pump lifting costs.

- Water injection for enhanced oil recovery: on the purpose of increasing oil production, producers flood water into the well. With time, the amount to be injected increases even more, and consequently, the amount of produced water steadily increases.

- Poor mechanical integrity: corrosion or wear cause many mechanical problems with the casting holes, thereby leading to more water entries. Other mechanical flaws include splits caused by flows and excessive pressure.

- Geological formations and underground communications: these problems might happen near wellbores and include channeling, barrier breakdowns, and fracturing out of zone.

C.8 Impacts of Discharge

The constituents of produced water pose a major threat on the environment if produced water is discharged onto open resources. Dumping of produced water will significantly threaten aquatic life and crops if it is discharged to a river, or used for irrigation. Different factors define the degree of seriousness, some of which are temperature, pH, dilution, precipitation, adsorption, and content of dissolved organic material.

Discharge of produced water into marine or terrestrial environments, increases salinity that is a major contributor to toxicity, heavy metals that adversely affect aquatic life, treatment chemicals that accumulate in marine sediments, and risky radionuclides.

C.9 Produced Water Management

The decision on the way produced water should be managed has to be made in accordance with technical feasibility, site location, cost, regulatory compliance, and availability of necessary equipment and infrastructure. Veil et al. proposes a hierarchy for taking the decision, which includes produced water minimization, reuse and recycling, and disposal as the last option [62].

C.9.1 Production Minimization

In order to minimize produced water volumes, water needs to be restricted from entering the wellbore. Typically, water enters due to a pressure gradient that occurs when hydrocarbons are extracted from hydrocarbon-bearing strata. Hence, strategies targeted to minimize volumes of produced water have to be able to block the water from entering the hydrocarbon zone. Some mechanical blocking devices may be used to achieve so. Examples include straddle packers, cement, bridge plugs, infill drilling, sand plugs, tubing patches, and pattern flow control [74]. Moreover, shut-off chemicals that block fractures or water channels may be used. Most of the times, these chemicals are in the form of polymer gels, or gelants that selectively enter pathways and replace water.

At another level, volumes of produced water can be minimized by keeping water that already entered the wellbore from reaching the surface. This can be accomplished through a dual completion well technique proposed by Wojtanowicz et al. primary completion is done at the zone of high oil production, and the secondary at the zone of high water production, the two being separated by packers. Oil is driven up to the surface, while water is pushed

down to underlying formations. Two separate pumps and strings are used here. This process is often referred to as downhole water sink. Another option is to use downhole oil-water separation techniques, by which oil is separated from oil in the wellbore itself rather than after extraction. After this separation, oil is lifted by a pump to the surface and water is injected underground at the same time. A similar technique has been used in gas wells.

C.9.2 Reuse and Recycle

Sometimes, produced water can be used directly without treatment, particularly when it is clean to start with (like in some cases of CBM water) or the target use does not require high water quality (industries, or water flooding operations). In many other cases, produced water has to be treated before meeting its end use. The cost factor is very important to consider in these cases. Some of the beneficial uses of this water include:

- Underground injection for enhanced oil recovery: In the US, 71% of the water injected underground is used to maintain pressure or hydraulically drive oil up to the surface, while the other 29% is sequestered in non-producing formations [62]. In this case, produced water is employed as a resource and no longer considered a waste.
- Injection for future use: This is known as aquifer storage and recovery.
- Use by animals: Animals can tolerate some level of contaminants in their water; hence, some treatment of produced water may make it usable by livestock as a source of drinking water, or as a habitat as in the case of fish.
- Irrigation of crops: Some pretreatment is necessary in this case because there are ions that have adverse effects on the healthy growth of plants.
- Rangeland restoration

- Industrial use: Examples include dust control, vehicle and equipment washing, drilling fluids, fire control, and use for power generation.

It is noteworthy that this is a very important topic of research, because the value of water increases with its scarcity. Hence, in countries where water resources are dwindling, cost-effective usage of produced water might be a viable valid option.

C.9.3 Disposal

Some oil or natural gas production companies dispose of produced water by re-injection into non-producing formations. Others try to discharge it to nearby water bodies or even the ocean if they are allowed to. Whether or not water has to be treated before disposal is a study subject to a number of factors, the most important of which is the regulations set by a country or defined by international laws.

C.9.4 Produced Water Treatment

Treatment is considered the healthiest and most effective way of managing produced water even though some treatment technologies may be energy and cost intensive. Typically, treatment is considered to meet beneficial use effluent standards [57]. The most pressing treatment needs would include any of the following:

- De-oiling: oil and grease removal
- Soluble organics removal: decreased concentrations of benzene (and BTEX)
- Desalination or removal of TDS
- Decreased concentrations of Biological Oxygen Demand (BOD)
- Control of suspended solids and sand

- Disinfection
- Dissolved gas removal (CO2 and H2S)
- Softening, removing excess water hardness
- Removing NORM
- Adjustment of Sodium Adsorption Ratio to avoid soil damage in land application
- Removal of special constituents like Boron that would restrict irrigation, or sodium that would obstacle proper crop cultivation.

Several well-established technologies as well as a number of emerging ones are being used for treatment of produced water. Moreover, many novel technologies that could be tested are being proposed. These technologies could be stand-alone ones, of hybrid configurations, or even some commercial packages that treat oil and gas produced water and zero liquid discharge.

In order to assess technologies, a number of parameters have to be considered. Some of these are industrial status, contaminant range, product water quality, water recovery, energy consumption, robustness, mobility, modularity, life cycle, O&M considerations, capital cost, pre and post treatment, infrastructure requirements, applicability in produced and frac water treatment and concentrate management.

C.10 Oil-Water Separation Technologies

Basic separation technologies are stand-alone ones that are well-established in industry and have always showed optimal performance as they employ the usage of natural forces like gravity or centrifugal force enhanced through inlet conditions.

These technologies will be divided into two categories according to oil concentration in produced water.

C.10.1 Oil Content $\geq$ 1000ppm

C.10.1.1 API oil-water separators

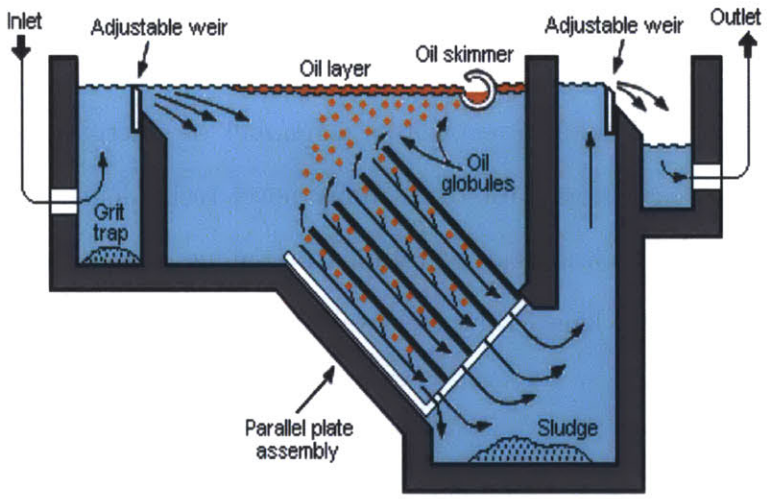

Figure C.2: API Separator

The American Petroleum Institute oil-water separator, shown above, is a device designed to the institute's standards used to separate gross amounts of oil and suspended solids from produced water. It is extensively used to treat wastewater effluents of petroleum refineries, petrochemical plants, and natural gas processing wells. This device is a gravity-separation one, that uses Stokes law to define the rise velocity of oil droplets based on their density and size. Since the specific gravity difference between oil and wastewater is much smaller than that between suspended particles and wastewater, most of the suspended particles will settle to the bottom as a sediment layer, oil particles will float to the surface, and wastewater will form the middle layer. Typically, a skimmer is used to restore the oil layer that is

re-processed or disposed of. A chain and flight scraper and a sludge pump are used to help the removal of the sediments [75]. And water is sent to further treatment. API separators can be circular or rectangular. However, rectangular units are much more commonly used because of size compatibility. Three-phase separators are also available with an additional gas drawoff connection.

In general, API separators promote very good quiescent separation of water and free oil. They perform well in the treatment of elevated oil concentrations, achieves high removal rate of 50-99%. Particulates above 150μ are removed [57]. The reason behind this wide range of efficiency is the presence of other similar designs of oil water separators. One of these is the parallel plate separator that is designed based on the same concept. However, this one includes a tilted parallel plate assembly or parallel packs that enhance the coalescence of suspended oil particles into larger globules due to the larger surface area offered by the design. Therefore, with less space considerations a parallel plate separator can offer the same removal rate as an API separator.

Rudolfs et al. states that the limitations of these devices lie with the minimum globule size they tackle [73]. Some oil globules are much less in diameter than 150μ. Also, free oil concentrations can be in the range of 15-100 ppm which is far less than the concentration these devices can remove. Hence, soluble total petroleum hydrocarbons are not efficiently removed with these processes. Last but not least, though these devices can handle very large flow, the retention time used for separation is very long, which does not make separation efficiency very preferable.

C.10.1.2 Coalescing Plate Separators

These devices are often referred to as CPI. Their design is a variant of the API separators. They consist of corrugated plates or a bundle of slanted tubes at 60 degrees in a vessel

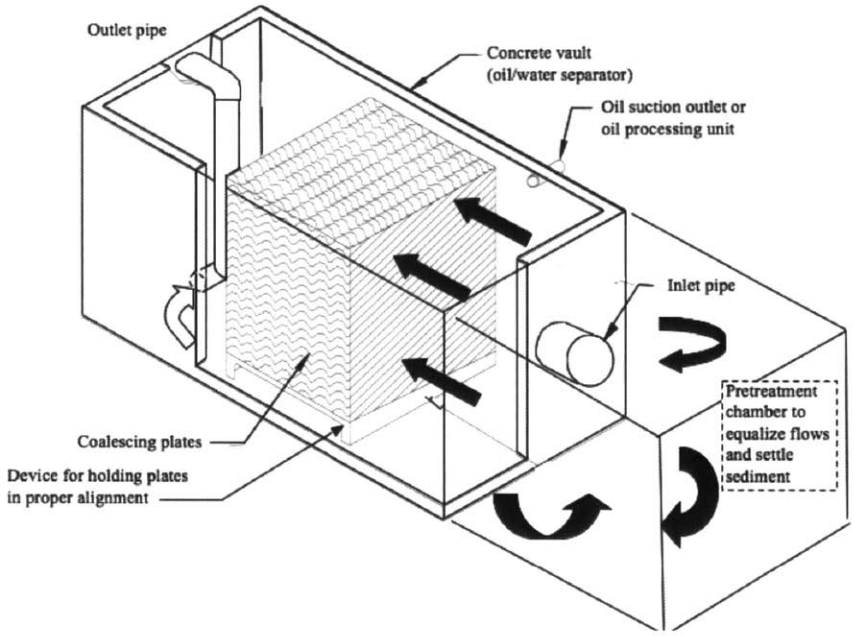

Figure C.3: CPI

or tank. The plates can be placed vertically too. However, it has been found that if the plates are tilted at 60 degrees, the solids will slide down the plates and be collected at the bottom. The settling surface of these plates is the projected horizontal area above of which coalescence of oil globules takes place; hence CPI surface takes less space, estimated to be one fifth of that occupied by APIs [76]. CPIs are much better than APIs when it comes to removal efficiency (95%) and they remove particles as small as 40μ; however, they are not that desirable in petroleum refineries because they cannot handle the same shock load or very high flow rates.

C.10.1.3 Hydrocyclone

Lawrence and Miller define a hydrocyclone as a device of cylindrical construction that is fitted with one or more tangential inlets which cause the fluid entering the cyclone to follow a circular path around the wall of the process. Hydrocyclones are used to separate solids from liquids based on the density of the materials to be separated. Wastewater is fed tangentially

at the top cylindrical section that mounts a conical base. The angle of the latter determines the separating efficiency of the hydrocyclone. Hydrocyclones have no moving parts, and could be made from different materials, like metals, plastic, or ceramics. The hydrocyclone has two exits, one at the bottom called underflow or reject for more dense fractions and one at the top called overflow or product for less dense fraction of the dense stream [77].

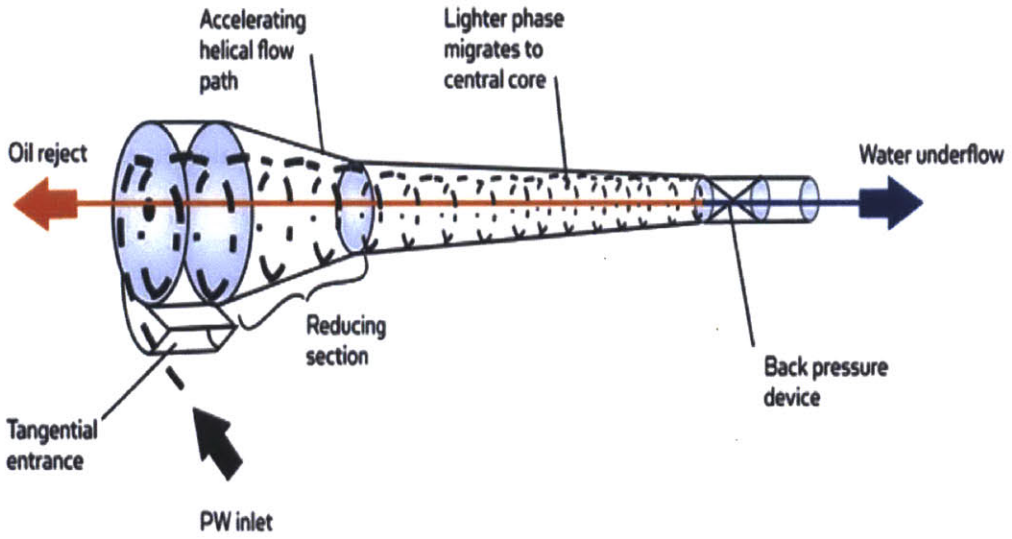

Figure C.4: Hydrocyclone

In case of produced water, rotation of the feed stream generates a centrifugal force of magnitude thousands of times greater than the earth's gravitational force of attraction. Heavy water and solids migrate to the outer wall, lighter material moves towards the center and the light oil is rejected through the underflow outlet.

Hydrocyclones are examples of well-established and known technologies in the oil and gas industries that are able to remove small diameter of oil droplets down to 15μ. They are

very useful for polishing the effluent as the O&G removal rate can go up to 95%. Also, they can be used with organo-clays as pretreatment steps of reverse osmosis. Hydrocyclones do not require any pre or post treatment and the design needs no energy requirements unless a forwarding pump to deliver water to the inlet is used. Yet, soluble TPH compounds are still not removed.

C.10.1.4 Flotation

Flotation is a process in which fine gas bubbles are used to separate small, suspended particles that are difficult to separate by settling or sedimentation. After the gas in injected to produced water, suspended oil particles, colloids, and particulates are attached to the bubbles, and they both rise to the surface. The dissolved gas could be air, nitrogen, or any inert gas. Dissolved air flotation units have been the most commonly used to treat produced water on purpose of removing volatile organics and oil and grease [78]. Gas flotation technologies could be dissolved gas flotation (DGF) or induced gas flotation (IGF). The two apply the same concept of design. However, each presents a way of bubble generation and consequently each generates a certain size of the bubbles. In DGF units, air is usually fed into the chamber that is filled with wastewater. Then vacuum or rapid pressure drop is applied, and air is released. On the other hand, IGF units use mechanical shear or propellers to create bubbles at the bottom of the chamber. To further enhance separation, some producers use flocculants or coagulants, which are chemical additives that speed up coalescence, as a pretreatment to flotation. Flotation works well in cold temperatures and it is excellent for removing natural organic material.

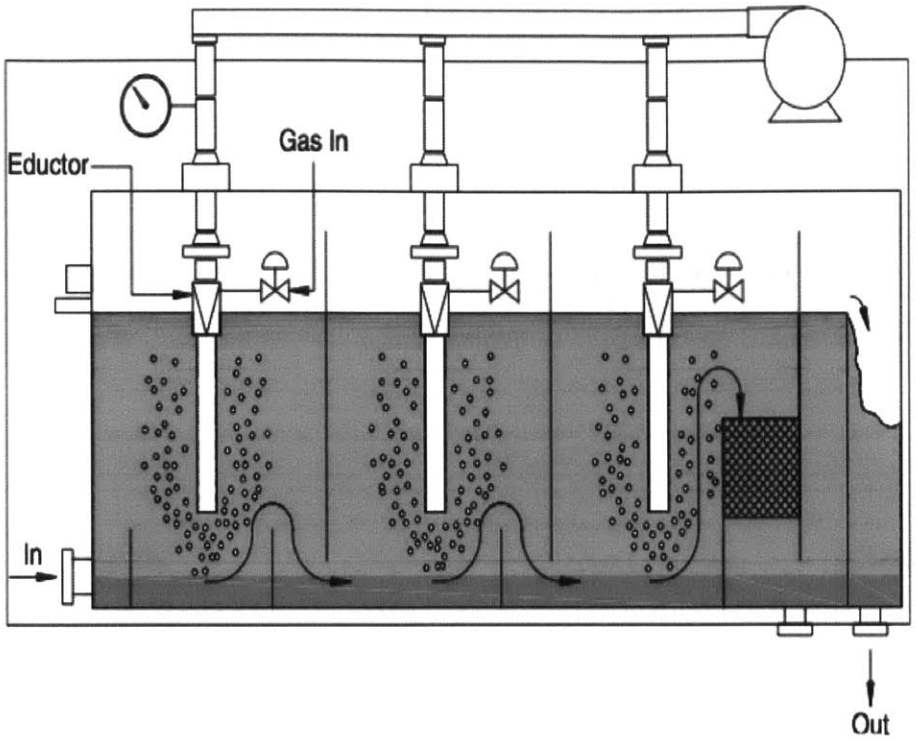

Figure C.5: Induced Gas Flotation

DAF (Dissolved Air Flotation) can remove particles as small as 25μ, and if flocculants are added, DAF can remove contaminants 3 to 5μ in size [79]. Flotation is well established in oil and gas industries, and can achieve a removal rate of 93% for O&G [80], 75% for COD, and 90% for H_2S [81]. Treatment costs are estimated to be \$0.60/m3 [81]. However, flotation does not remove soluble oil compounds. .

C.10.2 Oil Content $\leq$ 1000ppm

C.10.2.1 Biological Aerated Filters (BAFs)

The term biological aerated filter refers to a class of technologies including fixed film and attached growth processes, roughing filters, intermittent filters, packed bed media filters, and conventional trickling filters. A BAF comprises of a permeable medium like gravel,

upon which a microbial film is generated due to interaction with the fed wastewater. Gravel will then facilitate removal of organic constituents. This process, being aerobic, causes the microbial layer to get thicker until the slimy layer becomes anaerobic and the microbial layer starts sloughing off [82]. The technology is optimal for oil content less than 60ppm. The medium used should be durable, inexpensive, and should allow pore space that does not clog flow through the filter. BAFs remove oil, suspended solids, ammonia, nitrogen, COD and

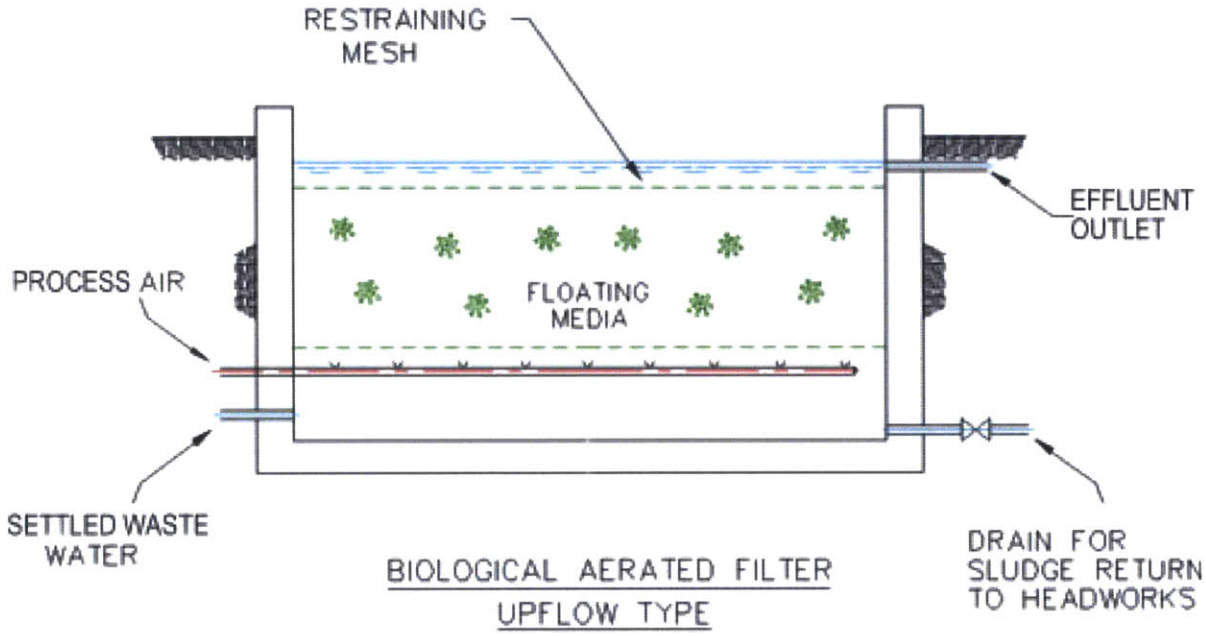

Figure C.6: Biological Aerated Filter

BOD, iron, manganese, heavy metals, and H2S. High salinity might reduce the effectiveness of the filter because it causes toxicity. BAF is a well-established technology in produced water treatment. It is primarily used for oil-field production activities. Removal capability varies with hydraulic loading rate. Generally, typical rates are 60 to 90% nitrification, 50 to 70% total nitrogen, 70 to 80% oil, 30 to 60% COD, 85 to 95% BOD, and 75 to 85% of suspended solids [83]. BAFs provide a 100% water recovery. Some energy might be needed because pumps and fans are used for aeration and distribution nozzles. Estimated energy is 1 to 4 kWh/day.

C.10.2.2 Adsorption

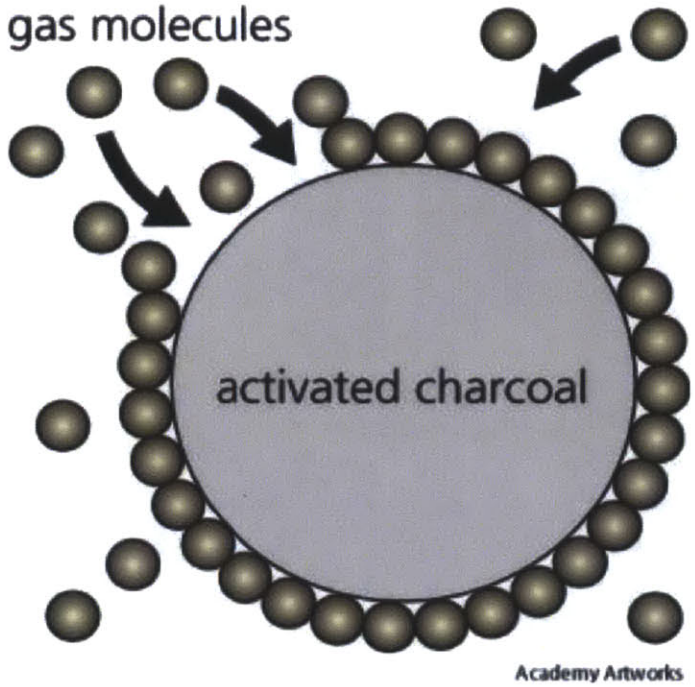

Figure C.7: Adsorption against Activated Carbon

Adsorption is defined to be the accumulation or sticking of ions, molecules, or gases to a surface. In produced water treatment, several surfaces can be used, the most common of which are zeolites, organo-clay, activated alumina, and activated carbon. Chemicals might be used to restore media when all active sites are occupied. And the media is periodically washed to remove trapped particulates. Adsorption is gravity fed, and needs no energy supply. It is best used as a polishing step rather than for primary treatment. Adsorbents are capable of removing iron, manganese, total organic carbon, BTEX, heavy metals, and oil. Removal rate of heavy metals is $\geq$80% [84]. Water recovery is nearly 100%.

C.10.2.3 Media Filtration

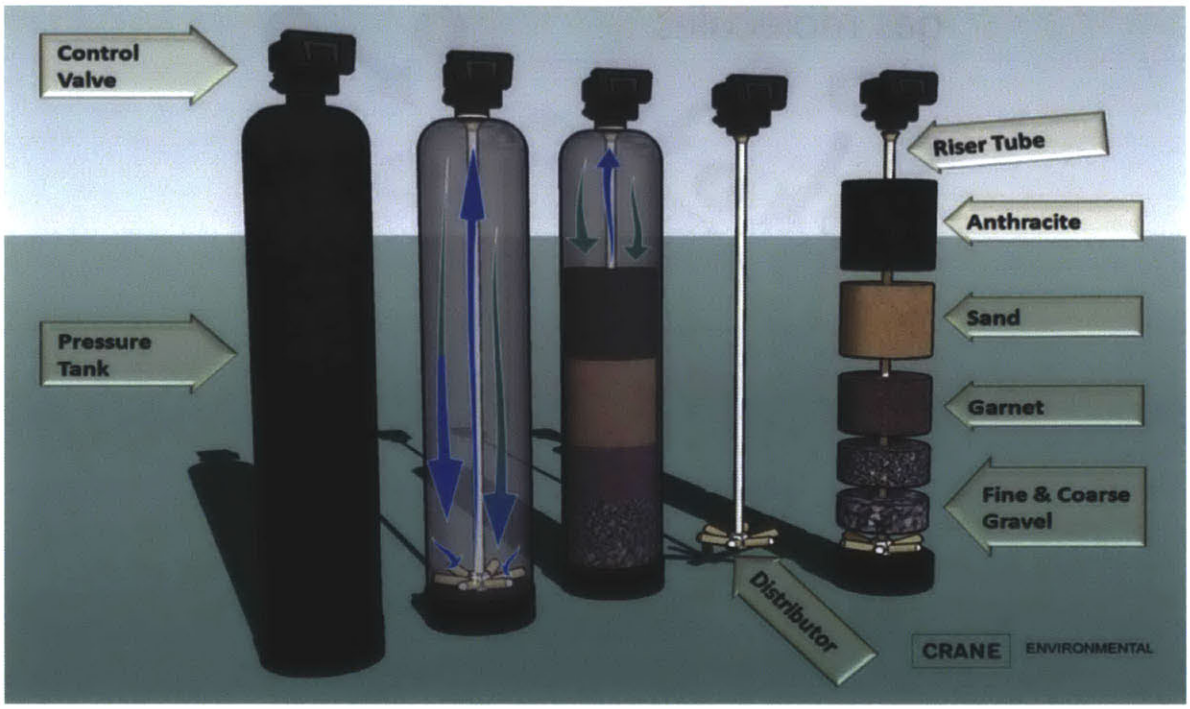

Figure C.8: Various Media Filtration Systems

Media filtration is also referred to as deep bed filters that are beds of stratified granular materials designed to achieve removals of particulates. Media that can be used in this technology cover a wide range of materials, the most common of which are sand, anthracite, and walnut shell. Dual medium filter beds are also available. The granular media is at least four feet deep in a vertical tank. Wastewater is added and is let to settle within the media. This technology is primarily used for treatment of water produced in oilfields. It is able to remove small diameter oil particles [85], and its removal rate is enhanced by addition of flocculants upstream the filter. Deep bed filters are not recommended for oil concentrations over 100ppm, and they do not remove any of the soluble TPH compounds or even fine particulates.

The different oil-water separators have different treatment requirement based on the minimum oil particles' size as shown in the following figure.

Oil Removal Technology	Minimum size of particles removed (microns)
API gravity separator	150
Corrugated plate separator	40
Induced gas floatation (no flocculants)	25
Induced gas floatation (with flocculants)	3 – 5
Hydroclone	10 – 15
Mesh coalescer	5
Media filter	5
Centrifuge	2
Membrane filter	0.01

(Source: Argonne National Laboratory)

Figure C.9: Minimum Oil Particle Size Removed for Different Oil Removal Technologies

C.11 TDS Removal

Several technologies have been established and used in oil and gas industries for treatment of total dissolved solids. High salinity contributes to the toxicity in water; hence, reduction of TDS concentrations is one of the primary needs behind treatment of produced water.

C.11.1 1,000 ppm $\leq$TDS $\leq$ 10,000 ppm

C.11.1.1 Oxidation

Chemical oxidation treatment can be used to remove iron, manganese, sulfur, odor, and synthetic organic chemicals, dissolved in produced water. Chemical oxidation takes place through a set of oxidation/reduction reactions, where some substances lose electrons to be received by others. In water treatment applications, oxidants most commonly used are chlorine, permanganate, oxygen, and ozone. Chemical oxidation is well established, reliable, and requires minimal equipment [86]. Removal capability is a function of contact time, and applied chemical dosages.

C.11.1.2 Electrodialysis and Electrodialysis Reversal

ED and EDR are electrochemical charge driven processes in which ions migrate through selectively permeable membranes under the effect of an applied potential difference. Exchange membranes are usually made up of ion exchange polymers and they are able to pass ions of one charge and reject ions of the opposite charge. In wastewater treatment an ER stack is used, in which cation exchange membranes and anion exchange membranes are arranges alternatively between a cathode and an anode. Ions of different charges will migrate to opposite compartments. EDR is similar to ED except that it uses periodic reversal of polarity to effectively reduce scaling and fouling, allowing the system to operate at higher recoveries [87]. These methods are effective for produced water reclamation with low TDS concentrations (up to 8000ppm) and they have high water recoveries. To avoid scaling or fouling on ion exchange membranes, pretreatment is sometimes recommended. Softening, pH lowering, and filtration of suspended solids before feeding wastewater into the system are effective pretreatment methods. Biological growth can be avoided by adding a small amount of chlorine given that ED membranes are not susceptible to degradation by chlorine. Despite the system's efficiency in desalinating brackish water, it is not widely used because of its high treatment cost and potential fouling problems.

C.11.2 10,000 $\leq$ TDS $\leq$ 80,000ppm

Pressure-Driven Membrane Technologies are very effective candidates for removal of TDS with concentration within this range. These systems utilize hydraulic pressure to overcome the osmotic pressure of the feed solution and force the permeate-pure water- to diffuse through a dense, non-porous membrane [88]. Globally, Reverse Osmosis seawater desalination technologies are dominant with a 58% share of the market and still growing [73]. However, there are also some thermally driven membrane technologies that offer good solutions.

C.11.2.1 Nanofiltration

Just like other membranes, Nanofiltration membranes are thin films of synthetic organic or inorganic materials, which are selectively permeable according to size or molecular weight. Nanofiltration is one of the most studied membrane technologies that are utilized in treatment of brackish water. It is known to show good performance with desalination of municipal water supplies. However, there have been a lot of questions about its usage as a standalone technology in remediation of produced water, which has made it a better candidate as a pretreatment technique for other systems such as Reverse Osmosis Membranes. NF membranes are designed to reject contaminants as small as 0.001μm. This allows NF to achieve high rejection of divalent ions (Mg, Ca, Ba, SO4), heavy metals ($\geq$99% of MgSO4 [87]), and radionuclides. It is also applicable for certain classes of organic compounds. Hence, NF is best suited for softening applications and removal of most metals. The nominal TDS range for NF application sis between 1,000 and 35,000ppm [89]. Water recovery ranges from 75 to 90% but may require addition of scale inhibitors depending on feed water quality. NF membranes (approximately 0.08 kWh/bbl. [90]) require less energy than RO membranes but they share similar maintenance, robustness, reliability, mobility, modularity and operational footprint.

C.11.2.2 Seawater Reverse Osmosis-SWRO

SWRO membrane systems are most applicable for feed streams up to 47,000 ppm TDS that is seawater level [91]. RO membranes are highly selective, capable of rejecting contaminants as small as 0.0001μ. Monovalent and multivalent ions, molecules, and metals are easily rejected by RO membranes. Primarily, their main use is to reject NaCl (salt) with a rate in excess of 99%. Other rejected contaminants include Boron and Silica. Because of the high molecular weight of radionuclides, they are also rejected by RO membranes. However, they are unable to offer a significant barrier to dissolved gases and certain low molecular weight

organic molecules [92]. The main limitation of RO systems is the potential fouling due to the formation of an oil film on the membrane and abrasion of membrane due to precipitation. Water recovery is also low and is frequently restricted to 30-60% because of the relatively high osmotic pressure of the feed stream. Produced and Frac water in specific are sometimes overwhelming for RO systems. Membrane fouling and scaling, being the primary concern

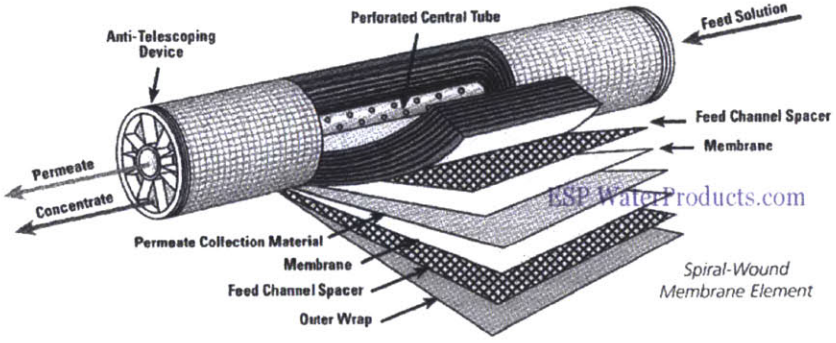

Figure C.10: Reverse Osmosis Membrane

of RO operation, necessitate pretreatment to remove organic foulants and sometimes the addition of scale inhibitors. If appropriate design considerations are not met, RO systems end up being energy and cost intensive. SWRO technology has one of the smallest footprints of all technologies. However, residual management costs may be substantial due to low water recovery. Post treatment is normally required to separate biomass, solids, and dissolved gases. RO is a major component in many hybrid systems used today in different industries.

C.11.2.3 Brackish Water Reverse Osmosis- BWRO

BWRO membranes are designed to achieve moderately high rejections of dissolved constituents ($\geq$94% NaCl). BWRO generally may achieve water recovery up to 85%. It rejects metals and divalent ions to a high degree, and has similar limitations like SWRO for organics removal, pretreatment necessity, and inorganic scaling control. The hydraulic pressure required to overcome the osmotic pressure of the feed water is lower than that of SWRO.

Hence, operational costs are reduced. The higher recovery of BWRO reduces concentrated brine management.

One study of BWRO examined the potential of harvesting iodide from produced water, and used 4 BWRO membranes and 3 NF membranes. It showed effective results when tested on water produced in a natural gas production facility in Eastern Montana [93].

C.11.2.4 Membrane Distillation

Membrane distillation is a thermally driven separation process that utilizes a low-grade heat source to facilitate mass transport through a hydrophobic, microporous membrane. A vapor pressure gradient, generated due to the temperature difference across the membrane, behaves as the driving force for mass transfer. There is no present documentation that MD has been used for produced water treatment in the past. However, it is an effective desalination technology that treats feed water with TDS in excess of 35,000ppm. Theoretically, MD membranes remove 100% of all non-volatile solutes. As a standalone technology, MD possesses a water recovery similar to that of BWRO. However, when coupled with a crystallizer, an MD system is able to reduce scaling and achieve a recovery of 80% [40].

Generally, MD membranes have to be porous, should not be wetted by process liquids, must not allow any capillary condensation inside the pores, and should only transport vapor through [41]. Moreover, MD requires that the feed water temperature be elevated beyond that of the permeate side, yet a large thermal gradient is not required for mass transfer. Scaling and fouling are possible, and regular maintenance is needed. MD is very flexible, can be readily integrated in mobile platforms, and highly modular.

C.11.2.5 Freeze-Thaw Evaporation

It is a process that combines natural processes of freezing and evaporation to provide the driving force for demineralization of produced water. Two cycles take place: freeze crystallization followed by thawing. It has low power requirements, yet it can be used only in areas that have the required freezing days.

C.11.2.6 Vapor Compression

In vapor compression distillation system, heat is provided by the compression of vapor rather than a direct source of boiler produced steam. High pressure steam is used. The cycle is made up of four stages. Low temperature vapor compression distillation is a simple, reliable, and efficient process. The choice of a high capacity compressor is key for scale formation reduction. VCD is applicable to feed water with TDS$\geq$40,000ppm, no matter what the chemistry makeup entails. Water recovery is around 40%, which is higher than that provided by Multi Effect Distillation or Multi-Stage Flash

C.11.3 Very High TDS Concentration

C.11.3.1 Multi-Effect Distillation

An MED evaporator consists of several consecutive cells (or effects) maintained at decreasing levels of pressure (and temperature) from the first (hot) cell to the last one (cold). Sufficient energy is applied to bring the feed water to its boiling temperature and then to deliver the extra energy needed for the heat of vaporization to transform part of the saline water to steam. The final step is to condense the process steam as pure water. Different effects are kept at reduced pressures to attain boiling at reduced temperatures, and consequently, makes the system less energy-intensive. The vapor produced at one effect heats the water

in the next one. MED systems have not been widely explored with produced waters though they cover a wide range of TDS because a number of problems were associated with the old designs. Mainly, scaling and low heat transfer rate problems have been very common. MED offers great potential of reducing the plant's footprint.

C.11.3.2 Multi-Stage Flash

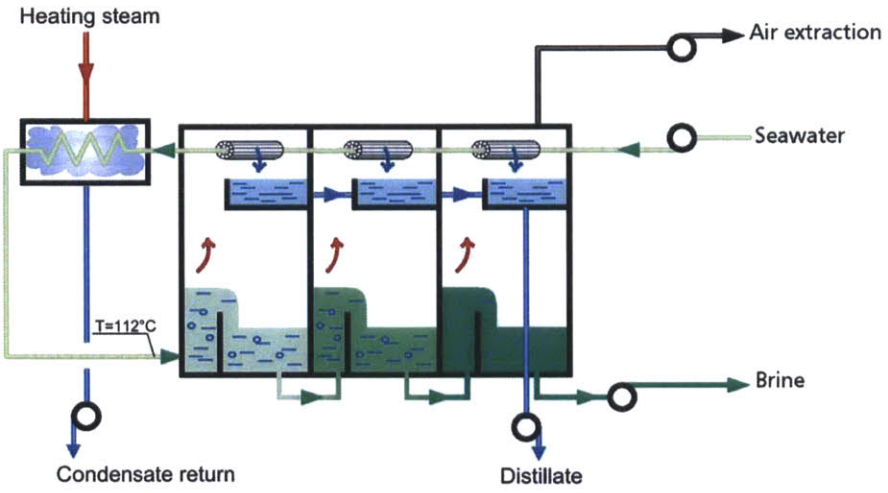

Figure C.11: Multi Stage Flash System

Flash evaporation is the process by which water is evaporated due to a reduction in pressure rather than an increase in temperature. Multi stage flash systems primarily operate based on the concept of flash evaporation. Steam is collected at each stage, and pure water is recovered after condensation. Post-treatment is sometimes needed. MSF had the largest market share before 2005, when membrane technologies-particularly reverse osmosis- started to take over [62]. A multi effect distillation- vapor compression hybrid system is commonly used and it has much more enhanced energy efficiency.

C.11.3.3 Crystallizers

Crystallization is an equilibrium-based separation and evaporation technology that uses energy as the separating agent and can be comprised of a combination of treatment processes

that are more energy efficient at removing water from lower TDS waters. For instance, RO is commonly used for an initial pass through if TDS levels are sufficiently low. Crystallization processes can then be used to further concentrate the RO concentrate stream by extracting water from the brine solution; the total volume of the liquid concentrate is reduced while the associated TDS increases significantly. Crystallization has proven to treat water with the highest salinity (up to 650,000ppm). 95% return rates of frac and produced water can be achieved. The systems are energy and cost intensive.

C.11.4 Total Suspended Solids Removal

C.11.4.1 Microfiltration/Ultrafiltration

Microfiltration (MF) has the widest pore size (0.1-3μm) of the wide variety of membrane filtration systems. Ultrafiltration (UF) pore sizes range from 0.01 to 0.1μm. In terms of particle size, MF range covers the lower portion of the conventional clays and the upper half of the range for humic acids. This size is smaller than that of bacteria and algae, but larger than that of viruses. MF is typically utilized for turbidity removal and suspended colloids volume reduction. UF, in turn, is able to remove viruses, odor and other colloidal natural organic matter. Both membranes are low-pressure systems, and both are well-established methods used as pretreatment for RO systems and Electrodialysis techniques and other TDS removal systems, as they themselves cannot remove salt. MF membranes can operate in either cross-flow separation or dead-end filtration where there is no concentrate flow. And the pump configurations could be pressure-driven or vacuum-type systems. Water recovery ranges from 85 to 95% [94]. Membrane selection, in general, is based on a number of criteria that include, but not limited to cost, percent recovery, end use, pretreatment, percent rejection, and pressure. MF/UF membranes are available in ceramic and polymer form.

Ceramic membranes are made of oxides, nitrides or carbides of metals like aluminum, zir-

conium, or titanium [95]. They are very resilient, mechanically strong, chemically and thermally stable, and can achieve high flux rates. They are capable of removing particulates, O&G, and metal oxides. A strainer can be used as pretreatment of water fed into a ceramic MF/UF membrane.

Polymeric membranes are made of materials like polyacrylonitrile and polyvinylidene. They are relatively inexpensive but less resilient than ceramic membranes. They are applicable to any feed water bin, independent of salt type and concentration. Nearly all non-dissolved organic carbon is removed, while 10% of the dissolved type is guaranteed. Suspended solids removal rate is nearly 100%.

C.11.4.2 Settling

Settling is implemented in a basin or a pond, where gravity is the main force that causes particulates to settle. Settling ponds have a large footprint and they pose some risk on wildlife. There are no chemical requirements though sedimentation enhancement chemicals are sometimes added. The main factor that determined the rate of removal is the retention time in the pond.

C.11.4.3 UV Disinfection

This is a widely used well-established technology that has gained popularity by virtue of its ease of operation lack of chemical requirements, and no formation of any disinfection byproducts. Water is pumped through a UV reactor which is equipped with an array of UV lamps that provide a disinfection dosage of 30-50 mJ/cm^2. UV light is known to inactivate the DNA and/or RNA of pathogens. Typically, UV disinfection is a polishing technique and is the last treatment stage in most water treatment facilities.

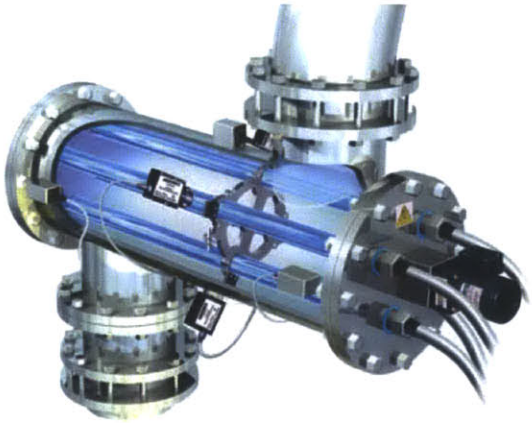

Figure C.12: UV Disinfector

C.12 Comments

The performance of some oil removal and TDS removal technologies can be summarized with Fig. C.13 and C.14. Choice of the most convenience technology for a plant is decided based on different technical and economic parameters. Fig C.15 compares the performance of different produced water remediation technologies.

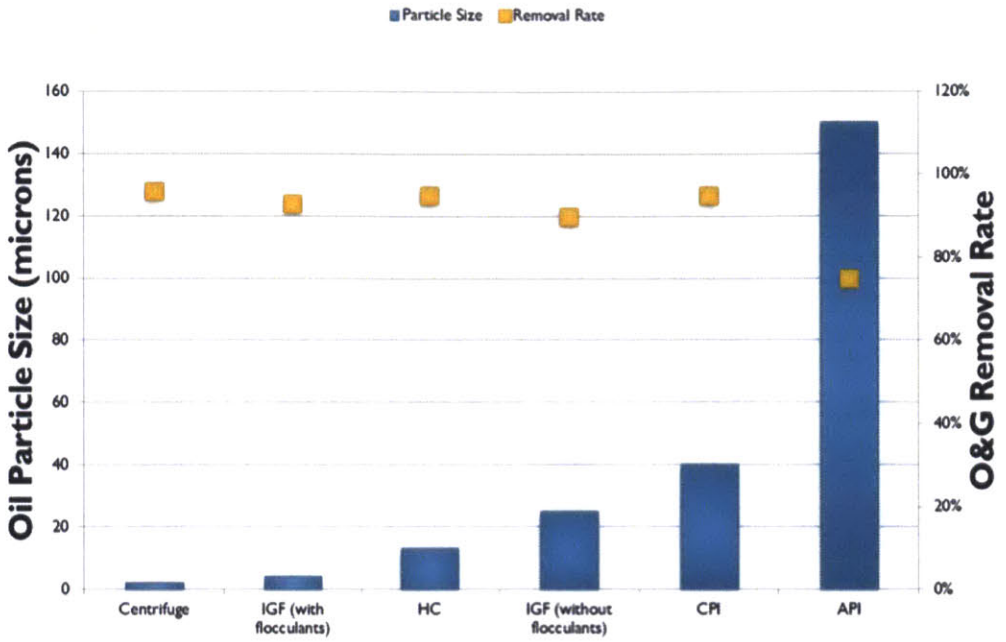

Figure C.13: Removal Rate and Particle Size for Oil Removal Technologies

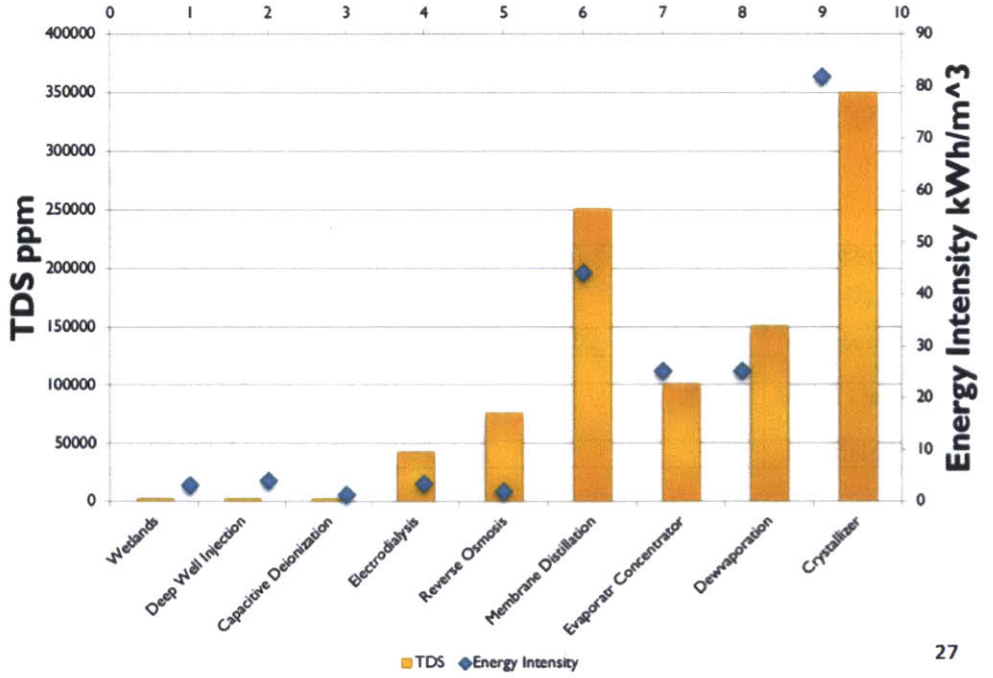

Figure C.14: Energy Intensity and TDS limit for TDS Removal Technologies

Primary Application	Technology	O&G	TDS	TSS	BOD/COD	Water Recovery	Energy	Cost ($/m3)
Oil Content >1000ppm	API	50-95%	-	-	-	-	Low	-
	CPI	Up to 95%	-	-	-	-	Minimal	-
	Hydrocyclone	Up to 95%	-	high	-	high	Forwarding pump	-
	Centrifuge	Up to 96%	-	-	-	-		-
	Floatation	93%	-	-	75% COD	~100%	Pressurize the System	0.6
Oil Content <1000ppm	BAFs	70-80%	-	75-85%	60% COD 85-95% BOD	~100%	1-4 kWh/day	C- high O-low
	Adsorption	-	>80% HM	-	-	~100%	Minimal	-
	Media Filtration	>90%	-	-	-	~100%	Minimal (Backwash)	-
TDS 1000-10,000	Oxidation	-	f(Oxidant)	-	-	100%	18% of O&M Cost	C:2.64/d O:0.013
	ED	-	>90%	-	-	80-90%	0.31-0.44 kWh/kg NaCl	0.94
	FTE	-	~1000ppm	>90%	-	50%		f(Site)
TDS >10,000ppm (<80,000)	NF	-	>99%Dival <90%Mono	-	~90%	75-90%	0.5kWh/m^3	C:220-1070 O:0.188
	MD	-	2-10 ppm	-	-	60-95%	Operates by waste heat	C:0.94 O:0.37
	SWRO	-	>99.4%	80%NH_3 50% B	98%COD	30-60%	2.89-4.2kWh/m^3	C:792/d O:0.5
	BWRO	-	100-1500ppm	60-80%NH_3	95%COD	60-85%	0.12-0.817kWh/m^3	C:211-1056 O:0.18
TDS>80000ppm	VC	-	Very high	-	-	40%	15-26 kWh/m^3	C:880-1572 O:0.47
	MED	-	Very high	-	-	20-35% Horizontal and Vertical Tube Design 67% Stacked	2.9+10 kWh/m^3	C: 1572-2076 O: 0.69
	MSF	-	2-10 ppm	-	-	10-20%	(2.83-5.67)+21 kWh/m^3	C:1572-2264 O:1.19
	Dewvaporation		20 ppm		-	90%	-	-
TSS	Ceramic MF/UF	10%	-	100%	-	90-100%	-	-
	Polymeric MF/UF	10%	-	100%	-	85-100%	-	C:6.3-12.6 O:6.3-12.6
	UV Disinfection	-	-	-	90-99%	100%	3.25 kWh/day	34.3/d

Figure C.15: Performance Comparison of Produced Water Remediation Technologies

Bibliography

[1] Zahid Amjad. Fouling in heat exchangers, 2001.

[2] T.R. Bott. *Fouling of Heat Exchangers.* Chemical Engineering Monographs. Elsevier Science, 1995.

[3] T. Kuppan. *Heat Exchanger Design Handbook.* Dekker Mechanical Engineering. Taylor & Francis, 2000.

[4] R.K. Shah and D.P. Sekulic. *Fundamentals of Heat Exchanger Design.* Wiley, 2003.

[5] Mostafa M. Awad. Fouling of heat transfer surfaces. Technical report, Mansoura University, Egypt, 2011.

[6] *Proceedings from the Tenth Annual Industrial Energy Technology Conference, Houston, TX*, 1988.

[7] H.C. Flemming. Biofouling in water treatment. In Hans-Curt Flemming and GillGregory Geesey, editors, *Biofouling and Biocorrosion in Industrial Water Systems*, pages 47–80. Springer Berlin Heidelberg, 1991.

[8] Joshi M.H., Balamurugan P., Venugopalan V.P., and Rao T.S. Dense fouling in acid transfer pipelines by an acidophilic rubber degrading fungus. *The Journal of Bioadhesion and Biofilm Research*, 27:621–629, 2011.

[9] Johnsen S.G., Henetho S.M., P. Tetlie, and S.T. Johansen. Studies of paraffin wax deposition on coated and non-coated steel surfaces. In *Proceedings of International Conference on Heat Exchanger Fouling and Cleaning*, 2011.

[10] Panchal C.B. Review of fouling mechanisms. In *Proceedings of International Conference on Mitigation of Heat Exchanger Fouling and its Economic and Environmental Implications*, 1999.

[11] Norman Epstein. Particulate fouling of heat transfer surfaces: Mechanisms and models. In L.F. Melo, T.R. Bott, and C.A. Bernardo, editors, *Fouling Science and Technology*, volume 145 of *NATO ASI Series*, pages 143–164. Springer Netherlands, 1988.

[12] Jovan Mitrovic, editor. *Heat Exchangers: Basic Design Applications.* InTech, 2012.

[13] K.J. Bell and A.C. Mueller. *Wolverine Heat Transfer Databook II.* Wolverine Tube, 2001.

[14] J Darby, George Tchobanoglous, et al. Providing reliable supply of safe drinking water poses challenges. *California Agriculture*, 54(5):69–77, 2000.

[15] Sandberg and Jan. *Fouling in Biomass Fired Boilers.* PhD thesis, Malardalen University, School of Sustainable Development of Society and Technology, 2011.

[16] J.Y. Huang, Y.M.J. Chew, and D.I. Wilson. Freezing fouling caused by fat crystallization on cooled surfaces. In *Proceedings of International Conference on Heat Exchanger Fouling and Cleaning*, 2011.

[17] J. Taborek, G.F. Hewitt, N.H. Afgan, International Center for Heat, and Mass Transfer. *Heat Exchangers: Theory and Practice.* Proceedings of the International Centre for Heat and Mass Transfer. McGraw-Hill, 1983.

[18] L. Melo, T.R. Bott, and C.A. Bernardo. *Fouling Science and Technology.* Nato Science Series E: (closed) Series. Springer, 1988.

[19] E.F.C. Somerscales, J.G. Knudsen, and Rensselaer Polytechnic Institute. *Fouling of Heat Transfer equipment.* Hemisphere Pub. Corp., 1981.

[20] S.N.Kazi. Fouling and fouling mitigation on heat exchanger surfaces. Technical report, University of Malaya, Kuala Lumpur, Malaysia, 2012.

[21] F. Kreith. *The CRC Handbook of Thermal Engineering.* The Mechanical engineering handbook series. CRC Press, 2000.

[22] T.R. Bott and J.S. Gudmundsson. Rippled silica deposits in heat exchanger tubes. In *6th International Heat Transfer Conference*, 1978.

[23] Crittenden B.D. and Khater E.M.H. Fouling from vaporizing kerosine. *Journal of Heat Transfer*, 109(3):583–589, 1987.

[24] Bansal B. *Crystallisation Fouling in Plate Heat Exchangers.* PhD thesis, Department of Chemical and Materials Engineering, The University of Auckland, New Zealand, 1994.

[25] Mueller, STEINHAGEN, and J. MIDDIS. Particulate fouling in plate heat exchangers. *Heat Transfer Engineering*, 10(4):30–36, 1989.

[26] Bohnet and Matthias. Fouling of heat transfer surfaces. *Chemical Engineering & Technology*, 10(1):113–125, 1987.

[27] B. J. Reitzer. Rate of scale formation in tubular heat exchangers. mathematical analysis of factors influencing rate of decline of over-all heat transfer coefficients. *Industrial & Engineering Chemistry Process Design and Development*, 3(4):345–348, 1964.

[28] Demopolous. Aqueous precipitation and crystallization for the production of particulate solids with desired properties. *Hydrometallurgy*, 96:199–214, 2009.

[29] James J. De Yoreo and Peter Vekilov. Principles of crystal nucleation and growth. Technical report, Lawrence Livermore National Laboratory, California, 2003.

[30] Tlili, Rousseau, Ben Amor, and Gabrielli. An electrochemical method to study scaling by calcium sulphate of a heat transfer surface. *Chemical Engineering Science*, 63:559–566, 2008.

[31] M. Brusilovsky, J. Borden, and D. Hasson. Flux decline due to gypsum precipitation on {RO} membranes. *Desalination*, 86(2):187 – 222, 1992.

[32] B.H. Rankin and W.L. Adamson. Scale formation as related to evaporator surface conditions. *Desalination*, 13(1):63 – 87, 1973.

[33] Junghahn. Memethod zum herabsetzen oder verhidern der krustenbildung. *Chemie Ingenieur Technik*, 36:60–67, 1964.

[34] J. Marriott. Where and how to use plate heat exchangers. *Chemical Engineering*, 78(8):127–134, 1971.

[35] B.A. Garrett-Price. *Fouling of Heat Exchangers: Characteristics, Costs, Prevention, Control, and Removal.* Noyes Publications, 1985.

[36] Z Amjad. Calcium sulfate dihydrate (gypsum) scale formation on heat exchanger surfaces: The influence of scale inhibitors. *Journal of Colloid and Interface Science*, 123(2):523 – 536, 1988.

[37] Lancia, Amedeo, Musmarra, Dino, Prisciandaro, and Marina. Measuring induction period for calcium sulfate dihydrate precipitation. *AIChE Journal*, 45:390–397, 1999.

[38] Otakar Sohnel and John W Mullin. Interpretation of crystallization induction periods. *Journal of Colloid and Interface Science*, 123(1):43 – 50, 1988.

[39] C.A. Branch. *Heat Transfer and Heat Transfer Fouling in Evaporators with Kraft Pulp Black Liquor.* University of Auckland, 1991.

[40] S.H. Najibi, H. Muller-Steinhagen, and M. Jamialahmadi. Calcium sulphate scale formation during subcooled flow boiling. *Chemical Engineering Science*, 52(8):1265 – 1284, 1997.

[41] Ramsdell L. and Partridge E. The crystal forms of calcium sulphate. *Mineralogical Society of America*, pages 59–74, 1977.

[42] Z. Amjad. Gypsum scale formation on heat exchanger surfaces: The influence of natural and synthetic polyelectrolytes. *Tenside, Surfactants, Detergents*, pages 214 – 219, 2004.

[43] Z Amjad. Scale inhibition in desalination applications: an overview in corrosion 96. In *The NACE International Annual Conference and Exposition*, 1996.

[44] J.C. Cowan and D.J. Weintritt. *Water-formed scale deposits.* Gulf Pub. Co., Book Division, 1976.

[45] Deparment of Geology and Planetaty Science at University of Pittsburgh. Gypsum mineral. Online.

[46] D. Q. Kern and R. E. Seaton. A theoretical analysis of thermal surface fouling. *British Chemical Engineering*, 4(5):258–262, 1959.

[47] Thermal-Fluids Center. Scale analysis of natural convection. online, 2010.

[48] Anthony F. Mills. *Heat Transfer*, chapter 5, pages 455–565. Prentice Hall, 1998.

[49] J.W. Gibbs, H.A. Bumstead, R.G. Van Name, and W.R. Longley. *The collected works of J. Willard Gibbs.* Number v. 2 in The Collected Works of J. Willard Gibbs. Longmans, Green and Co., 1902.

[50] M. Volmer. *Kinetik der phasenbildung.* Chemische Reaktion. J. W. Edwards, 1939.

[51] J.W. Mullin. *Crystallization- Fourth Edition.* Reed Educational and Professional Publishing Ltd, 2001.

[52] Volmer M. and Schultz W. *Kondensation an Kristalen.* Zeitschrift fur Physikalische Chemie, 1931.

[53] Oleg D. Linnikov. Investigation of the initial period of sulphate scale formation part 1. kinetics and mechanism of calcium sulphate surface nucleation at its crystallization on a heat-exchange surface. *Desalination*, 122(1):1 – 14, 1999.

[54] David Hasson, Alexander Drak, and Raphael Semiat. Induction times induced in an ro system by antiscalants selaying caso4 precipitation. *Desalination*, 157:193 – 207, 2003.

[55] Fahiminia, Feridoun, Watkinson, A. Paul, Epstein, and Norman. Early events in the precipitation fouling of calcium sulphate dihydrate under sensible heating conditions. *The Canadian Journal of Chemical Engineering*, 85(5):679–691, 2007.

[56] Scott Sinex. Edta- a molecule with a complex story. Prince George's Community College.

[57] Tom Hayes and Dan Arthur. Overview of emerging produced water treatment technologies. In *11th Annual International Petroleum Conference, Albuquerque, NM*, 2004.

[58] Colorado Department of Public Health and Environment. Discharges associated with produced water treatment facilities. Technical report, Water Quality Control Division.

[59] Aaron D. and Horn. Breakthrough mobile water treatment converts 75% of fracturing flowback fluid to fresh water and lowers co2 emissions. In *SPE Americas E&P Environmental and Safety Conference*, 2009.

[60] Ahmadun Fakhruâ Al-Razi, Alireza Pendashteh, Luqman Chuah Abdullah, Dayang Radiah Awang Biak, Sayed Siavash Madaeni, and Zurina Zainal Abidin. Review of technologies for oil and gas produced water treatment. *Journal of Hazardous Materials*, 170:530–551, 2009.

[61] Harish R. Acharya, Claire Henderson, Hope Matis, Hareesh Kommepalli, Brian Moore, and Hua Wang. Cost effective recovery of low-tds flowback water for reuse. Technical report, Department of Energy, 2011.

[62] John V., Markus P., Deborah E., and Robert J. A white paper describing produced water from production of crude oil, natural gas, and coal bed methane. Technical report, US Department of Energy, 2004.

[63] Breit G., Klett T.R., Ferderer D.A., and Kharaka. National compilation of information about water co-produced with oil and gas. In *5th International Petroleum Environmental Conference*, 1998.

[64] P.J.C. Tibbetts, I.T. Buchanan, L.J. Gawel, and R. Large. A comprehensive determination of produced water composition. In JamesP. Ray and F.Rainer Engelhardt, editors, *Produced Water*, volume 46 of *Environmental Science Research*, pages 97–112. Springer US, 1992.

[65] R.P.W.M. Jacobs, R.O.H. Grant, J. Kwant, J.M. Marquenie, and E. Mentzer. The composition of produced water from shell operated oil and gas production in the north sea. In JamesP. Ray and F.Rainer Engelhardt, editors, *Produced Water*, volume 46 of *Environmental Science Research*, pages 13–21. Springer US, 1992.

[66] BR Hansen and SRH Davies. Review of potential technologies for the removal of dissolved components from produced water. *Chemical Engineering Research and Design*, 72(A2):176–188, MAR 1994.

[67] P. Ekins, R. Vanner, and J. Firebrace. Zero emissions of oil in water from offshore oil and gas installations: Economic and environmental implication. *Journal of Cleaner Production*, 15:1302 1315, 2007.

[68] M.T. Stephenson. A survey of produced water studies. In JamesP. Ray and F.Rainer Engelhardt, editors, *Produced Water*, volume 46 of *Environmental Science Research*, pages 1–11. Springer US, 1992.

[69] Utvik T.I.R. Characteristics of produced water in the north sea. Technical report, ProducedWaterWorkshop, Aberdeen, Scotland, 2003.

[70] T. Gafvert, I. Faerevik, and A.L. Rudjord. Assessment of the discharge of norm to the north sea from produced water by the norwegian oil and gas industry. In P. Povinec and J.A. Sanchez-Cabeza, editors, *Radionuclides in the Environment Int. Conf. On Isotopes in Env. Studies*, volume 8 of *Radioactivity in the Environment*, pages 193 – 205. Elsevier, 2006.

[71] Weidong W., Ximing L., Yong C., Songting Z., and Yan J. The technology of microbial treatment of drained water of oilfields. In *SOEPE Asia Pacific Improved Oil Recovery Conference*, 2001.

[72] Dal Ferro B. and Michael S. Global onshore and offshore water production. Technical report, Douglas-Westwood Lts.

[73] Rodney R. *Produced Water and Associated Issues*, 2003.

[74] Robert Lee, Randy Seright, Mike Hightower, Allan Sattler, Martha Cather, Brian McPherson, Lori Wrotenbery, David Martin, and Mike Whitworth. Strategies for produced water handling in new mexico. In *Ground Water Protection Council Produced Water Conference*, pages 16–17, 2002.

[75] Milton R Beychok. *Aqueous wastes from petroleum and petrochemical plants.* Wiley New York, NY, 1967.

[76] Total water management for the petroleum and petrochemical industries. Technical report, Water Technologies- Siemens, 2009.

[77] P Rogoshewski. Remedial action technology for waste disposal sites. 1983.

[78] AL Casaday. Advances in flotation unit design for produced water treatment. In *SPE Production Operations Symposium*, 1993.

[79] National Energy Technology Laboratory. *Produced Water Management Technology Descriptions Fact Sheet.*

[80] All Consulting. Handbook on coal bed methane produced water: Management and beneficial use alternatives, 2003.

[81] Dennis A Burke. Application of the agf (anoxic gas flotation) process. In *The 4th International Conference: Flotation in Water and Waste Water Treatment, Helsinki Finland, Finnish Water and Waste Water Works Association*, 2000.

[82] O.K. Scheible, A. Gupta, National Small Flows Clearinghouse, United States. Environmental Protection Agency. Office of Municipal Pollution Control, Inc HydroQual, and United States. Environmental Protection Agency. *Assessment of Single-stage Trickling Filter Nitrification.* US Environmental Protection Agency Design Manual. The Office, 1991.

[83] Delin SU, Jianlong WANG, Kaiwen LIU, and Ding ZHOU. Kinetic performance of oilfield produced water treatment by biological aerated filter. *Chinese Journal of Chemical Engineering*, 15(4):591 – 594, 2007.

[84] F.R. Spellman. *Handbook of Water and Wastewater Treatment Plant Operations.* Taylor & Francis, 2003.

[85] Clifford J Hensley. Filter media for filter systems, April 18 1995. US Patent 5,407,574.

[86] Environmental Resources Team (U.S.). Water Engineering and Research Group. *Water Treatment Primer for Communities in Need.* Advanced water treatment research program report. U.S. Dept. of the Interior, Bureau of Reclamation, Technical Service Center, Water Treatment Engineering and Research Group, 2001.

[87] David S Kosson, Hans A van der Sloot, Florence Sanchez, and Andrew C Garrabrants. An integrated framework for evaluating leaching in waste management and utilization of secondary materials. *Environmental Engineering Science*, 19(3):159–204, 2002.

[88] KS Spiegler and O Kedem. Thermodynamics of hyperfiltration (reverse osmosis): Criteria for efficient membranes. *Desalination*, 1(4):311–326, 1966.

[89] Long beach water department prototype seawater desalination testing facility test plan, 2006.

[90] Claire Ventresque, Greg Turner, and Guy Bablon. Nanofiltration: from prototype to full scale. *Journal-American Water Works Association*, 89(10):65–76, 1997.

[91] M. Wilf and L. Awerbuch. *The Guidebook to Membrane Desalination Technology: Reverse Osmosis, Nanofiltration and Hybrid Systems, Process, Design, Applications and Economics.* Balaban Desalination Publications, 2007.

[92] Simon Judd and Bruce Jefferson. *Membranes for industrial wastewater recovery and re-use.* Elsevier Science, 2003.

[93] M Adewumi, J Erb, and RW Watson. Design considerations for a cost effective treatment of stripper oil well produced water. *Produced Water: Technological/Environmental Issues and Solutions, Plenum Publishing Corp., New York*, pages 511–523, 1992.

[94] S.J. Randtke, American Water Works Association, M.B. Horsley, and American Society of Civil Engineers. *Water Treatment Plant Design 5/E.* McGraw-Hill's AccessEngineering. McGraw-Hill Education, 2012.

[95] Marcel Mulder. Basic principles of membrane technology. *The Netherlands: Kluver Academic Publischers*, 2003.